Department of Precision and Microsystems Engineering

Enhancing AFM

Speeding up an AFM measurement by altering the Q-factor

R.H.A. Swuste

Report no : SOM 2017.026
Coach : dr. M.H. van Es
Professor : dr. ir J.F.L. Goosen
Specialisation : SOM
Type of report : MSc. Thesis
Date : 6 July 2017

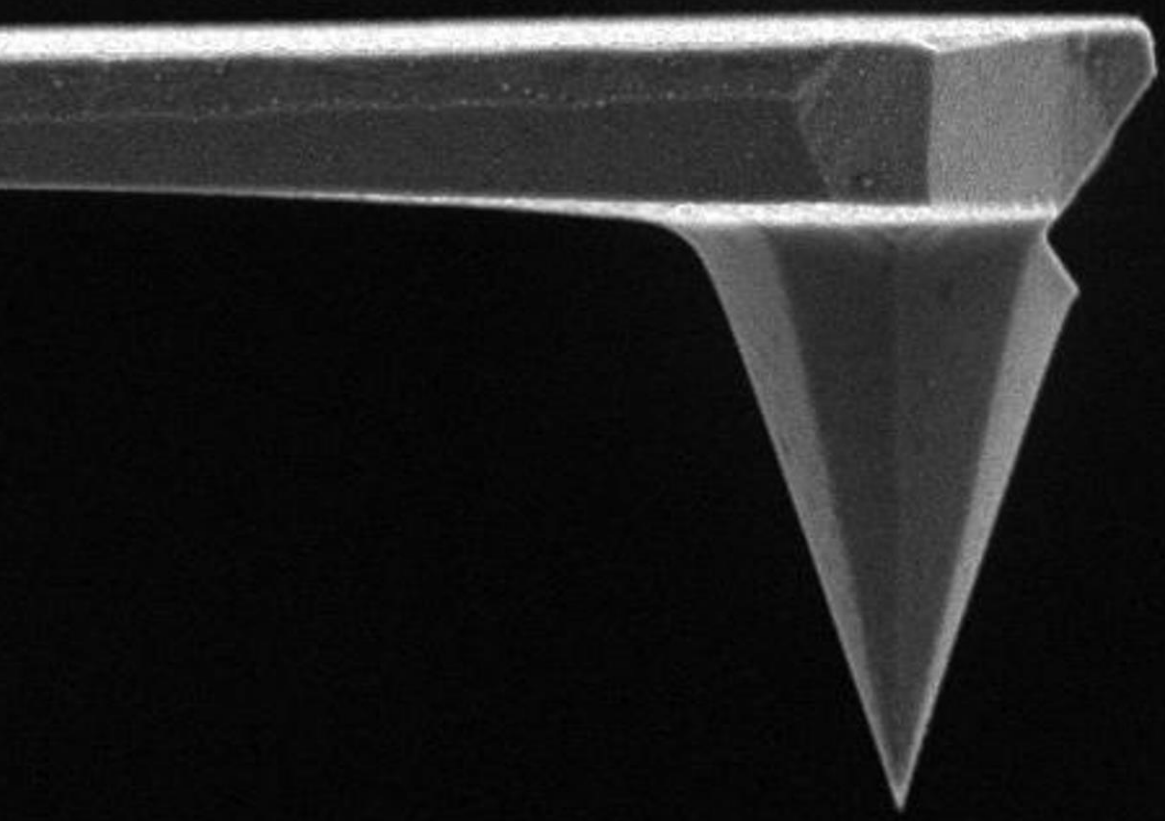

TU Delft

TNO innovation for life

Enhancing AFM

Speeding up an AFM measurement by altering the Q-factor

by

R. H. A. Swuste

in partial fulfilment of the requirements for the degree of

Master of Science
in Mechanical Engineering

at the Delft University of Technology,
to be defended publicly on Thursday July 6th, 2017 at 12:45.

Student number:	1323954	
Supervisors:	dr.ir. J.F.L. Goosen	TU Delft
	dr. M.H. Van Es	TNO
Thesis committee:	dr. M.K. Ghatkesar	TU Delft
	B. Sajadi, MSc	TU Delft

An electronic version of this thesis is available at http://repository.tudelft.nl/.

TU Delft Delft University of Technology

Abstract

The Atomic Force Microscope (AFM) is a small scale measuring device, with a lot of benefits over other existing measuring techniques. Unfortunately, measurement speed is not one of them. Many have tried and succeeded to improve the measurement speed, but there is still room for improvement. By passively lowering the Q-factor, a measurement can be sped up, while still be compatible with other speed improvement techniques.

To passively lower the Q-factor, we propose measuring in a medium more dense then air. First in a liquid, de-mineralized water, to prove the effect, and later in a gas, CO_2, to keep the samples clean.

Our models predict a speed increase of 0.3559 ms per measured point, or 6.941 min per image of 5 µm × 5 µm with 512 lines in liquid. The experiments show an increase of 0.4180 ms per point, or 8.155 min per measurement. In the much less dense gas a 0.031 01 ms per point or 0.6550 min per frame is calculated. The experiments show an increase of 0.027 29 ms per point with a total of 0.5300 min per frame.

Both in liquid and in gas an improvement is observed. When measuring in a liquid, the speed increase of 8.155 min per frame is noticeable when a small area on a single sample is measured. Measurements in gas, with an increase of 0.5300 min per frame only become interesting when multiple frames need to be measured, since a gas measurement does take longer to set up. Changing the used measurement gas to a more dense gas could make single frame measurements more interesting.

Contents

Acknowledgements

In my years as a student, which is quite sometime now, I have roamed the halls and corridors of 3ME (and for a short period of time also Industrial Design). In this time I have had the fortune of meeting a lot of people who have inspired me, helped me with projects (educational and personal) or were there to socialize with. There are not only my fellow students, but also the academic and support staff. A special thanks goes out to Taylor and Marleen, for all the adventures we had and for those yet to come. But also for TNO, Maarten especially for allowing my to do my research with them and guiding me trough the process.

Rolf Swuste
Delft, July 2017

Nomenclature

Symbols

Symbol	Units	Description
a_{free}	m	Free air amplitude
a_{SP}	m	Desired tapping amplitude
B	Hz	Measurement bandwidth
b_{c}	m	Width of the cantilever
C_{n}	–	nth positive root of $0 = 1 + \cos C_{\mathrm{n}} \cosh C_{\mathrm{n}}$, where $n = 1, 2, \ldots$.
f_{c}	Hz	Cantilevers first resonance frequency
$f_{\mathrm{fb,z}}$	Hz	Feedback frequency z-scanner
F_{n}	N	Smallest measurable force
$\overline{H}$	–	The ratio of the separation between the cantilever beam and the surface to the width of the cantilever beam
h_0	m	Sample height
h_{c}	m	Height of the cantilever
K	–	modified Bessel function of the second kind
$k_{\mathrm{b}}T$	N m	Thermal energy
k_{c}	$\mathrm{N\,m^{-1}}$	Spring constant of the cantilever
l_{c}	m	Length of the cantilever
M	$\mathrm{g\,mol^{-1}}$	Molar mass
m_{c}	kg	Mass of the cantilever
N_{s}	–	Number of scan lines
P	Pa	Pressure
Q	–	Quality factor
Q_{c}	–	Cantilever's quality factor
R	$\mathrm{m^3\,Pa\,K^{-1}\,mol^{-1}}$	Gas Constant:8.314 459 8 $\mathrm{m^3\,Pa\,K^{-1}\,mol^{-1}}$
Re	–	Reynolds number
T	K	Temperature
r_{t}	m	Tip radius
r_{s}	m	Sample radius
V_{image}	frames/s	Maximum image acquisition rate
vol%	–	Volume percent
W_{s}	m	Scan range
w	m	Apparent width of surface features
α	–	Feedback phase delay factor
Γ	–	Hydrodynamic function
η	Pa s	Viscosity
κ	–	Normalized mode number

μ_c	$\mathrm{kg\,m^{-1}}$	Mass per unit length of the cantilever
ρ	$\mathrm{kg\,m^{-3}}$	Density
$\Sigma\tau_n$	s	Sum of time delays
τ	s	Response Time
τ_c	s	Cantilever response time
τ_I	s	Integral time error
τ_m	s	Oscillation measuring time
τ_p	s	Parachuting time
τ_z	s	Z-scanner time delay
τ	–	$\tau = \log \mathrm{Re}$
φ_{closed}	rad	Closed loop phase delay
φ_z	rad	Phase delay at feedback frequency $f_{fb,z}$
Ω	–	Correction function Hydrodynamic function
ω	$\mathrm{rad\,s^{-1}}$	Resonance frequency of mode n in vacuum

Acronyms

Acronym	Explanation
AFM	Atomic Force Microscope
DUT	Delft University of Technology
FE-SEM	Field Emission Scanning Electron Microscope
FFT	fast Fourier transform
NDIR	Non Dispersive Infra-Red
OBD	Optical Beam Deflection
PSD	Position Sensitive Detector
SEM	Scanning Electron Microscope
STM	Scanning Tunneling Microscope
TEM	Transmission Electron Microscope
TNO	Netherlands Organisation for Applied Scientific Research

1

Introduction

The Atomic Force Microscope (AFM) has been around for thirty years, in this time the small scale measuring device went from being complicated and limited, to a cheap and easy microscope which can be used for a wide variety of measurements. Unlike an optical microscope, the AFM is not bound to the wavelength of light to define the resolution [2]. It can therefore observe smaller details than an optical microscope. The AFM is not the only existing small scale imaging method. It has to compete with much faster measurement methods like the Field Emission Scanning Electron Microscope (FE-SEM), the Scanning Electron Microscope (SEM) and the Transmission Electron Microscope (TEM) which are the most used alternatives, operating in the same lengthscale (Figure 1.1).

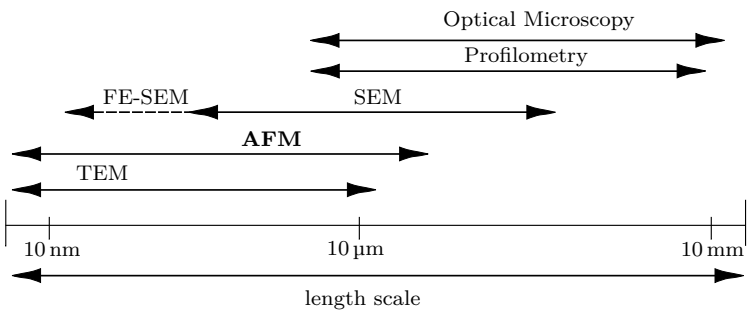

Figure 1.1: Comparison of length-scales of various microscopes [19].

The FE-SEM, SEM and TEM require conductive samples or samples with a conductive coating, and a special environment like a vacuum or gas environment. Measuring with an AFM however, requires little to no sample preparations and works in any environment (Table 1.1). This makes the AFM a very easy and cheap measuring device and is therefore often used in research. But since the AFM physically has to scan every line, it is a very slow device. The speed makes it impractical to scan surfaces greater then $100\,\mu m^2$, it is therefore not widely used in commercial applications [43]. This thesis, commissioned by Netherlands Organisation for Applied Scientific Research (TNO), is a small part of a larger research group, tasked with making the AFM more suitable for commercial applications, increasing not only the measurement speed, but also the throughput and abilities of the AFM.

Table 1.1: Comparison of AFM with SEM and TEM [19].

	AFM	SEM	TEM
Sample preparation	**Little or none**	From a little to a lot	From a little to a lot
Resolution	**0.1 nm**	5 nm	**0.1 nm**
Relative cost	**Low**	Medium	High
Sample environment	**Any**	Vacuum(SEM) or gas (environmental SEM)	Vacuum
Depth of field	Poor	**Good**	Poor
Sample type	**Conductive or insulating**	Conductive	Conductive
Time for image	2-10 minutes	**0.1-1 minute**	**0.1-1 minute**
Maximum field of view	100 µm	**1 mm**	100 nm
Maximum sample size	**Unlimited**	30 mm	2 mm
Measurements	**3 dimensional**	2 dimensional	2 dimensional

1.1. History of the AFM

The history of the AFM is quite long. The first working principle behind the AFM has been documented 88 years ago, although it was meant for a large scale imaging device. 58 years later, the first AFM was created. Since then various members of the scientific community have been working on improving the device, leading to the useful imaging device it is today.

Stylus Profiler In 1929 Prof. Schmalz described a mechanical machine which could be used to capture a surface topography with a magnification factor greater then a 1000× [39]. This device was called the stylus profiler (Figure 1.2). The profiler consisted of a large arm, the cantilever, with a mirror mounted on top under an angle and a probe, the stylus, on the bottom. The cantilever was mounted to a spring, allowing it to move in the vertical direction. When the probe was placed on a moving surface, it would follow the height of that surface. These small movements created a rotation in the mirror. A light source would shine a focussed beam of light on the mirror, which was then recorded on a photographic film. Because the light had to travel a relatively long distance from the mirror to the film, a small change in the mirror's angle had a large effect on the position of the beam reflected on the film. The film moved at the same speed as the sample to 'record' the sample surface.

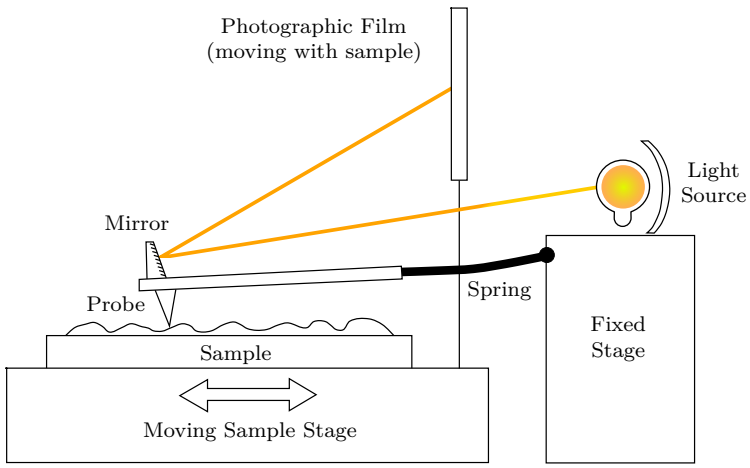

Figure 1.2: An early model of the stylus profiler as designed by Prof. Schmalz in 1929. A lightsource would be focussed and shine on a mirror attached to a probe. The beam would be reflected on photosensitive film. Due to the setup, small variations in height of the probe would be enlarged on the film [19].

Early AFM In 1981 Binnig *et al.* [12, 11] introduced the Scanning Tunneling Microscope (STM), an apparatus which used a potential difference to measure the distance between a surface and the STM tip . In order to function, the STM needed a conductive sample surface. To overcome this disadvantage, a conductive cantilever was added, handmade from gold with a diamond tip glued to it (Figure 1.3).

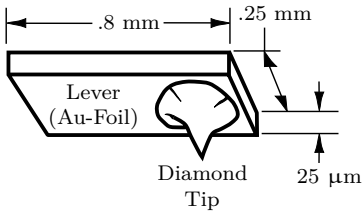

Figure 1.3: The first cantilever created by G. Binnig *et al.*[10]. It was handmade from gold with a small diamond tip glued to it. The changes in height would be measured using the STM.

This became the first AFM, in 1986 [10]. The AFM had the same working principle as the stylus profiler, but used the very precise STM to measure the deflection of the cantilever instead of the profilers' optical system. It was capable of imaging non-conductive (and conductive) surfaces on an atomic scale. In 1987 Binnig *et al.* [9] found a way to create cantilevers using micro fabrication techniques, which was less labour intensive. These cantilevers where designed to be used with STM as the measuring method. In 1988, the Optical Beam Deflection (OBD) system first replaced the STM to measure the deflection [31]. The OBD system used a laser in combination with a Position Sensitive Detector (PSD) to measure the deflection of the cantilever (Figure 1.4), much like the old stylus profiler. This made the AFM a lot simpler and cheaper while still remaining sensitive to minor deflections.

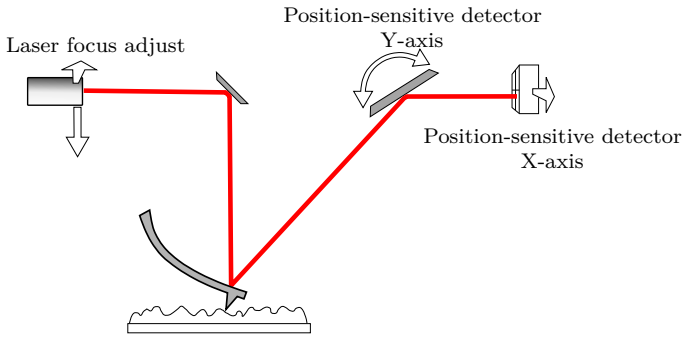

Figure 1.4: An AFM optical beam deflection system. This system has a lot of similarities with the earlier stylus profiler, but now with a small laser as a light source and a photosensitive detector as a sink [19].

Tapping Mode One of the drawbacks of the early AFM was the wear on the sample surface and the probe, due to the continuous contact and the corresponding lateral forces. Zong *et al.* [47] introduced a different operating mode in 1992, defining the old mode as 'contact mode' (Figure 1.5a) and his new mode as 'tapping mode'(Figure 1.5b). In tapping mode, the cantilever is excited just below its resonance frequency (f_c), the frequency where the cantilever has the largest free amplitude (a_{free}), above the surface. A control system moves the cantilever towards the surface. When the vibrating probe reaches the surface, the small impacts ('tapping') will reduce the free amplitude. When the cantilever had reached the amplitude set point (a_{SP}), a predetermined part of the free amplitude, the control system will maintain the height. The cantilever then moves along the surface, still tapping it. The controller has to keep the amplitude the same as the amplitude set point. The deflection is then used to plot the surface topography. Although the probe and sample still come into contact, the probe does not apply shear forces to the sample any more, which greatly reduces the damages on both tip and sample.

Measurements in liquid In 1987 the first measurements in liquid where demonstrated by Marti *et al.* [30, 5]. They imaged graphite and sodium chloride surfaces, not in water, but in paraffin oil, to protect the specimens from moisture. Measuring deflection with the STM in liquid was complicated, since the STM could not come into contact with conducting liquids because it would measure the liquid instead of the cantilever. The arrival of the OBD has made liquid measurements more convenient.

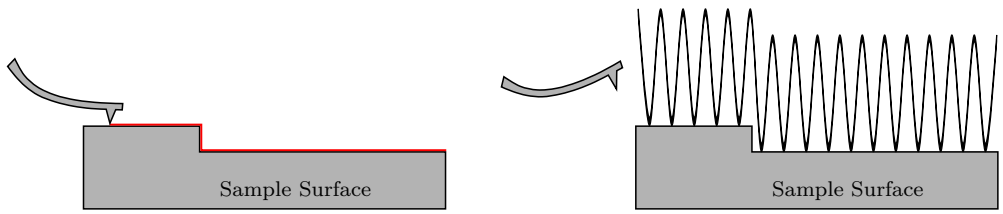

(a) In contact mode, the cantilever follows the surface topography. The constant contact can create wear on the tip but also on the sample, mostly due to lateral forces.

(b) In tapping mode the cantilever taps the surface at a certain interval. This reduces wear on tip and sample, since the lateral forces are almost completely eliminated.

Figure 1.5: Two different operating modes of the AFM. These modes are two of the three main modes used for creating topographies [19].

The ability to measuring in liquid is important because many biological samples cannot survive a dry environment. Since this first measurement, cells have been studied extensively with the AFM. Häberle *et al.* [23] investigated the effect of viruses in living cells in 1992, Henderson *et al.* [24] studied glial cells, but due to the shear and normal forces applied by the cantilever, the cells would always deform. *"contact mode* AFM *shows underlying submembrane structures, such as the cytoskeletal fibers, due to local deformation of the cell envelope.[35]"* But the cells could also be easily destroyed when too much force was applied. In 1994 Lantz *et al.* [28] and Putman *et al.* [36] measured cells in a liquid environment using tapping mode. Because the AFM would 'tap' the cell, the viscoelastic properties of the cell membrane caused it to act as a 'hard' material, until the cell surface slowly relaxed under the applied pressure to a new equilibrium. Thanks to the high tapping frequency, the cell remains 'hard' throughout the measurement. This created the ability to image the surface of the cell, opening a door to many new studies.

Measuring in liquid also has disadvantages. The smallest detectable force (F_n) increases considerably. When the F_n is high, more force will be exerted on the sample, creating a high probability to cause damages, especially on biological or other soft samples. This force is defined as:

$$F_\mathrm{n} = \sqrt{\frac{2k_\mathrm{c}k_\mathrm{b}TB}{\pi Q_\mathrm{c}f_\mathrm{c}}}. \tag{1.1}$$

Where k_c is the cantilevers spring constant, $k_\mathrm{b}T$ is the thermal energy, B is the measurement bandwidth, Q_c the Q-factor and f_c the resonance frequency of the cantilever. In a liquid such as water, the added mass of the water which adheres to the cantilever causes the resonance frequency to drop to one third of the original frequency and the Q_c drops by a factor 50, this is due to the added damping when submerged. Ziegler *et al.* [49] have found a way to minimize F_n by encasing the cantilever, limiting the contact with water and thus the damping. (Figure 1.6).

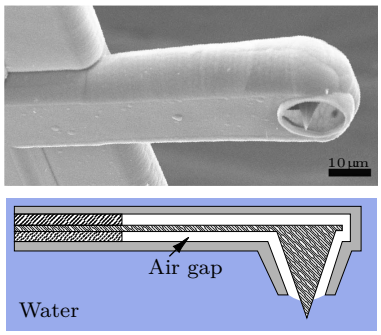

Figure 1.6: Encased cantilever as designed by Ziegler *et al.* [49, 48] to minimize the force needed to perform a measurement on a sensitive sample. The air gap makes it possible to measure in liquid while retaining most properties of an air measurement.

1.2. Current AFM

The AFM today is very easy to handle. There is no need for a STM to measure the movement of the cantilever. The main method for measuring is through an OBD system, but there are also cantilevers with integrated sensors to measure the deflection. Cantilevers now have standardised bodies and are created 'en masse' on wafers by various companies (Figure 1.7). They can be produced in all kinds of shapes and dimensions with varying properties and extra options. These cantilevers allow for more than only the surface topography measurements, such as force spectroscopy, magnetic, electrochemical and thermal measurements.

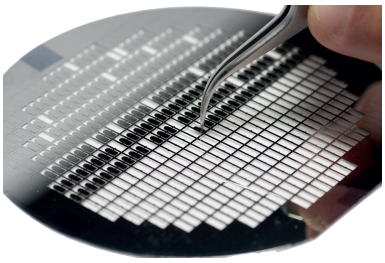

Figure 1.7: A batch of Olympus silicon probes still on the wafer in/on which they where created [37].

Speeding up an AFM Measurement Ever since the creation of the AFM, there have been different approaches to speed up an AFM measurement. Below is a small overview of the techniques used, together with the achieved speed and resolution.

1991 Barrett *et al.* [8] managed to reach a velocity of $1\,\mathrm{cm\,s^{-1}}$ with an unknown resolution. This speed was achieved using contact mode and constant-height mode, where the cantilever is set to a constant height and does not follow the contours of the sample. Constant-height mode requires no feedback. The measurements worked great on hard samples such as silicon, but damaged the softer PMMA sample (acrylic glass).

1992 Butt *et al.* [17] have calculated the scan speed limit in constant-force contact mode. In contrast to constant-hight mode, constant-force mode uses feedback to follow the contours of the sample. The theoretical limit found for a 0.1 nm resolution was $0.1\,\mathrm{\mu m\,s^{-1}}$. In water, a higher speed of $3\,\mathrm{\mu m\,s^{-1}}$ was possible due to the added damping.

1996 Manalis *et al.* [29] have reached speeds of $1\,\mathrm{cm\,s^{-1}}$ and unknown resolution using a cantilever with a build in piëzo actuator. The scan speed dropped to $0.5\,\mathrm{mm\,s^{-1}}$ for high, but still unknown resolution. In both cases contact mode and constant-force mode where used. In constant force mode feedback is used to create a constant force on the sample, changing the height as it goes.

1998 Paloczi *et al.* [33] used small cantilevers, with a high resonance frequency of 100 kHz (300 kHz in air) and low spring stiffness of $0.66\,\mathrm{N\,m^{-1}}$, in water. They reached speeds of $52\,\mathrm{\mu m\,s^{-1}}$ in tapping mode with a 2 nm resolution.

1998 Ookubo *et al.* [32] combined the tapping mode drive frequency with the feedback signal to obtain a $458\,\mathrm{\mu m\,s^{-1}}$ tip velocity with a 8.95 nm resolution.

2000 Sulchek *et al.* [41] measured with a speed of $3\,\mathrm{mm\,s^{-1}}$ an a 50 nm resolution. They used a cantilever with integrated actuator for tapping mode in liquid.

2001 Ando *et al.* [4] utilized the high frequencie (around 650 kHz) and small spring constant (around $150\,\mathrm{pN\,m^{-1}}$) from his cantilever and optimized the electronics to reach a tip velocity of $600\,\mathrm{\mu m\,s^{-1}}$ this at a 2.4 nm resolution.

2005 Humphris *et al.* [26] used a micro resonator as scan stage, together with a mechanical feedback system. With this setup a scanning speed of $22.4\,\mathrm{cm\,s^{-1}}$ an a vertical resolution of 1 nm and lateral resolution of 30 nm can be achieved in contact mode.

2006 Picco *et al.* [34] used a tuning fork and flexture-stage scanning system to image in contact mode with no feedback with 1300 frames/s and a tip velocity reaching $20\,\mathrm{cm\,s^{-1}}$. The resolution was not given but is believed to lay around 5 nm. All this was reached without doing significant damage to the sample.

Since 2006 no fundamental changes to speed up a measurement have been achieved.

The scan speeds reached by the different researchers are hard to compare to each other. Different definitions are used to indicate their improvement. Some use tip velocity, others scan frequency or frames per second. The velocities mentioned above are recalculated to tip velocity, making the comparison easier. In order to speed up an measurement, there are multiple factors that have to be looked at. Equation (1.2) composed by Ando *et al.* [5, 3] shows the components which are needed to create the maximum imaging rate, the number of images that can be taken per second.

$$V_{\mathrm{image}} = \frac{\alpha w}{16 W_{\mathrm{s}} N_{\mathrm{s}} \Sigma\tau_{\mathrm{n}}} \tag{1.2}$$

The maximum image acquisition rate V_{image} is a relation between the feedback phase delay factor α the factor by which the feedback controller compensates for the phase delay in the feedback loop. The apparent width of the surface features w, approximated by the convolution of the tip radius r_{t} and the sample radius r_{s} ($w \approx \sqrt{r_{\mathrm{t}} r_{\mathrm{s}}}$). The scan range, W_{s} for a $W_{\mathrm{s}} \times W_{\mathrm{s}}$ image. The number of scan lines N_{s} and the sum of time delays $\Sigma\tau_{\mathrm{n}}$ (Equation (1.3)). The $\Sigma\tau_{\mathrm{n}}$ is the sum of delays in Table 1.2.

$$\Sigma\tau_{\mathrm{n}} = \tau_{\mathrm{c}} + \tau_{\mathrm{p}} + \tau_{\mathrm{z}} + \tau_{\mathrm{m}} + \tau_{\mathrm{I}} \tag{1.3}$$

Table 1.2: Time delays which contribute to $\Sigma\tau_{\mathrm{n}}$ [5, 3].

	Definition	Formula	
τ_{c}	Cantilever Response Time. The time the cantilever needs to reach a steady state value after reacting to a change in surface topography (Figure 1.8). It is a combination of the cantilevers Q-factor Q_{c} and resonance frequency f_{c}.	$\tau_{\mathrm{c}} = \frac{Q_{\mathrm{c}}}{\pi f_{\mathrm{c}}}$	(1.4)
τ_{m}	Oscillation Measuring Time. Time required to measure oscillation, it depends on the measuring method, and can be as little as half a vibration period $\tau_{\mathrm{m}} = \frac{1}{2f_{\mathrm{c}}}$. When measuring with a lock-in amplifier the τ_{m} will be around three times the vibration period.	$\tau_{\mathrm{m}} \approx \frac{3}{f_{\mathrm{c}}}$	(1.5)
τ_{z}	Z-Scanner Response Time. The time the z-scanner needs to react to a change in surface topography. It depends on the phase delay (φ_{z}) and the Z-scanners feedback loop resonance frequency ($f_{\mathrm{fb,z}}$).	$\tau_{\mathrm{z}} = \frac{\varphi_{\mathrm{z}}}{2\pi f_{\mathrm{fb,z}}}$	(1.6)
τ_{I}	Integral Time of the Error at the PID Controller. The time the PID controller needs to process the error signal. It is experimentally approximated with h_0 as sample height, a_{free} as the free oscillation amplitude and $\varphi_{\mathrm{closed}}$ as the closed loop phase delay.	$\tau_{\mathrm{I}} = 4h_0 \frac{\sin(\frac{\varphi_{\mathrm{closed}}}{2})}{a_{\mathrm{free}} f_{\mathrm{c}}}$	(1.7)
τ_{p}	Parachuting Time. The time it takes when, after encountering a steep incline, the tip completely detaches from the surface and lands on it again as described by Ando *et al.* [5]. With $\beta = \arccos\left((a_{\mathrm{free}} - a_{\mathrm{SP}})/(5h_0 \sin(\varphi_{\mathrm{closed}}/2))\right)$	$\tau_{\mathrm{p}} = \frac{\frac{\tan\beta}{\beta-1}}{f_{\mathrm{c}}}$	(1.8)

1.3. Research goal and problem statement

Where others focus on perfecting the feedback loop, or the mechanical design of the AFM and/or cantilever [3, 8, 13, 14, 27, 29], this research focusses on reducing the cantilever response time. The goal is to do this by passively reduce the Q-factor. Passively, to avoid having to use custom made cantilevers or complicate the AFM design more than necessary.

Cantilever response time The cantilever response time, τ_c, is the time the cantilever needs to react to a change in the surface. When the τ_c is low, the cantilever reacts faster on changes (Figure 1.8b). It is a combination of Q_c and f_c as can be seen in Equation (1.4). The Q-factor is proportional to the

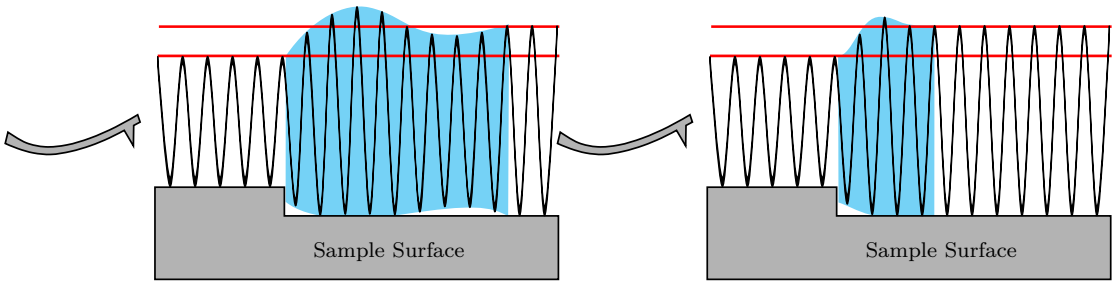

(a) A large response time: It takes longer for the cantilever to reach a new steady state value after encountering a change in topography.

(b) A Short response time: The cantilever reacts faster to changes in surface topography and thus reaches the new steady state value sooner.

Figure 1.8: The effect of the response time (τ_c) is isolated from other effects and visualized. The AFM is operated in constant-height mode.

amount of cycles needed to dissipate excess energy and the f_c indicates the frequency of those cycles. The response time will decrease if the Q_c decreases or if the f_c increases. A lot of effort has been put in increasing the f_c[18]:

$$f_c = \frac{1}{2\pi}\sqrt{\frac{k_c}{0.24 m_c}}. \tag{1.9}$$

This was achieved by either lowering the cantilevers mass (m_c), and/or increasing the cantilevers spring stiffness (k_c) [3]. The cantilevers have been perfected to be as small and as light as practically possible while still being large enough to properly deflect the OBD's laser [43]. There is, however, still room to reduce the Q-factor.

Q-factor To reduce the Q-factor, it is important to understand what the Q-factor is. The Q factor came to life in 1914 as the K factor. It was used to show inductive purity. In 1920 it became the Q-factor mostly because the Q wasn't used yet. It was a little after 1924 that the term Quality factor first appeared [40]. Currently it describes how under-damped an oscillator is and the relation between the bandwidth and the centre frequency. A higher Q-factor means a more narrow bandwidth and a

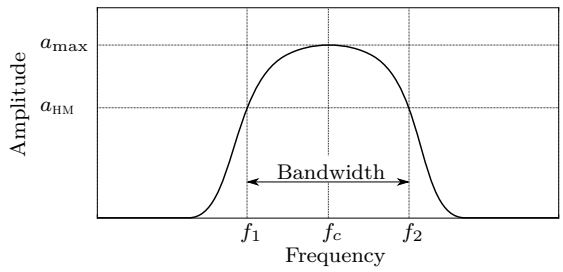

Figure 1.9: The bandwidth is the frequency range from f_1 to f_2, Δf. At these points the amplitude has half the power of the maximum amplitude, e.g. $\frac{1}{\sqrt{2}}\, a_{max}$.

sharper peak (Figure 1.9). This can also be seen in Equation (1.10) where Δf is the Full Width Half Maximum, the frequency range in which the power is equal or higher than half the maximum power at f_c.

$$Q_c = \frac{f_c}{\Delta f} \tag{1.10}$$

A higher Q-factor also means the system is a more efficient oscillator because there is less energy dissipated per cycle. Vice versa a low Q-factor dissipates more energy per cycle:

$$Q = 2\pi \cdot \frac{\text{total energy}}{\text{dissipated energy}}. \tag{1.11}$$

There are improvements to be made by passively lowering the Q_c. Balantekin *et al.* [7], Fairbain *et al.* [20] and Gunev *et al.* [22] have done this actively, obtaining promising results, but passively there is not much progress. Passively lowering Q_c would be preferred, to keep the AFM and the cantilevers as simple and cheap as possible. A lower Q-factor in liquid was also observed by others, but deemed undesirable since they where mostly working on biological samples [49]. Lowering the Q_c has a drawback, as seen in Equation (1.1), the smallest detectable force will grow larger. This means that more force has to be exerted on the sample to retrieve usable measurement data. This could be a problem for biological samples. The harder samples like silicon, used by the semiconductor branch, are less prone to damage [8]. For this branch, changing the measurement medium is a viable option to lower the measurement time.

Problem statement Measuring a small scale surface with an AFM is relatively easy and cheap, unfortunately it is a very slow process. Since its creation it has become faster, but is still not as fast as other alternatives. For the AFM to become a useful instrument in the semi-conductor industry, the measurement speed has to increase further. This will be achieved by lowering the Q-factor. Preferably without further complicating the device and the measurement itself. If this can be done by changing the measurement medium, it can possibly coexist with other techniques to speed up a measurement.

Research Goal Investigate if it is possible to lower the Q-factor passively by changing the measurement medium to a liquid or a gas. If the speed does improve, find out if it is significant enough to further explore the benefits in a commercial application.

Research Questions When the problem statement and the research goal are combined, two research questions can be formulated. These questions will be answered at the end of the thesis.

- How much faster can an AFM measurement become by lowering the cantilever response time via passively lowering the Q-factor, by measuring in a liquid environment?
- By how much does the measurement speed increase in a gas filled environment with a higher density than air, compared to air?

Thesis outline The thesis starts with an introduction in the current chapter, Chapter 1, here, the reader will be introduced with the alternatives, the history, the relevant theory and the current state of the AFM, as well as the the goal of this research, the questions which are going to be answered. Chapter 2 starts with an explanation of the models and data analysis scripts that are used. Next it focusses on the materials and equipment used for the experiments and describes the steps done to conduct the experiments. Chapter 3 contains a selection of the results of the models and the experiments. The results will be discussed in Chapter 4. The thesis ends at Chapter 5 with the conclusions and the recommendations for further research.

Additional information is supplied in the appendices. Appendix A explains different theories and principles used in the thesis. Appendix B shows the code written for the models and the data analysis. Appendix C holds the specifications of the used equipment. Appendix D contains the designs of a special cantilever holder for measurements in liquid, designed for the Anfatec AFM. The full set of results can be found in Appendix E.

2

Methods & Materials

To obtain a lower Q-factor and thus to speed up an AFM measurement, external damping will be added by measuring in a more dense fluid. First in a liquid, then in a gas. The behaviour of the cantilever will be estimated with the help of a simplified model. Using these estimations as a guideline, a measurement plan is developed to measure the response of the cantilever in the different fluids, in a reliable and repeatable manner.

2.1. Description of the models

The simplified model estimates the behaviour of the cantilever in air, liquid and various gas concentrations and mixes. The model can be divided into a part which estimates the behaviour when the cantilever is vibrating freely, and into a part which estimates the behaviour of the cantilever near the surface. The model is written in Python 2.7 and can be found in Appendix B.

Cantilever behaviour This part of the model uses the dimensions of the cantilever, together with the properties of silicon and the used mediums to estimate the first and second resonance frequency, the Q-factor and the relation to the Q-factor in air. This is done with the help of the hydrodynamic function [38]. This function is used to compensate for the difference in density and viscosity of other fluids than air:

$$\Gamma_{\mathrm{circ}}(\omega_{\mathrm{R,n}}) = 1 + \frac{4i\ \mathrm{K}_1(-i\sqrt{i\ \mathrm{Re}(\omega_{\mathrm{R,n}})})}{\sqrt{i\ \mathrm{Re}(\omega_{\mathrm{R,n}})}\ \mathrm{K}_0(-i\sqrt{i\ \mathrm{Re}(\omega_{\mathrm{R,n}})})}. \tag{2.1}$$

The equation uses the modified Bessel function of the second kind (K_0, K_1). The hydrodynamic function was originally created for circular bodies and needs to be multiplied with a correction factor ($\Omega(\omega_{\mathrm{R,n}})$) for rectangular beams. More on the modified Bessel function, a complete explanation of the first and second resonance frequency as well as the hydrodynamic function can be found in Appendix A. It also the uses the Reynolds number ($\mathrm{Re}(\omega_{\mathrm{R,n}})$) for medium R and resonance mode n . It is defined by:

$$\mathrm{Re}(\omega_{\mathrm{R,n}}) = \frac{\rho_{\mathrm{R}}\ \omega_{\mathrm{R,n}}\ b_{\mathrm{c}}^2}{4\ \eta_{\mathrm{R}}}, \tag{2.2}$$

and will further be displayed as Re. The ρ_{R} is the density of the medium, $\omega_{\mathrm{R,n}}$ the resonance frequency in $\mathrm{rad\,s^{-1}}$, η_{R} the viscosity of the medium and b_{c} the width of the cantilever. The circular hydrodynamic function is then multiplied by the correction factor $\Omega(\omega_{\mathrm{R,n}})$ (Equation (A.10)) for rectangular bodies such as cantilevers:

$$\Gamma(\omega_{\mathrm{R,n}}) = \Omega(\omega_{\mathrm{R,n}})\ \Gamma_{\mathrm{circ}}(\omega_{\mathrm{R,n}}). \tag{2.3}$$

With the help of this new rectangular hydrodynamic function the Q-factor can be obtained using the mass per meter (μ_c):

$$Q_{\mathrm{R,n}} = \frac{\frac{4\,\mu_c}{\pi\,\rho_R\,b_c^2} + \Gamma_r(\omega_{\mathrm{R,n}})}{\Gamma_i(\omega_{\mathrm{R,n}})}. \tag{2.4}$$

The Q-factor, together with the resonance frequency in $\mathrm{rad\,s^{-1}}$ are used to calculate the cantilever rise time:

$$\tau_c = \frac{2Q_{\mathrm{R,n}}}{\omega_{\mathrm{R,n}}}. \tag{2.5}$$

This model is valid for air, gas and liquid. For different gas mixtures the corresponding densities and viscosities have to be inserted in Equation (2.2). The mixture density and viscosity are calculated with

$$\rho_{\mathrm{mix}} = \frac{(\mathrm{vol\%}_1 M_1 + \mathrm{vol\%}_2 M_2)P}{TR} \tag{2.6}$$

and

$$\eta_{\mathrm{mix}} = \frac{\mathrm{vol\%}_1\eta_1\sqrt{M_1} + \mathrm{vol\%}_2\eta_2\sqrt{M_2}}{\mathrm{vol\%}_1\sqrt{M_1} + \mathrm{vol\%}_2\sqrt{M_2}} \tag{2.7}$$

respectively [15]. Here vol% is the volume percentage, M is the molar mass [mol], T represents the temperature [K], P absolute pressure [Pa] and R is the ideal gas constant [$\mathrm{m^3\,Pa\,K^{-1}\,mol^{-1}}$].

Cantilever behaviour near the surface This part of the model repeats the calculation made by the first part, but it substitutes the hydrodynamic function for a cantilever beam with a more complicated hydrodynamic function which takes near surface effects into account:

$$\Gamma(\omega_{\mathrm{R,n}}) = \Gamma_r(\omega_{\mathrm{R,n}}) + i\Gamma_i(\omega_{\mathrm{R,n}}) \tag{2.8}$$

with

$$\begin{aligned}\Gamma_r(\omega_{\mathrm{R,n}}) = a_0 &+ a_1\tau + a_2\tau^2 + a_3\tau^3 + a_4\tau^4 + a_5\tau^5 \\ &+ a_6\tau^6 + a_7\tau^7 + a_8\tau^8 + a_9\tau^9 + a_{10}\tau^{10} \\ &+ a_{11}\tau^{11} + a_{12}\tau^{12} + a_{13}\tau^{13} + a_{14}\tau^{14} + a_{15}\tau^{15} \\ &+ a_{16}\tau^{16} + a_{17}\tau^{17} + a_{18}\tau^{18} + a_{19}\tau^{19} + a_{20}\tau^{20},\end{aligned} \tag{2.8a}$$

$$\begin{aligned}\Gamma_i(\omega_{\mathrm{R,n}}) = b_0 &+ b_1\tau + b_2\tau^2 + b_3\tau^3 + b_4\tau^4 + b_5\tau^5 \\ &+ b_6\tau^6 + b_7\tau^7 + b_8\tau^8 + b_9\tau^9 + b_{10}\tau^{10} \\ &+ b_{11}\tau^{11} + b_{12}\tau^{12} + b_{13}\tau^{13} + b_{14}\tau^{14} + b_{15}\tau^{15} \\ &+ b_{16}\tau^{16} + b_{17}\tau^{17} + b_{18}\tau^{18} + b_{19}\tau^{19} + b_{20}\tau^{20}\end{aligned} \tag{2.8b}$$

and

$$\tau = \log_{10}\mathrm{Re}. \tag{2.8c}$$

The a_n and b_n are experimentally found coefficients by Green *et al.* [21] and can be found in Tables A.1 and A.2 for the different values of $\overline{H}$:

$$\overline{H} = [0.1 \quad 0.2 \quad 0.3 \quad 0.5 \quad 1]\,,$$

where $\overline{H}$ is the ratio of the separation between the cantilever beam and the surface (h_c) to the width of the cantilever beam (b_c),

$$\overline{H} = \frac{h_0}{b_c}. \tag{2.9}$$

The found values for the hydrodynamic function are inserted into Equations (2.4) and (2.5) to calculate the Q-factor and cantilever rise time.

2.2. The equipment

To see the effect of the different mediums on the Q-factor, two thermal spectra per medium will be taken, one spectrum when the cantilever is hovering above the surface and another when the cantilever is near the surface. These spectra will later be used to determine the Q-factor. First the Bruker FastScan AFM will be used for the thermal spectra in air and liquid. Next the Anfatec AFM will be used for the thermal spectra in air and in gas. The equipment used throughout this research has been supplied by TNO and the Delft University of Technology (DUT). The details and specification of the equipment can be found in Appendix C.

Anfatec AFM All the experiments were originally planned to be performed on a small tabletop AFM, the Anfatec AFM (Figure 2.1a). It has the ability to measure at an ambient set-up and is designed with the main connections integrated into the granite base, so that the whole system can be placed under a bell jar (Figure 2.1b). The used bell jar has a volume of 9.6L and is designed to suit vacuum applications. It is useful for acoustic isolation or measurements in a higher or lower pressure than normal. This AFM does not allow for liquid measurements, therefore a special sample holder is designed and produced using rapid prototyping techniques. A small summary of this design can be found in Appendix D. Half a year into this thesis research, TNO purchased a Bruker FastScan AFM, which has the native ability to measure in liquid, making the custom sample holder obsolete.

(a) Tabletop AFM produced by Anfatec [6].

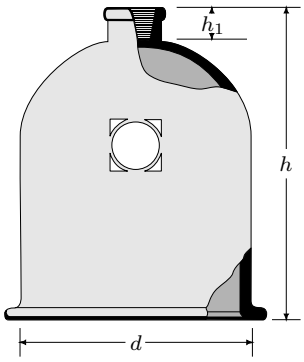

(b) Schott DURAN bell jar with neck bore, for vacuum use, 300 x 215 mm

Figure 2.1: The Anfatec AFM with bell jar. It is very useful for research purposes, since it allows for a high degree of customization. The supplied bell jar is used mostly for acoustic isolation.

Bruker Dimension FastScan AFM The Bruker Dimension FastScan AFM is a semi-automatic commercial AFM (Figure 2.2)[16]. It is located in a vibration and acoustic isolated box which is not suited to create a controlled gas environment. The Bruker AFM is simpler to operate than the Anfatec AFM, but less flexible.

Figure 2.2: The Bruker Dimension FastScan is a semi-automatic commercial AFM [16].

The cantilever The cantilever chip used throughout this study is the HQ:NSC35 chip, fabricated by MikroMash (Figure 2.3). It has three rectangular cantilevers, all with a different lengths, resonance frequency and stiffness. The dimensions and resonance frequencies can be found in Table 2.1. The

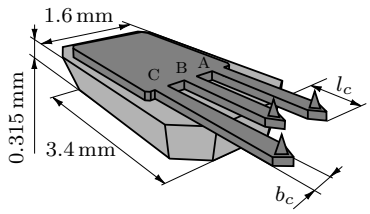

Figure 2.3: The HQ:NSC35/Cr-Au BS cantilever chip. The chip consists of 3 cantilevers each with their own length. This gives them different resonance frequencies. From the front to the back, there is cantilever C, B, A.

cantilevers are available with different coatings. The versions used is the HQ:NSC35/Cr-Au BS and is fitted with a thin chromium-gold coating to enhance reflectivity and is designed to be operated in tapping mode. It is fitted with a tip which is between 12 µm and 18 µm in height.

Table 2.1: HQ:NSC35 Resonance frequencies and dimensions of the cantilever.

NSC35 Cantilevers	Resonance Frequency (kHz) min.	**typ.**	max.	Length $l_c \pm 5$ (µm)	Width $b_c \pm 3$ (µm)	Thick. $h_c \pm 0.5$ (µm)
A	130	**205**	290	110	35	2.0
B	185	**300**	430	90	35	2.0
C	95	**150**	205	130	35	2.0

Measurement mediums The measurements will take place in three different fluids: ambient air, a liquid and a gas. For the liquid, de-mineralized water or demi-water is used, because of the wide availability and the low residue when evaporated. For the gas, CO_2 is chosen since it is easily obtainable and non-toxic in the used concentrations. The gas is supplied in 16 gr. cylinders which hold enough gas to fill 8.66L at ambient pressure. It has a 99.95% purity and is entered into the system using a small hand held bicycle pump (Figure 2.4). The properties of the mediums can be found in Table 2.2.

Table 2.2: Densities and viscosity in [kg m^{-3}] and [Pa s^{-1}] per medium at T = 291 K and p = 1.1013 bar [42].

Medium	Density	Viscosity
Air	1.214	1.813e-5
Demi-water	998.6	1.053e-3
CO_2	1.852	1.459e-5

(a) A small and portable bicycle pump. **(b)** 16gr. gas cannister, filled with CO_2

Figure 2.4: The CO_2 supply system. This low cost pump is a cheap and effective way to introduce CO_2 in the measurement set-up. The small size makes it safer to administer the gas, since it only contains 8.66 L, too little gas to fill an entire room. Two of the small cannisters are used to fill a bell jar.

CO_2 sensor To measure the CO_2 concentration inside the bell jar, a CozIR wide range CO_2 sensor is used. It is a non dispersive infra-red sensor. This sensor has a range from 0 to 1 000 000 ppm with

an error of ±5% of the reading and is fitted with a cap which allows for in-line measurements. The CO_2 concentration is fed to a pc using a serial connection. Details on the working principle of the sensor can be found in Appendix A.

Figure 2.5: The CozIR wide range CO_2 sensor has a range from 0 to 1 000 000 ppm and is used to determine the CO_2 concentration inside the bell jar. The used sensor has an adapter fitted on top to allow for in-line measurements.

Data logging The data gathered from the experiments is processed and logged with the help of a Zurich Instruments lock-in amplifier. The device uses a fast Fourier transform (FFT) algorithm to convert the signal of the deflection of the cantilever from the time domain into the frequency domain [50].

Figure 2.6: The UHFLI lock-in amplifier from Zurich Instruments is used to convert the obtained deflection signal from the AFM into a frequency spectrum using a FFT algorithm.

2.3. Measurement plan

To measure the effects of the different fluids on the Q-factor, two AFM's are used. On the Bruker AFM, the measurement in liquid will be conducted. The Anfatec AFM will be used for the measurement in gas. Before each measurement, a measurement under normal conditions (e.g. air) is made. A measurement consists of at least two thermal spectra. The first spectrum is made when the cantilever is vibrating freely, away from the sample surface. Next the cantilever is calibrated and moved to a set distance from the surface. Here, the 'near surface' thermal spectrum is measured. For the measurement in gas, both spectra are taken at a range of gas concentrations. The thermal spectra are analysed and the results are compared to those of the measurements in air. This leads to an improvement ratio of the Q-factor.

'Free vibrating' thermal spectrum This is the first thermal spectrum made of every cantilever. First the OBD is aligned properly, and at a few millimetres from the surface. Without exciting the cantilever, the vibration, due to thermal motion of the cantilevers surroundings, is recorded. The lock-in amplifier transforms this signal to a frequency spectrum using the FFT algorithm. This results in an undriven thermal spectrum such as is shown in Figure 2.7.

Calibration Next, the cantilever is lowered towards the surface until a deflection is observed. At this point the cantilever is retracted a few micrometers and a force spectroscopy curve is generated. Here, the cantilever is slowly driven into the surface while the deflection is measured. Since the movement of the AFM is known, a deflection versus displacement curve can be plotted, an example

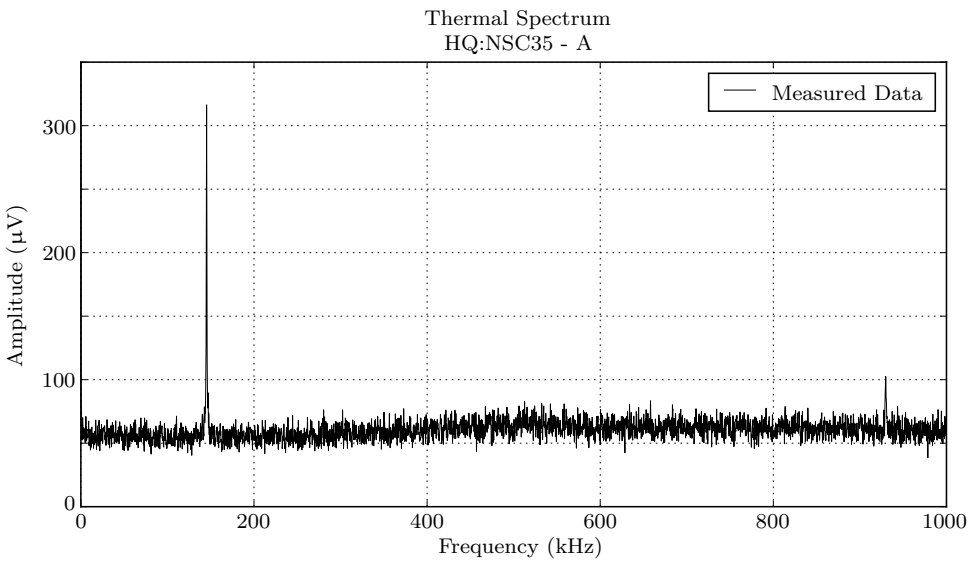

Figure 2.7: Example of an undriven thermal spectrum. The first and second resonance frequency can be found around 175kHz and 930kHz respectively.

of this curve is shown in Figure 2.8. In this curve, the slope is measured from the point after the cantilever touches the surface (after point (2) in Figure 2.8). From this slope the displacement per deflection can be deduced in [nm V^{-1}].

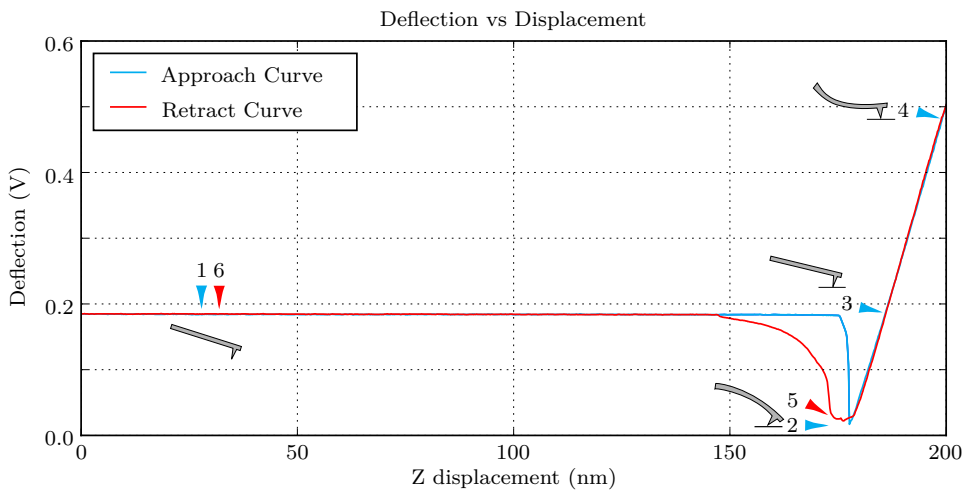

Figure 2.8: Deflection vs. displacement graph. (1) The cantilever is far away from the surface and starts to approach it. (2) The cantilever is so close to the surface that the Van Der Waals force makes it snap to the surface. (3) The cantilever is now at the height that it would touch the surface if the attraction forces from the surface would't already have attracted it. (4) The cantilever is pushing in the surface. At this point the cantilever has approached the set distance and starts to retract again. (5) Due to capillary forces, the cantilever sticks to the surface longer than when it approached it. (6) The cantilever returns to the starting position.

'Near surface' thermal spectrum To see what the influences of the tip-sample interactions are, a second thermal spectrum is made near the surface. The cantilever is too close to the surface to vibrate feely. Therefore the cantilever is excited on the second resonance frequency. Because the cantilever is now touching the surface, a clear thermal spectrum can only be made if the cantilever is excited (Figure 2.9). In order to drive the cantilever without disturbing the results, the cantilever is

driven at the second resonance frequency. We assume that the driven and undriven thermal spectra are similar around the first resonance frequency.

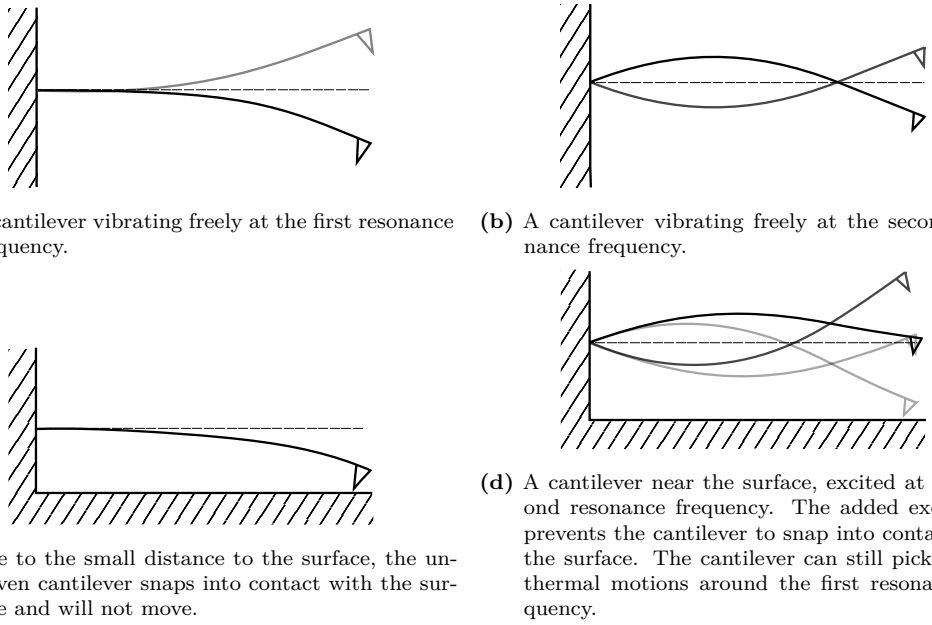

(a) A cantilever vibrating freely at the first resonance frequency.

(b) A cantilever vibrating freely at the second resonance frequency.

(c) Due to the small distance to the surface, the undriven cantilever snaps into contact with the surface and will not move.

(d) A cantilever near the surface, excited at the second resonance frequency. The added excitation prevents the cantilever to snap into contact with the surface. The cantilever can still pick up the thermal motions around the first resonance frequency.

Figure 2.9: An illustration of a cantilever vibrating free and on the surface in various resonance frequencies.

Using the data obtained in the calibration process, the cantilever is driven at the second resonance frequency with a free amplitude (a_{free}) of 10 nm. The cantilever is set to approach the surface until it reaches the amplitude set point (a_{SP}) at 85% or 8.5 nm from the surface. Here the final thermal spectrum is taken.

Data analysis The data gathered from the measurements is processed by a Python script. This script imports the data-points and plots them, the black line in Figure 2.10. The script will try to fit a Lorentzian curve on them using:

$$L(x) = \frac{a \cdot b^4}{(x^2 - b^2)^2 + (x\frac{b}{c})^2} + d. \tag{2.10}$$

This fit is plotted in blue. The parameters of this equation are linked to the performance of the cantilever. The a, b, c and d can be exchanged with the resonance frequency f_{c}, the amplitude at the resonance frequency, the Q-factor Q_{c} and the background noise respectively. This leads to Equation (2.11):

$$L(x) = \frac{\text{amp} \cdot f_{\text{c}}^4}{(x^2 - f_{\text{c}}^2)^2 + (x\frac{f_{\text{c}}}{Q_{\text{c}}})^2} + \text{noise}. \tag{2.11}$$

Once the script has successfully fitted the curve using the Least-Squared method, the Q-factor is found. To help the script fit the data, it searches for high, but broad peaks, to rule out outliers and estimates the values of the resonance frequency, maximum amplitude, Q-factor and noise level. These values are used to create an initial guess, represented as the red line in Figure 2.10. The initial guess can be altered manually if the data is not as expected.

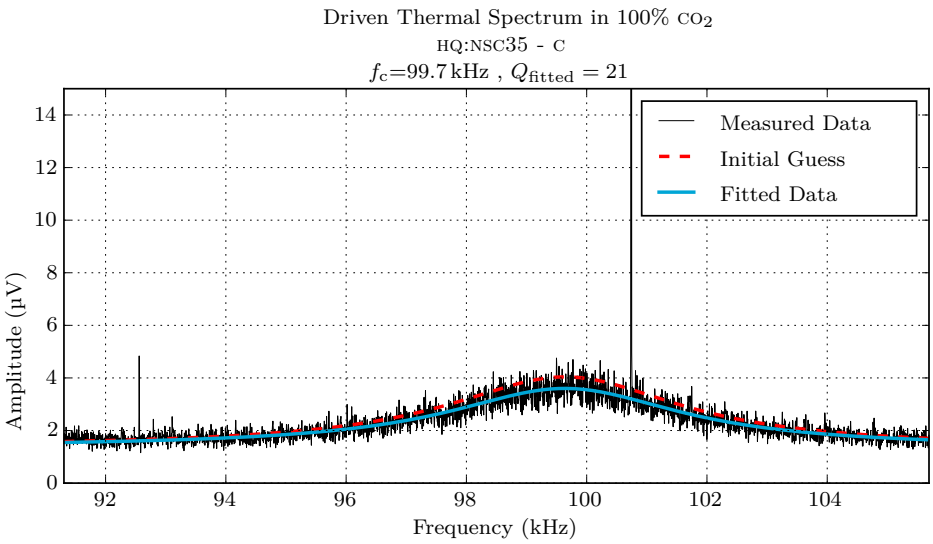

Figure 2.10: Example of a fit of an Anfatec measurement made by `result_fit.py`. The black line represents the measurement data. The red line represents the initial guess and the blue line is the fit created by the algorithm.

Liquid measurements On the Bruker FastScan AFM, the measurements in air and liquid are performed. The measurements in air work as previously described. For the liquid measurements, a drop of de-mineralized water is placed on the cantilever. A second drop is placed on the sample surface. If there are air bubbles trapped inside the bubble they will be removed. When the cantilever hovers above the surface and the two drops merge, a liquid meniscus forms (Figure 2.11) in which the measurements take place. The rest of the experiment follows the before mentioned procedure.

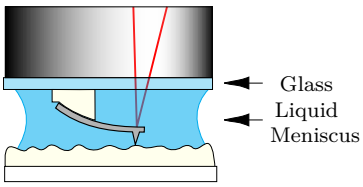

Figure 2.11: For the measurements in liquid, a liquid meniscus is created by covering the cantilever and the sample in a big drop of liquid. When the cantilever is positioned above the sample and the two drops touch, the meniscus is created.

Gas measurements The gas measurements make use of the Anfatec AFM. It starts again with a measurement in air. For the gas measurements the AFM is covered by the bell jar. The gas is supplied through a tube to the bottom of the jar (Figure 2.12).

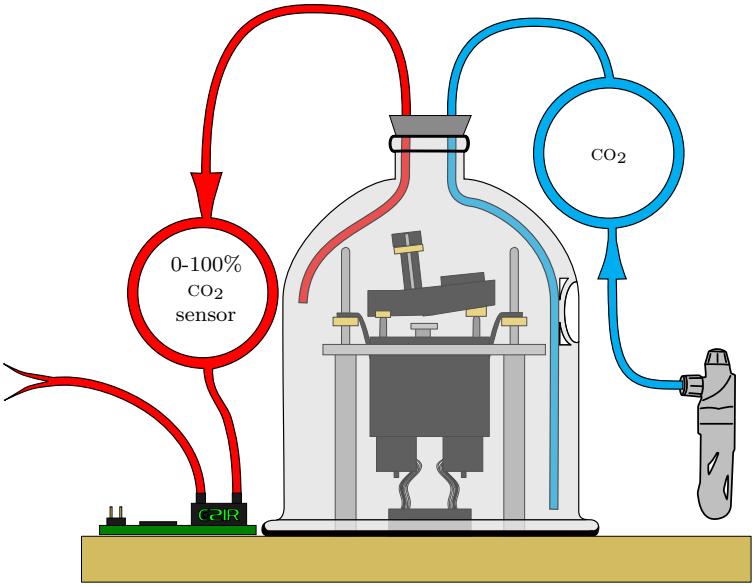

Figure 2.12: The measurement setup of the Anfatec AFM. The bell jar is filled with CO_2 from a cannister. The CO_2 is released at the bottom of the jar, the exhaust tube is located at the height of the cantilever. The exhausted gas will flow through the 0-100% CO_2 sensor before ending into the open air.

The excess gas can escape trough a second tube, with the outlet at the height of the experiment. The gas concentration of the outflow tube is monitored using the CozIR CO_2 sensor. The measurement is started in air (0.15% CO_2). After each thermal spectrum the gas concentration is increased. When the gas reaches 100%, a last thermal spectrum is measured, away from the surface. Next the cantilever is lowered into place near the surface. The set-up is calibrated and the gas refilled. As soon as the gas concentration reaches 100% again, the final thermal spectrum is measured

2.4. Revised gas measurement

After evaluation, the measurement in gas is repeated. This time with a revised measurement plan and other equipment, to gain more control over the experiment and have a higher density of data points.

Revised equipment For the second set of gas measurements, a different Lock-in amplifier is used. The simpler HF2LI from Zurich Instruments. It only allows for 2048 data points per spectrum, but is able to focus those data points into a region of interest, resulting in a higher data density.

Figure 2.13: The HF2LI lock-in amplifier from Zurich Instruments, is a simpler lock-in amplifier, is used to convert the obtained deflection signal from the AFM into a frequency spectrum using a FFT algorithm.

Revised measurement plan The reference measurement in air remains unchanged. At the start of the gas measurement, the system is flushed with nitrogen gas (N_2) until the CO_2 concentration reaches 0 ppm. Here, the first thermal spectrum is measured. Next, CO_2 is slowly released into the system. A thermal spectrum is measured at several points between 0 ppm and 1 000 000 ppm. When 100% gas concentration is reached, the calibration process starts, followed by a single near surface

thermal spectrum in a completely gas filled environment. Since the gas concentration cannot be lowered reliably, the bell jar is lifted to let the gas escape, and the system is washed again with N_2. Now, the rest of the thermal spectra near surface are measured, again with an increasing gas concentration, from 0 ppm to 1 000 000 ppm.

3

Results

In the previous chapter, the used materials are listed along with the used methods, to perform the simulations and experiments. A selection of the results of these simulations and experiments are listed in this chapter. The first results are from the models, to predict the behaviour of the cantilever in different fluids. This is then followed by the results of the actual experiments in air and liquid, performed on the Bruker FastScan AFM. The last results in this chapter are from the Anfatec AFM, which is used to measure in air and different gasses. Only a selection of the obtained results are shown, the full dataset can be found in Appendix E.

3.1. Models

The models create a reference for the actual experiments, they help to make a prediction of the cantilevers behaviour in different fluids. Only the results of the free vibrating models are shown, the results near the surface are unusable and will be further discussed in Chapter 4. The different models use the parameters listed in Tables 3.1 and 3.2, together with Equations (2.4), (2.5) and (A.5). Due to the uncertainties in the fabrication of the cantilever chip, the results can vary up to 40%, and serve therefore as a rough estimation. The model used to obtain these results can be found in Appendix B.

Table 3.1: Densities and viscosity in [$\mathrm{kg\,m^{-3}}$] and [$\mathrm{Pa\,s^{-1}}$] per medium at T = 291 K and p = 1.1013 bar [42].

Medium	Density	Viscosity
Air	1.214	1.813e-5
Demi-water	998.6	1.053e-3
CO_2	1.852	1.459e-5

Table 3.2: Parameters used to model the behaviour of the cantilevers in different fluids at $T = 291\,\mathrm{K}$.

Medium	ρ ($\mathrm{kg\,m^{-3}}$)	η ($\mathrm{Pa\,s}$)
Air	1.214	1.813e-5
Liquid	998.6	1.053e-3
CO_2	1.852	1.459e-5
N_2	1.174	1.750e-5

3.1.1. Air model

This model calculates the Q-factor, resonance frequency and cantilever rise time in the open air. Table 3.3 shows the results.

Table 3.3: The resonance frequency (f_c), Q-factor and cantilever rise time (τ_c) of the HQ:NSC35 cantilever chip in open air. The model has a 40% error margin.

NSC35 Cantilevers	Free vibration f_c (kHz)	Q (–)	τ_c (ms)
A	226.1	257	0.3613
B	337.9	315	0.2971
C	161.9	215	0.4236

3.1.2. Liquid model

Table 3.4 holds the results of the simulation in the heavier de-mineralized water.

Table 3.4: The resonance frequency (f_c), Q-factor and cantilever rise time (τ_c) of the HQ:NSC35 cantilever chip measuring in a liquid environment. The model has a 40% error margin.

NSC35 Cantilevers	Free vibration f_c (kHz)	Q (–)	τ_c (ms)
A	77.49	6	0.02508
B	117.9	7	0.01942
C	54.50	5	0.03118

3.1.3. Gas model

The gas model calculates the cantilevers response in two different gasses, CO_2 and N_2, but also in a variation of different compositions of the two gasses. Table 3.5 shows the result of an environment completely filled with N_2. This is used to wash the environment of gasses, so as to start the measurement with a known gas. After the wash, the environment is filled with CO_2. Table 3.6 shows the expected reaction when measuring in CO_2.

Table 3.5: The resonance frequency (f_c), Q-factor and cantilever rise time (τ_c) of the HQ:NSC35 cantilever chip before the measuring gas is inserted, a filled N_2 environment. The model has a 40% error margin.

NSC35 Cantilevers	Free vibration f_c (kHz)	Q (–)	τ_c (ms)
A	226.2	266	0.3740
B	338.0	327	0.3075
C	161.9	223	0.4385

Table 3.6: The resonance frequency (f_c), Q-factor and cantilever rise time (τ_c) of the HQ:NSC35 cantilever chip in a 100% CO_2 environment. The model has a 40% error margin.

NSC35 Cantilevers	Free vibration f_c (kHz)	Q (–)	τ_c (ms)
A	225.6	234	0.3303
B	337.2	286	0.2696
C	161.5	198	0.3899

Using Equations (3.1) and (3.2) the density and viscosity are calculated for different ratios of the two gasses.

$$\rho_{\text{mix}} = \frac{(\text{vol}\%_1 M_1 + \text{vol}\%_2 M_2)P}{TR} \tag{3.1}$$

$$\eta_{\text{mix}} = \frac{\text{vol}\%_1 \eta_1 \sqrt{M_1} + \text{vol}\%_2 \eta_2 \sqrt{M_2}}{\text{vol}\%_1 \sqrt{M_1} + \text{vol}\%_2 \sqrt{M_2}} \tag{3.2}$$

The corresponding Q-factors can be found in Figure 3.1. On the left side of this graph, the measurement space is filled with N_2. On the right it is filled with 100% CO_2.

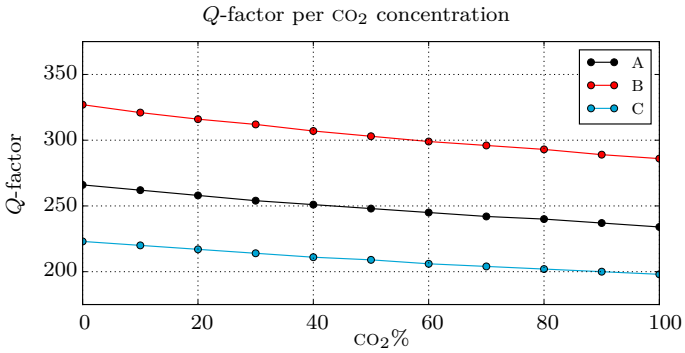

Figure 3.1: Calculated Q-factors for a range of gas concentrations, starting with 100% N_2 and ending up at 100% CO_2.

3.2. Experimental Results

The liquid and gas experiments are conducted on the two different AFM's. Prior to these experiments a thermal spectrum in air is measured for a reference. The results of these measurements can be found in the following sections.

3.2.1. Liquid experiment

For the experiments in liquid, the Bruker FastScan AFM is used. The experiment starts with the measurement of a thermal spectrum in air. First, when the cantilever is vibrating freely and it is repeated with the cantilever positioned near the surface. Then the thermal spectrum is measured again. The results can be found in Table 3.7.

Table 3.7: Reference measurement in air: resonance frequency and Q-factor for the HQ:NSC35 on the Bruker Fastscan AFM.

NSC35 Cantilevers	Free vibration f_c (kHz)	Free vibration Q (–)	Near surface f_c (kHz)	Near surface Q (–)
A	145.2	181	143.6	50
B	214.8	255	212.1	43
C	107.0	158	106.7	51

Next de-mineralized water is added to the cantilever and on the surface to submerge it inside a liquid meniscus as can be seen in Figure 2.11. The volume of this meniscus is large enough to measure the free vibration as well as the vibrations near surface. The results are shown in Table 3.8.

Table 3.8: Measurement in liquid: resonance frequency and Q-factor for the HQ:NSC35 on the Bruker Fastscan AFM.

NSC35 Cantilevers	Free vibration f_c (kHz)	Free vibration Q (–)	Near surface f_c (kHz)	Near surface Q (–)
A	67.29	4	95.42	2
B	105.0	6	127.9	3
C	47.64	3	55.39	2

3.2.2. Gas experiment

The experiments in gas are conducted on the Anfatec tabletop AFM, together with the supplied bell jar and the COZIR 0-100% CO_2 sensor. For this experiment a fresh cantilever is used. Therefore a

new thermal spectrum in air, without the bell jar is measured. First, when the cantilever is vibrating freely, and next near the surface. The results are found in Table 3.9

Table 3.9: Reference measurement in air: resonance frequency and Q-factor for the HQ:NSC35 on the Anfatec AFM.

NSC35 Cantilevers	Free vibration		Near surface	
	f_c (kHz)	Q (–)	f_c (kHz)	Q (–)
A	141.2	120	136.9	26
B	208.1	170	208.3	35
C	102.7	125	101.1	7

For the experiment in gas, the bell jar is placed on top of the system and the CO_2 sensor is connected similar to Figure 2.12. The CO_2 is released into the system in a controlled manner. At various points in time the thermal spectrum is measured and the CO_2 concentration is noted. Using these steps the thermal spectra in the range between regular air and 100% CO_2 are measured with the cantilever vibrating freely. Next the cantilever is positioned near surface, the gas is replenished, and a final thermal spectrum in 100% CO_2 is measured. The end result can be found in Table 3.10, while the change of Q-factor per concentration with the cantilever away from the surface, can be seen in Figure 3.2.

Table 3.10: Measurement in gas: resonance frequency and Q-factor for the HQ:NSC35 in 100% CO_2 on the Anfatec AFM.

NSC35 Cantilevers	Free vibration		Near surface	
	f_c (kHz)	Q (–)	f_c (kHz)	Q (–)
A	141.2	147	133.1	11
B	208.0	183	202.4	29
C	102.6	99	99.15	20

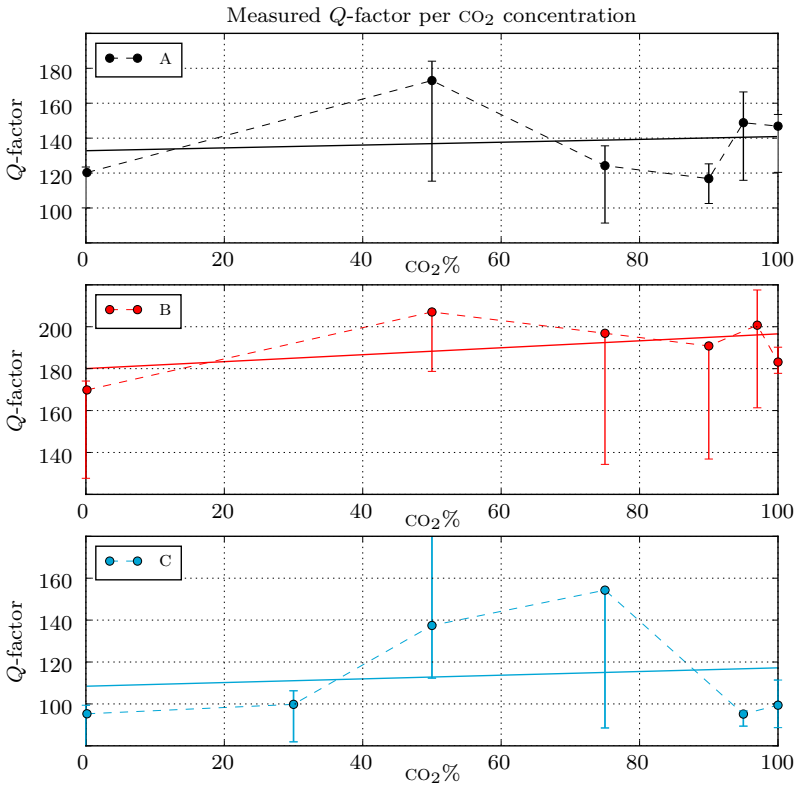

Figure 3.2: Measured Q-factors of the cantilevers versus the gas concentrations, starting with regular air (0.15% CO_2) and ending up at 100% CO_2.

3.2.3. Revised gas measurement

The experiment is repeated with a fresh cantilever chip, but only the behaviour of the C cantilever is measured. A different lock-in amplifier is connected to generate more data points within the region of interest. At the start of the experiment the bell jar is washed with N_2. After that the CO_2 gas is supplied, slowly increasing the concentration in the jar. In Table 3.11 the measured data is given, starting with the reference measurement in air.

Table 3.11: Measured resonance frequency and Q-factor for the HQ:NSC35-C. This measurement is done with a fresh cantilever, a higher resolution around the area of interest and a controlled starting environment. Only the longest cantilever C is examined.

NSC35 C	Free vibration		Near surface	
	f_c (kHz)	Q (–)	f_c (kHz)	Q (–)
Air	103.3	162	101.7	66
N_2	103.3	159	103.3	139
CO_2	103.2	161	101.3	35

In Figure 3.3 the Q-factor is plotted versus the CO_2 concentration. Here the blue dashed line represents the trend line and the solid blue line the trend line without the last point.

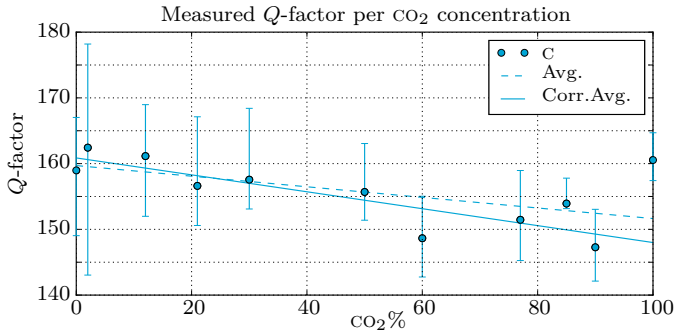

Figure 3.3: Measured Q-factors of the C cantilever in a range of gas concentrations, starting with 100% N_2 and ending up at 100% CO_2.

In Figure 3.4 the Q-factor is plotted versus the CO_2 concentration near the surface. Here the red data point at 100 % is the first point of the measurement, after which the measurement is continued at 0 %.

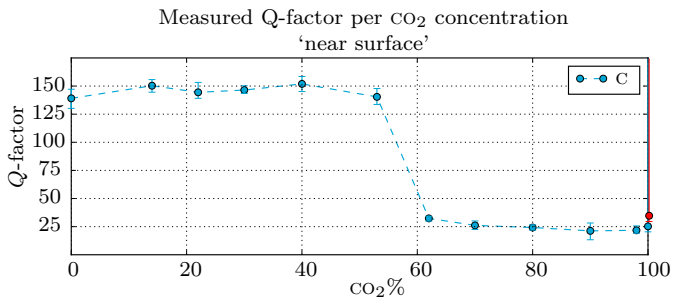

Figure 3.4: Measured Q-factors of the C cantilever near the surface as a function of gas concentrations, starting with N_2 and ending up at 100% CO_2. The red data point is the first measurement after which the system is washed with N_2 until the CO_2 concentration again reaches 0 %.

4

Discussion

The previous chapter described the most important results needed to find out if the Q-factor can be lowered. These results will be discussed in this chapter. First, the used models, for air, liquid and gas, are discussed separately, followed by the liquid and gas measurements. The chapter will be concluded with a general discussion.

4.1. Models

For the measurement in liquid, the model shows an improvement of the cantilever response time, τ_c, with as much as a factor 15, as can be seen in Table 4.1. A large improvement is to be expected with such a dense medium.

Table 4.1: Estimated improvement of τ_c when measuring in liquid, according to the model.

NSC35 Cantilevers	Q-factor Air (–)	Q-factor Liquid (–)	τ_c Air (ms)	τ_c Liquid (ms)	Times Faster (×)
A	257	6	0.3613	0.02508	14.41
B	315	7	0.2971	0.01942	15.30
C	215	5	0.4236	0.03118	13.58

Although the longest cantilever (C) is expected to show the largest decrease in Q-factor, the model shows that the shortest cantilever (B) shows the most improvement. This is most likely caused by the difference of the cantilevers resonance frequency. Since damping is proportional speed, a faster vibrating cantilever experiences more damping than a slow cantilever. By measuring in liquid, the cantilevers own resonance frequency also changes. The liquid adheres to the cantilever, effectively increasing the cantilever's mass. This will result in a lower resonance frequency, f_c:

$$f_c = \frac{1}{2\pi}\sqrt{\frac{k_c}{0.24 m_c}}. \tag{4.1}$$

The change of f_c will influence multiple delays, τ_m,τ_I and τ_p, in the total sum of time delays $\Sigma\tau_n$. These delays strongly depend on the measurement set-up and can be minimized by selecting the appropriate equipment. The main delay effected is the oscillation measuring time, τ_m, and while it can also be sped up by using different equipment. Since a lock-in amplifier is used, τ_m will be around three times the vibration period:

$$\tau_m \approx \frac{3}{f_c}. \tag{4.2}$$

Other detection methods could lower this number. The increase in τ_m is small, compared to the decrease of the τ_c, as is shown in Table 4.2

Table 4.2: Estimated increase of τ_m when measuring in liquid, according to the model.

NSC35 Cantilevers	f_c Air (kHz)	f_c Liquid (kHz)	τ_m Air (ms)	τ_m Liquid (ms)	Times Slower (×)
A	226.1	77.49	0.01327	0.03871	2.918
B	337.9	117.9	0.008878	0.02545	2.866
C	161.9	54.50	0.01854	0.05504	2.970

The much less dense CO_2 also shows an increase in speed, but here only a 10% gain can be observed. See also Table 4.3. The shortest cantilever (B) still experiences the largest change, but since the gas does not increase the resonance frequency noticeably, the improvement difference between the B and C cantilever is much less. This also means there is no significant change in τ_m. This is visible in Table 4.4. These models only supply a rough estimation due to the error margin of 40%.

Table 4.3: Estimated improvement of τ_c when measuring in gas, according to the model.

NSC35 Cantilevers	Q-factor Air (–)	Q-factor Gas (–)	τ_c Air (ms)	τ_c Gas (ms)	Times Faster (×)
A	257	234	0.3613	0.3303	1.094
B	315	286	0.2971	0.2696	1.102
C	216	198	0.4236	0.3899	1.087

Table 4.4: Estimated increase of τ_m when measuring in gas, according to the model.

NSC35 Cantilevers	f_c Air (kHz)	f_c Gas (kHz)	τ_m Air (ms)	τ_m Gas (ms)	Times Slower (×)
A	226.1	225.6	0.01327	0.01329	1.002
B	337.9	337.2	0.008878	0.008897	1.002
C	161.9	161.5	0.01854	0.01858	1.002

Near surface model The near surface model results where omitted in the last chapter. The near surface model was created with an equation and parameters obtained from Green *et.al.*[21]. The parameters were experimentally obtained. This worked perfectly in the scenario which they had set. With other variables, such as a larger cantilever with a higher Q-factor and a lower resonance frequency, the results became 'unusable' and therefore are dismissed. These results for air are shown in Table 4.5. In the other mediums, the results are similar.

Table 4.5: Q-factors in air, near the surface, according to the model.

NSC35 Cantilevers	Q-factor for $\overline{H}$= 0.1 (–)	0.2 (–)	0.3 (–)	0.5 (–)	1 (–)
A	120	317	1127	-1147	-595
B	140	489	-12030	-612	-429
C	78	158	297	1251	-1817

4.2. Measurements

The measurements are taken away from the surface and near the surface. Near the surface an un-driven cantilever will stick to it, so a thermal spectrum can not be measured. To overcome this problem, the cantilever is driven at the second resonance frequency, this will prevent the cantilever from sticking to the surface. The assumption is made that the cantilever reacts equally around the region of interest (e.g. the first resonance frequency) when it is driven at the second resonance frequency, or not driven

at all since the resonance frequencies are not coupled. To check the validity of this assumption, two thermal spectra are taken, both when the cantilever is far from the surface. The first spectrum is un-driven, shown in Figure 4.1a, while the second spectrum, shown in Figure 4.1b, is driven at the second resonance frequency.

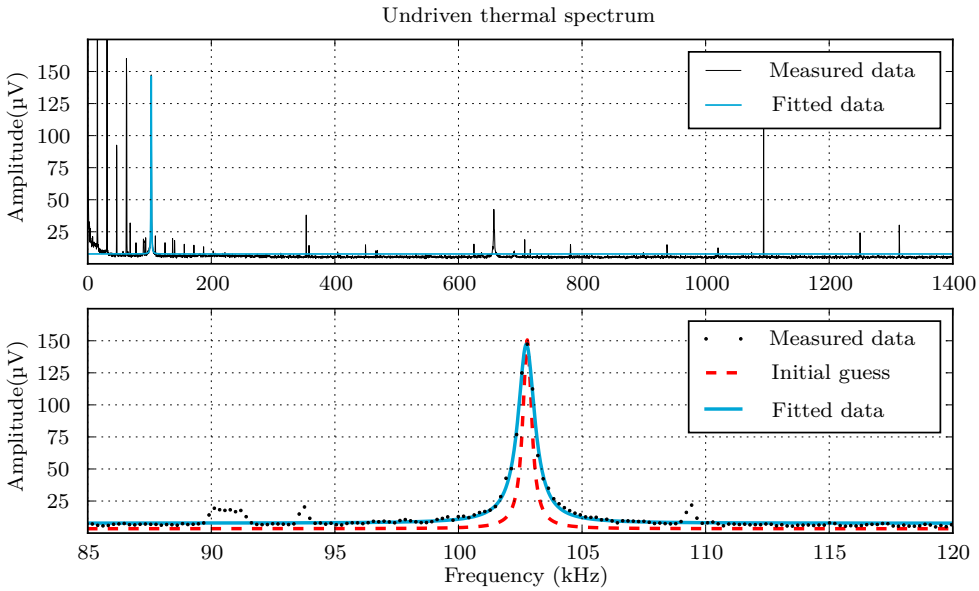

(a) Undriven thermal spectrum in air. It has a Q-factor of 125 at a resonance frequency of 102.7 kHz.

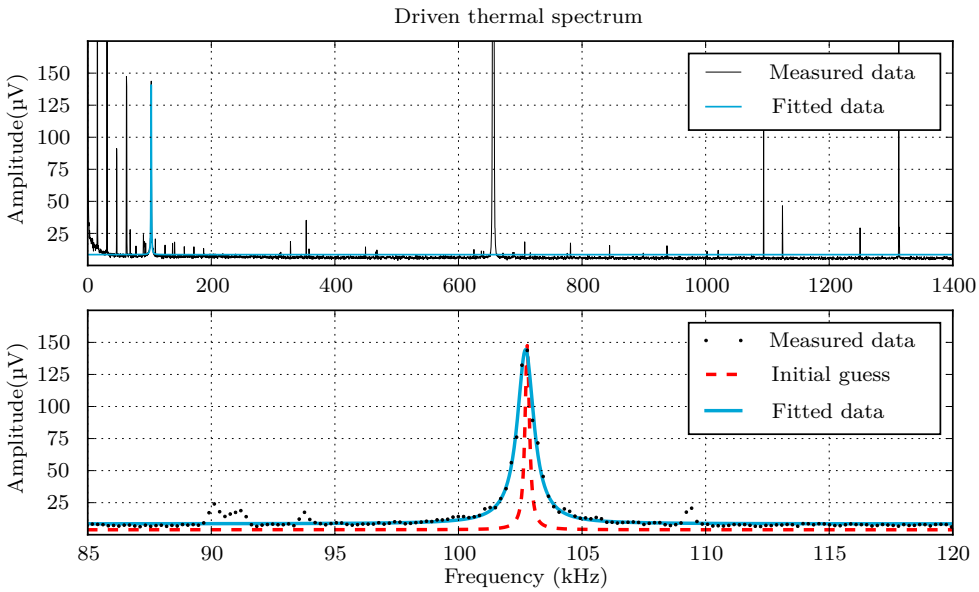

(b) Thermal spectrum of the same cantilever, driven at the second resonance frequency at 655.8 kHz. The first resonance frequency is located at 102.7 kHz With a Q-factor of 127.

Figure 4.1: Comparison of a un-driven and a driven thermal spectrum fit. Zoomed in on the region of interest, around the first resonance frequency at 102 kHz. This region is barely effected by the driving of the second resonance frequency.

The region around the first resonance frequency is barely effected by the cantilevers' excitation. This can also be seen in the Q-factor. The undriven spectrum has a Q of 125, while the driven cantilever has a Q of 127 and the noise level increases from 7.681 µV to 8.440 µV. These changes are small enough, for this thesis, to use this technique to measure a thermal spectrum near the surface.

4.2.1. Liquid

The initial measurements in liquid proved to be incredibly complicated. These measurements where performed on the Anfatec AFM, with a custom build liquid holder. It proved to be difficult to create repeatable measurements. The arrival of the Bruker FastScan AFM not only eliminated this problem, but made the measurements in liquid the least complicated experiments to complete. The data is sampled with a sample resolution of around 50 Hz, which proves to be sufficient for the fitting algorithm to find a decent fit.

Table 4.6: Decrease in Q-factor and τ_c, when measuring in liquid, free from the surface.

NSC35 Cantilevers	Q-factor Air (–)	Q-factor Liquid (–)	τ_c Air (ms)	τ_c Liquid (ms)	Times Faster (×)
A	181	4	0.3968	0.02027	19.57
B	255	6	0.3773	0.01668	22.62
C	158	3	0.4704	0.01743	26.99

Opposite of what the models suggested, the longest cantilever, C has the largest decrease in Q-factor, suggesting that the surface area of the cantilever plays a bigger role than the resonance frequency, for the Q-factor (Table 4.6). The change in f_c when measuring in liquid is in line with the models, as is shown in Table 4.7.

Table 4.7: Increase in τ_m, when measuring in liquid, free from the surface.

NSC35 Cantilevers	f_c Air (kHz)	f_c Liquid (kHz)	τ_m Air (ms)	τ_m Liquid (ms)	Times Slower (×)
A	145.2	67.29	0.02066	0.04459	2.159
B	214.8	105.0	0.01396	0.02858	2.046
C	107.0	47.64	0.02805	0.06297	2.245

When measuring thermal spectra near the surface, the improvement of the Q-factor decreases. When the cantilever nears a sample, tip-sample interactions come into play, causing mode damping, making the measurement faster, so that there is less to improve. Measuring near the surface decreases all the Q-factors, but since the Q-factor in air is effected more, the overall improvement is less. The difference between the cantilevers, however has increased. This is shown in Table 4.8.

Table 4.8: Measured decrease in Q-factor and τ_c, when measuring in liquid, near the surface.

NSC35 Cantilevers	Q-factor Air (–)	Q-factor Liquid (–)	τ_c Air (ms)	τ_c Liquid (ms)	Times Faster (×)
A	50	2	0.1111	0.008060	13.78
B	43	3	0.06482	0.007520	8.620
C	51	2	0.1510	0.008852	17.05

Near the surface, the resonance frequency in air decreases slightly, in liquid however, an increase is clearly visible in Table 4.9. One possible explanation for this phenomenon could be the more complex fluid dynamics of in a dense medium near a large body.

Table 4.9: Measured increase in τ_m when measuring in liquid, near the surface.

NSC35 Cantilevers	f_c Air (kHz)	f_c Liquid (kHz)	τ_m Air (ms)	τ_m Liquid (ms)	Times Slower (×)
A	143.6	95.42	0.02089	0.03144	1.505
B	212.1	127.9	0.01415	0.02346	1.658
C	106.7	55.39	0.02812	0.05417	1.926

4.2.2. Gas Measurement

The gas measurements can, unfortunately, not profit from the Bruker FastScan AFMs' benefits. These measurements are performed on the Anfatec AFM. Because these measurements use gas, which needs to be contained, the measurement quickly becomes more difficult. Not only being unable to make changes to the AFM because of the bell jar, but also the measuring of the gas concentration has its challenges. There is a small error introduced when measuring the gas concentration. Aside from the accuracy of the CO_2 sensor, the measurement procedure also introduces potential errors. The sensor is not located at the region of interest, but connected to a tube with its inlet near the region of interest. In practise, this means that the CO_2 concentration in the bell jar is, during the filling of the jar, always higher than the indicated concentration. The tube is relatively short, giving a delay between the actual concentration and the measures concentration. This delay is estimated to 1 second, which translates in an additional error of 1%. The measured Q-factors, shown in Table 4.10, do not behave as expected, but instead indicate that the system slows down for two of the three cantilevers, after the gas is injected. The f_c on the other hand behaves as expected, showing almost no change when the gas is added. This is shown in Table 4.11.

Table 4.10: Decrease in Q-factor and τ_c, when measuring in gas, free from the surface

NSC35 Cantilevers	Q-factor Air (–)	Q-factor Gas (–)	τ_c Air (ms)	τ_c Gas (ms)	Times Faster (×)
A	120	147	0.2711	0.3310	0.8190
B	180	183	0.2752	0.2803	0.9821
C	125	99	0.3875	0.3083	1.257

Table 4.11: Increase in τ_m, when measuring in gas, free from the surface.

NSC35 Cantilevers	f_c Air (kHz)	f_c Gas (kHz)	τ_m Air (ms)	τ_m Gas (ms)	Times Slower (×)
A	141.3	141.2	0.02124	0.02124	1.000
B	208.1	208.0	0.01441	0.01442	1.000
C	102.7	102.6	0.02920	0.02923	1.001

The results near the surface, shown in Table 4.12, again do not behave as expected, but this time, the only the C cantilever slows down, while the others speed up. The f_c, shown in Table 4.13, again behaves as expected.

Table 4.12: Measured decrease in Q-factor and τ_c, when measuring in gas.

NSC35 Cantilevers	Q-factor Air (–)	Q-factor Gas (–)	τ_c Air (ms)	τ_c Gas (ms)	Times Faster (×)
A	26	11	0.06059	0.02694	2.249
B	35	29	0.05316	0.04516	1.177
C	7	21	0.02151	0.06563	0.3277

Table 4.13: Actual increase in τ_m when measuring in gas, near the surface.

NSC35 Cantilevers	f_c Air (kHz)	f_c Gas (kHz)	τ_m Air (ms)	τ_m Gas (ms)	Times Slower (×)
A	136.9	133.1	0.02192	0.02254	1.029
B	208.3	202.4	0.01440	0.01482	1.029
C	101.1	99.15	0.02968	0.03026	1.019

A closer look at the fitted data reveals that the problem lies with the sample resolution. The first set of thermal spectra from the gas measurements is recorded at a sample resolution of 200 Hz, which

proves to be to low for accurate analysis. Because of the low resolution, outliers greatly effect the outcome. To overcome this handicap, the gas measurement is revised.

Revised gas measurement For the revised gas measurements, the measuring method is changed. Since the CO_2 supply is limited, only the largest cantilever, cantilever C is used for this measurement. Changes in fluid density should be most visible for the cantilever with the largest surface as the experiments in liquid showed. The gas measurement will now start in a better controlled environment, washed in N_2, so that the measurement can start at a true 0% concentration. The thermal spectra near the surface are now measured in a range of gas concentrations, to better understand what is happening near the surface. Finally the sample resolution is increased from around every 210 Hz to every 3.5 Hz.

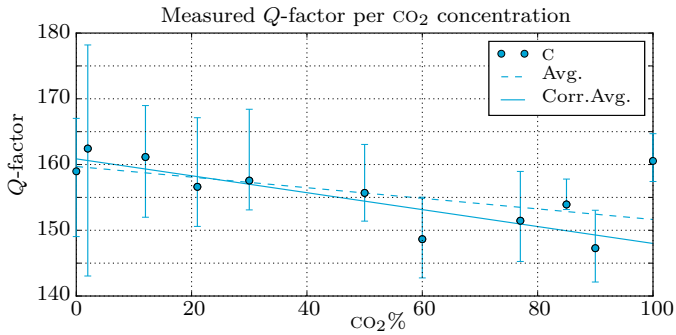

Figure 4.2: Measured Q-factors of the C cantilever in a range of gas concentrations, starting with 100% N_2 and ending up at 100% CO_2.

When the Q- factor is plotted against the gas concentration, in Figure 4.2, one point sticks out, the data point at 100%. This is believed to be an outlier, when compared to the rest of the data set. The Q-factor is higher than at the starting point. Therefore two trend lines are created. The blue dashed line shows the average of all the data points. The blue solid line shows the corrected average, the average of all the data points minus the final point. The improvement factor is calculated with an virtual point at 100%, located on the corrected average. This is shown in Table 4.14.

Table 4.14: Measured decreased in Q-factor and τ_c, with the 'free vibration' measurements for the corrected average and the actual data points.

NSC35 C	Q-factor Air (–)	Q-factor Gas (–)	τ_c Air (ms)	τ_c Gas (ms)	Times Faster (×)
'Free vibration'-Avg.	156.3	147.3	0.4816	0.4543	1.060
'Free vibration'-Data	156.3	160.5	0.4816	0.4952	0.9725
'Near surface'	66.38	25.24	0.2078	0.08026	2.589

Notice that the 'free vibration'-Avg. results are in the range expected for a gas measurement. The results near the surface, however, compare better to those of a liquid measurement. This is not valid for the change in f_c, shown in Table 4.15.

Table 4.15: Measured increased in τ_m,, with the 'free vibration' measurements for the corrected average and the actual data points.

NSC35 C	f_c Air (kHz)	f_c Gas (kHz)	τ_m Air (ms)	τ_m Gas (ms)	Times Slower (×)
'Free vibration'-Avg.	103.3	103.2	0.02904	0.02907	1.001
'Free vibration'-Data	103.3	103.2	0.02904	0.02907	1.001
'Near surface'	101.7	100.1	0.02950	0.02996	1.016

Thermal spectrum near surface The thermal spectrum near the surface is taken directly after the last measurement off the surface in a 100% CO_2 concentration. The cantilever is calibrated and lowered onto the surface. The gas is replenished until the concentration reaches 100% again. There the first thermal spectrum is measured. Since the lowering of the gas concentration cannot be measured accurately, the whole dome is washed with N_2, to reset the concentration back to 0%. Thermal spectra are again measured, while the gas concentration is increasing. The thermal spectrum near the surface raises some questions.

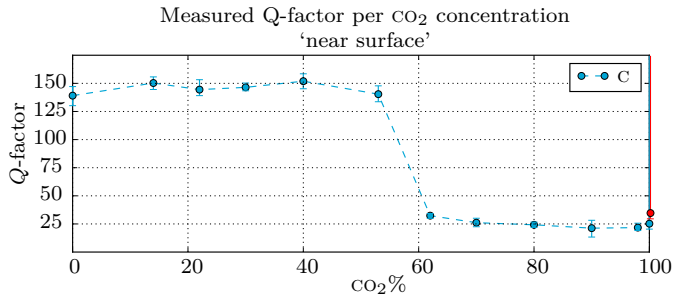

Figure 4.3: Measured Q-factors of the cantilevers near the surface in a range of gas concentrations, starting with N_2 and ending up at 100% CO_2. The red data point is the first measurement after which the system is washed with N_2 until the CO_2 concentration again reaches 0 %.

The error margins in this measurement set can be described as narrow, for every point, except the two points located at the 100% gas concentration point. These error margins are large (+450). A visual inspection of the data revealed that this is related to the fitting algorithm. Both point have a single point outlier in their data set. This point influences the error margins of the fit creating a large error estimation.

The second, and most obvious point is the large drop in Q-factor after it reaches a 50% concentration. While it is tempting to question only the large drop in the Q-factor, what happens before the drop is also quit interesting. The first thermal spectrum taken, away from the surface, in air shows that the Q-factor starts in a believable range. When this thermal spectrum is repeated near the surface, a drop in the Q-factor is visible, from 156 to 66. The same behaviour can also be seen with the reference measurements from the liquid experiment, in Tables 4.6 and 4.8. The decrease of Q-factor in gas is roughly twice as large than expected, but the most interesting part is before the drop. When the gas measurement starts, both away from the surface and near the surface, the bell jar in which the measurements are taken is washed with N_2. But when Figure 4.2 is compared to Figure 4.3, the decrease in Q-factor as the cantilever nears the surface is almost negligible. At this time it is unknown what causes this decrease in decrease.

4.3. General discussion

As the model and the results of the liquid experiments indicate, measuring in a liquid will speed up a measurement. This has already been proven by many others such as Sulchek *et.al.*[41]. In this experiment a theoretical time save of up to 0.3925 ms per tapping point is achieved. When the change of τ_m is taken into account, the time saved is reduced to 0.3559 ms per tapping point. With the time it takes for a measurement, V_{image}^{-1} defined by:

$$V_{\text{image}} = \frac{\alpha w}{16 W_s N_s \Sigma \tau_n}. \tag{4.3}$$

The parameters of an example measurement are chosen to be $\alpha = 1.4$, $w = 10\,\text{nm}$, $W_s = 5\,\mu\text{m}$, $N_s = 512$ lines. For the time delays, only τ_c and τ_m are taken into account: $\Sigma\tau_n = \tau_c + \tau_m$. A measurement in air with $\Sigma\tau_n = 0.4421\,\text{ms}$ results in a measurement time of 8.623 min. Measuring in liquid reduces the $\Sigma\tau_n$ to 0.086 22 ms resulting in a measurement time of 1.682 min. This is a reduction of 0.3559 ms for $\Sigma\tau_n$ and a 6.941 min reduction per measurement. An overview of the measurement time improvements for liquid can be found in Table 4.16.

Table 4.16: Measuring time for a 5 µm × 5 µm sample area with 512 scan lines using cantilever C in different mediums. The measuring time is based on τ_c and τ_m alone.

Medium	Model		'Free vibration'		'Near Surface'	
	$\tau_c + \tau_m$ (ms)	Total (min)	$\tau_c + \tau_m$ (ms)	Total (min)	$\tau_c + \tau_m$ (ms)	Total (min)
Air ref.	0.4421	8.623	0.4985	9.723	0.1791	3.493
Liquid	0.08622	1.682	0.08040	1.568	0.06302	1.229
Improvement	0.3559	6.941	0.4180	8.155	0.1161	2.264
Air ref.	0.4421	8.623	0.5106	9.959	0.2373	4.628
Gas	0.4085	7.968	0.4834	9.429	0.1102	2.149
Improvement	0.03101	0.6550	0.02729	0.5300	0.1271	2.479

According to the model, for the gas measurement, $\Sigma\tau_n$ can be reduced with 0.031 01 ms, or 0.6550 min per measurement. The experiments showed an improvement of 0.027 29 ms and 0.1271 ms or 0.5300 min and 2.479 min for a free measurement and a near surface measurement respectively, but the results near the surface are questionable, since the improvement is close to that of a liquid measurement.

This technique can also be used in conjunction with others to speed up a measurement even further. Measuring in liquid can however complicate the system and not all AFM's or samples might be able to be submerged in a liquid. Even though a measurement in gas only improves the measurement speed by roughly 1%, it can still be worth the effort to do so, if large batches need to be scanned. One of the benefits being that it can be implemented on top of almost all other speed improvement methods, without making the system much more complicated. To fully benefit from the speed improvements when measuring in gas, the system would most likely need an automated and constant control of the gas environment, combined with a semi-(or fully-) automated AFM. The experiments are performed in the non-inert CO_2, since it is cheaper and has a better availability, but there are gasses which are better suited for this measurement. One of the heavier inert gasses, Sulfur Hexafluoride (SF_6), would be a good candidate, as it is six times mode dense then air, as shown in Table 4.17.

Table 4.17: SF_6 properties, compared to the other measurement mediums ($T = 291K$)

Medium	ρ (kg m^{-3})	η (Pa s)
Air	1.214	1.813e-5
Liquid	998.6	1.053e-3
CO_2	1.852	1.459e-5
N_2	1.174	1.750e-5
SF_6	6.616	1.377e-5

When inserted into the model, an $\Sigma\tau_n$ of 0.1768 ms or 3.448 min per measurement are calculated, making it worth to investigate further. Although the alternatives of the AFM are still faster, the achieved increase of measurement speed, which can be combined with other existing speed up methods, help to reduces the difference in imaging speed and therefore reduces the obstacles for AFM applications.

5

Conclusion and recommendations

The purpose of this research has been to develop more knowledge on the use of gasses and liquids to increase the measurement speed by passively lowering the Q-factor, and to investigate if there is potential to use this principle to develop a commercial AFM. In the section below, the conclusions from the research are presented. These are followed by recommendations for further research.

5.1. Conclusion

Researching how much faster an AFM measurement would become if the measurement medium is switched with a more dense medium and thus by lowering the cantilevers Q-factor and cantilever response time, leads to the following results:

The models predicted a decrease in Q-factor in liquid from 215 to 5 for the C cantilever. This results in a decrease of time delays of 0.3559 ms, or 6.941 min per image of 5 µm × 5 µm with 512 lines. This is confirmed by the experiments, shown in Table 5.1. When measuring near the surface, tip-sample interaction becomes unpredictable. For this reason, the speed increase near the surface is lower than far from the surface when changing the measurement medium to a liquid.

Table 5.1: Measuring time for a 5 µm × 5 µm sample area with 512 scan lines using cantilever C in different mediums. The measuring time is based on τ_c and τ_m alone.

Medium	Model		'Free vibration'		'Near Surface'	
	$\tau_c + \tau_m$ (ms)	Total (min)	$\tau_c + \tau_m$ (ms)	Total (min)	$\tau_c + \tau_m$ (ms)	Total (min)
Air ref.	0.4421	8.623	0.4985	9.723	0.1791	3.493
Liquid	0.08622	1.682	0.08040	1.568	0.06302	1.229
Improvement	0.3559	6.941	0.4180	8.155	0.1161	2.264
Air ref.	0.4421	8.623	0.5106	9.959	0.2373	4.628
Gas	0.4085	7.968	0.4834	9.429	0.1102	2.149
Improvement	0.03101	0.6550	0.02729	0.5300	0.1271	2.479

The measurements in gas also showed improvement, for the model and the 'free vibration' measurements. Although this is only 0.5300 min for a 5 µm × 5 µm image, this could improve when more dense gasses are used. Measuring in a gas does make the measurement procedure more complicated, but this can be avoided with a automated gas compartment, build for gas measurements specifically. When measuring near the surface, a large improvement can be seen, comparable to the improvement when measuring in liquid. The reason of this change in Q-factor is not clearly understood and deserves further investigation. Measuring in a different, more dense, medium shows promising results, but the benefits are not sufficient for small scale measurements. If a large batch of samples, or a large area needs to be measured, changing the measurement medium becomes more interesting.

5.2. Recommendations for further research

This research will be concluded with a recommendations and steps which can help to successfully commercialize the project.

- While a reduction in measurement time was predicted and observed when measuring in liquid and gas, away from the surface, as well as near the surface, the effects near the surface still raise questions. A better understanding of phenomena near the surface in changing mediums can benefit further research.
- Design and create a custom build AFM which makes use of the method described, and possibly other methods to speed up a measurement. To complete this, a few hurdles have to be taken:
  - In the discussion, Sulfur Hexafluoride (SF_6) is opted as a candidate for a measurement medium. There are even more dense gasses available, such as Perfluorobutane (C_4F_{10} $11.21\,\mathrm{kg\,m^{-3}}$) or Radon (Rn $9.73\,\mathrm{kg\,m^{-3}}$), the heaviest noble gas. The most suitable gas(ses) have to be found through a gas study, to find the most dense, safe gasses, which can be used for the AFM measurements. The gas can be dependent of the industry using the AFM.
  - A seal-able compartment has to be designed for the AFM. The compartment must consist of a regulated gas inlet, various measurement systems for measuring the gas concentration, density, temperature and humidity, and a gas outlet to safely and responsibly dispose of the used gas. Preferably all automated, since it will decrease the set-up time per measurement drastically.
  - The AFM itself should be at least semi-automatic, such as the Bruker FastScan AFM. This prevents the need to clear the gas compartment every time an adjustment needs to be made. The automation will also reduce the set-up time of an experiment. Alternatively, an existing semi-automatic AFM can be retrofitted to measure in a closed compartment.

Taking into account these recommendations and the above mentioned required alterations to the atomic force microscope, the AFM could very well become even more attractive to use in commercial applications.

List of Figures

List of Tables

Bibliography

[1] How does an NDIR CO_2 sensor work? http://www.co2meter.com.

[2] E. Abbe. Beiträge zur theorie des mikroskops und der mikroskopischen wahrnehmung. *Archiv für Mikroskopische Anatomie*, 9(1):413–418, dec 1873.

[3] T. Ando. High-speed atomic force microscopy coming of age. *Nanotechnology*, 23(6):062001, Jan 2012.

[4] T. Ando, N. Kodera, E. Takai, D. Maruyama, K. Saito, and A. Toda. A high-speed atomic force microscope for studying biological macromolecules. *Proceedings of the National Academy of Sciences*, 98(22):12468–12472, oct 2001.

[5] T. Ando, T. Uchihashi, and T. Fukuma. High-speed atomic force microscopy for nano-visualization of dynamic biomolecular processes. *Progress in Surface Science*, 83(7-9):337–437, nov 2008.

[6] Anfatec Instruments AG. http://www.anfatec.de.

[7] M. Balantekin, S. Satır, D. Torello, and F. L. Değertekin. High-speed tapping-mode atomic force microscopy using a q-controlled regular cantilever acting as the actuator: Proof-of-principle experiments. *Rev. Sci. Instrum.*, 85(12):123705, dec 2014.

[8] R. C. Barrett. High-speed, large-scale imaging with the atomic force microscope. *J. Vac. Sci. Technol. B*, 9(2):302, mar 1991.

[9] G. Binnig, C. Gerber, E. Stoll, T. Albrecht, and C. Quate. Atomic resolution with atomic force microscope. *Surface Science*, 189-190:1–6, oct 1987.

[10] G. Binnig and C. F. Quate. Atomic force microscope. *Physical Review Letters*, 56(9):930–933, Mar 1986.

[11] G. Binnig and H. Rohrer. Scanning tunneling microscopy. *Surface Science*, 126(1-3):236–244, Mar 1983.

[12] G. Binnig, H. Rohrer, C. Gerber, and E. Weibel. Surface studies by scanning tunneling microscopy. *Physical Review Letters*, 49(1):57–61, Jul 1982.

[13] I. S. Bozchalooi, A. C. Houck, J. AlGhamdi, and K. Youcef-Toumi. Design and control of multi-actuated atomic force microscope for large-range and high-speed imaging. *Ultramicroscopy*, 160:213–224, jan 2016.

[14] I. S. Bozchalooi and K. Youcef-Toumi. Multi-actuation and PI control: A simple recipe for high-speed and large-range atomic force microscopy. *Ultramicroscopy*, 146:117–124, nov 2014.

[15] R. S. Brokaw. Approximate formulas for the viscosity and thermal conductivity of gas mixtures. II. *The Journal of Chemical Physics*, 42(4):1140–1146, feb 1965.

[16] Bruker Nano Surfaces Division. Dimension FastScan. https://www.bruker.com.

[17] H.-J. Butt, P. Siedele, K. Seifert, K. Fendler, T. Seeger, E. Bamberg, A. L. Weisenhorn, K. Goldie, and A. Engel. Scan speed limit in atomic force microscopy. *Journal of Microscopy*, 169(1):75–84, jan 1993.

[18] G. Y. Chen, R. J. Warmack, T. Thundat, D. P. Allison, and A. Huang. Resonance response of scanning force microscopy cantilevers. *Review of Scientific Instruments*, 65(8):2532, 1994.

[19] P. Eaton and P. West. *Atomic Force Microscopy*. Oxford University Press, Mar 2010.

[20] M. Fairbairn, S. Moheimani, and A. J. Fleming. Q control of an atomic force microscope microcantilever: A sensorless approach. *Microelectromechanical Systems, Journal of*, 20(6):1372–1381, Dec 2011.

[21] C. P. Green and J. E. Sader. Frequency response of cantilever beams immersed in viscous fluids near a solid surface with applications to the atomic force microscope. *Journal of Applied Physics*, 98(11):114913, Dec 2005.

[22] I. Gunev, A. Varol, S. Karaman, and C. Basdogan. Adaptive Q control for tapping-mode nanoscanning using a piezoactuated bimorph probe. *Review of Scientific Instruments*, 78(4):043707, Apr 2007.

[23] W. Häberle, J. Hörber, F. Ohnesorge, D. Smith, and G. Binnig. In situ investigations of single living cells infected by viruses. *Ultramicroscopy*, 42-44:1161–1167, jul 1992.

[24] E. Henderson, P. Haydon, and D. Sakaguchi. Actin filament dynamics in living glial cells imaged by atomic force microscopy. *Science*, 257(5078):1944–1946, sep 1992.

[25] R. C. Hibbeler. *Engineering Mechanics: Dynamics*. PRENTICE HALL, 2015.

[26] A. D. L. Humphris, M. J. Miles, and J. K. Hobbs. A mechanical microscope: High-speed atomic force microscopy. *Appl. Phys. Lett.*, 86(3):034106, 2005.

[27] N. Kodera, M. Sakashita, and T. Ando. Dynamic proportional-integral-differential controller for high-speed atomic force microscopy. *Rev. Sci. Instrum.*, 77(8):083704, 2006.

[28] M. A. Lantz, S. J. O'Shea, and M. E. Welland. Force microscopy imaging in liquids using ac techniques. *Appl. Phys. Lett.*, 65(4):409, 1994.

[29] S. R. Manalis, S. C. Minne, A. Atalar, and C. F. Quate. High-speed atomic force microscopy using an integrated actuator and optical lever detection. *Rev. Sci. Instrum.*, 67(9):3294, 1996.

[30] O. Marti, B. Drake, and P. K. Hansma. Atomic force microscopy of liquid-covered surfaces: Atomic resolution images. *Appl. Phys. Lett.*, 51(7):484, 1987.

[31] G. Meyer and N. M. Amer. Novel optical approach to atomic force microscopy. *Appl. Phys. Lett.*, 53(12):1045, 1988.

[32] N. Ookubo and S. Yumoto. Rapid surface topography using a tapping mode atomic force microscope. *Applied Physics Letters*, 74:2149, Apr 1999.

[33] G. T. Paloczi, B. L. Smith, P. K. Hansma, D. A. Walters, and M. A. Wendman. Rapid imaging of calcite crystal growth using atomic force microscopy with small cantilevers. *Applied Physics Letters*, 73:1658, Sep 1998.

[34] L. M. Picco, L. Bozec, A. Ulcinas, D. J. Engledew, M. Antognozzi, M. A. Horton, and M. J. Miles. Breaking the speed limit with atomic force microscopy. *Nanotechnology*, 18(4):044030, dec 2006.

[35] C. Putman, K. van der Werf, B. de Grooth, N. van Hulst, and J. Greve. Viscoelasticity of living cells allows high resolution imaging by tapping mode atomic force microscopy. *Biophysical Journal*, 67(4):1749–1753, oct 1994.

[36] C. A. J. Putman, K. O. Van der Werf, B. G. De Grooth, N. F. Van Hulst, and J. Greve. Tapping mode atomic force microscopy in liquid. *Appl. Phys. Lett.*, 64(18):2454, 1994.

[37] A. Research. Separating silicon probes from a wafer.

[38] J. E. Sader. Frequency response of cantilever beams immersed in viscous fluids with applications to the atomic force microscope. *Journal of Applied Physics*, 84(1):64, 1998.

[39] G. Schmalz. Über Glätte und Ebenheit als physikalisches und physiologisches Problem. *Verein Deutscher Ingenieure*, pages 1461–1467, Oct. 1929.

[40] K. L. Smith. On the Origins of the Quality Factor Q. *Quarterly Journal of the Royal Astronomical Society*, 27:695, Dec. 1986.

[41] T. Sulchek, R. Hsieh, J. D. Adams, S. C. Minne, C. F. Quate, and D. M. Adderton. High-speed atomic force microscopy in liquid. *Review of Scientific Instruments*, 71(5):2097, 2000.

[42] http://peacesoftware.de.

[43] M. van Es, J. Human, and H. Sadeghian. High speed imaging with the use of immersion AFM. Unpublished, 2015.

[44] C. A. Van Eysden and J. E. Sader. Resonant frequencies of a rectangular cantilever beam immersed in a fluid. *Journal of Applied Physics*, 100(11):114916, 2006.

[45] G. Watson. *A Treatise on the Theory of Bessel Functions*. Ca, 1995.

[46] E. W. Weisstein. "modified Bessel function of the second kind." from MathWorld–a Wolfram web resource.
http://mathworld.wolfram.com/ModifiedBesselFunctionoftheSecondKind.html.

[47] Q. Zhong, D. Inniss, K. Kjoller, and V. B. Elings. Fractured polymer/silica fiber surface studied by tapping mode atomic force microscopy. *Surface Science*, 290:L688–L692, Jun 1993.

[48] D. Ziegler and P. Ashby. Sensor for low force-noise detection in liquids, Sep 2014. US Patent App. 14/342,758.

[49] D. Ziegler, A. Klaassen, D. Bahri, D. Chmielewski, A. Nievergelt, F. Mugele, J. Sader, and P. Ashby. Encased cantilevers for low-noise force and mass sensing in liquids. In *Micro Electro Mechanical Systems (MEMS), 2014 IEEE 27th International Conference on*, pages 128–131, Jan 2014.

[50] Zurich Instruments. *UHFLI Lock-in Amplifier Product Specification*. Zurich Instruments, May 2015.

A

Explanations

Throughout this thesis, certain terms and functions, such as the resonance frequency or the hydrodynamical function, are used. These terms and functions are explained further in this Appendix. This to keep the main matter well organized.

A.1. First and second resonance frequency

The resonance frequency also known as the eigenfrequency is the frequency at which an object starts to resonate. At this frequency only a small external force is needed to obtain a maximum response amplitude. This can best be illustrated with a guitar string.

(a) First resonance frequency of a guitar sting. A half standing wave is clearly visible.

(b) Second resonance frequency of a guitar string. A whole standing wave can be seen here.

Figure A.1: First and second resonance frequencies in a guitar string, fixed on both sides.

When a note is played on a guitar, the sting starts to vibrate in it's resonance frequency (Figure A.1a). This is the frequency of the audible note. To change this tone, the tension of the string can be adjusted (tuning) or the string can be made shorter, when a note higher on the string is played. If the guitar string is excited very fast, near its second resonance frequency, it can produce a note twice as high (Figure A.1b). The same thing can be done with almost every object, although it might not always be audible. A beam clamped on one side for instance (Figure A.2). With the guitar string fixed on both sides there was a standing half wave visible. In the second resonance frequency a standing whole wave could be observed. When a beam, clamped on one side, vibrates at

(a) First resonance frequency of a beam fixed on one side. Unlike the sting fixed on both sides not even a half wave is visible.

(b) Second resonance frequency of a beam. At the point where the black and grey lines cross, there is no displacement, only rotation observed.

Figure A.2: First and second resonance frequencies in a beam, fixed on the left side.

the resonance frequency, not even one half of a standing wave can be observed (Figure A.2a). At the

second resonance frequency a little more then half a wave is visible (Figure A.2b). The AFM cantilever are very similar to a single side clamped beam. This means that the second resonance frequency is not double the frequency of the first. The theory states that the second resonance frequency is around 6.3 times the first frequency [25].

A.2. Hydrodynamic function

The hydrodynamic function is very helpful for predicting the behaviour of a cantilever, such as the Q-factor, in different mediums [38, 44, 21]. To calculate this function, first the normalized mode number (κ) of mode n has to be found:

$$\kappa_{\mathrm{n}} = C_{\mathrm{n}} \frac{b_{\mathrm{c}}}{l_{\mathrm{c}}}, \tag{A.1}$$

where b_{c} and l_{c} are the cantilevers width and length respectively. C_{n} is the nth positive root of:

$$1 + \cos C_{\mathrm{n}} \cosh C_{\mathrm{n}} = 0. \tag{A.2}$$

The normalized mode number is then used to make an approximation of the hydrodynamic function, known as the pade approximation (Γ_{pade}):

$$\Gamma_{\mathrm{pade}}(\kappa_{\mathrm{n}}) = \frac{1 + 0.74273\kappa_{\mathrm{n}} + 0.14862\kappa_{\mathrm{n}}^2}{1 + 0.74273\kappa_{\mathrm{n}} + 0.35004\kappa_{\mathrm{n}}^2 + 0.058364\kappa_{\mathrm{n}}^3}. \tag{A.3}$$

At the same time the resonance frequency in vacuum is calculated:

$$\omega_{\mathrm{vac,n}} = \frac{C_{\mathrm{n}}^2}{l_{\mathrm{c}}^2} \sqrt{\frac{E_{\mathrm{c}} I_{\mathrm{c}}}{\mu_{\mathrm{c}}}}, \tag{A.4}$$

where E_{c} and I_{c} are the Young's modulus and the moment of inertia of the cantilever. μ_{c} is the mass per length and is defined by $\mu_{\mathrm{c}} = \rho_{\mathrm{c}} \cdot b_{\mathrm{c}} \cdot h_{\mathrm{c}}$, the density, width and height of the cantilever respectively. The resonance frequency and the Pade approximation are used to determine the resonance frequency in $\mathrm{rad\,s^{-1}}$ ($\omega_{\mathrm{R,n}}$) of a specific medium R, where ρ_{R} is the density of the medium:

$$\omega_{\mathrm{R,n}} = \frac{\omega_{\mathrm{vac,n}}}{\sqrt{1 + \frac{\pi b_{\mathrm{c}} \rho_{\mathrm{R}}}{4 h_{\mathrm{c}} \rho_{\mathrm{c}}} \Gamma_{\mathrm{pade}}(\kappa_{\mathrm{n}})}}. \tag{A.5}$$

The resonance frequency is used to calculate the Reynolds number, here η_{R} is the viscosity of the medium as can be found in Table 2.2.

$$\mathrm{Re}_{\mathrm{R,n}} = \frac{\rho_{\mathrm{R}} \omega_{\mathrm{R,n}} b_{\mathrm{c}}}{4\eta_{\mathrm{R}}} \tag{A.6}$$

Next, the hydrodynamic function for circular bodies is calculated:

$$\Gamma_{\mathrm{circ}}(\omega_{\mathrm{R,n}}) = 1 + \frac{4i\ \mathrm{K}_1(-i\sqrt{i\ \mathrm{Re}_{\mathrm{R,n}}})}{\sqrt{i\ \mathrm{Re}_{\mathrm{R,n}}}\ \mathrm{K}_0(-i\sqrt{i\ \mathrm{Re}_{\mathrm{R,n}}})}. \tag{A.7}$$

This equation uses the Reynolds number for medium R ($\mathrm{Re}_{\mathrm{R,n}}$) and the modified Bessel function of the second kind (K_0, K_1). More on the modified Bessel function can found further in the appendix. To use the hydrodynamic function for a rectangular cantilever, it is multiplied by a correction factor $\Omega(\omega_{\mathrm{R,n}})$:

$$\Gamma(\omega) = \Omega(\omega)\ \Gamma_{\mathrm{circ}}(\omega) \tag{A.8}$$

with

$$\Omega(\omega) = \Omega_r(\omega) + i\Omega_i(\omega),$$

$$\begin{aligned}\Omega_r(\omega) =&(0.913242 - 0.48274\tau + 0.46842\tau^2 - 0.12886\tau^3\\ &+ 0.044055\tau^4 - 0.0035117\tau^5 + 0.00069085\tau^6)\\ &\times (1 - 0.56964\tau + 0.48690\tau^2 - 0.13444\tau^3\\ &+ 0.045155\tau^4 - 0.0035862\tau^5 + 0.00069085\tau^6)^{-1},\end{aligned} \tag{A.9}$$

$$\begin{aligned}\Omega_i(\omega) =&(-0.024134 - 0.029256\tau + 0.016294\tau^2 - 0.00010961\tau^3\\ &+ 0.000064577\tau^4 - 0.000044510\tau^5)\\ &\times (1 - 0.59702\tau + 0.55182\tau^2 - 0.18357\tau^3\\ &+ 0.079156\tau^4 - 0.014369\tau^5 + 0.0028361\tau^6)^{-1}\end{aligned} \tag{A.10}$$

and

$$\tau = \log_{10} \mathrm{Re}$$

With the help of this new rectangular hydrodynamic function the Q-factor can be obtained using the width of the cantilever (b_c), the mass per meter the (μ_c), and the density of the medium (ρ_R):

$$Q_{\mathrm{R,n}} = \frac{\frac{4\,\mu_\mathrm{c}}{\pi\,\rho_\mathrm{R}\,b_\mathrm{c}^2} + \Gamma_r(\omega_{\mathrm{R,n}})}{\Gamma_i(\omega_{\mathrm{R,n}})}. \tag{A.11}$$

A.2.1. Near surface hydrodynamic function

Near the surface the viscous damping effect changes. To model these effects, an alternative hydrodynamic function is used:

$$\Gamma(\omega) = \Gamma_r(\omega) + i\Gamma_i(\omega) \tag{A.12}$$

with

$$\begin{aligned}\Gamma_r(\omega) = a_0 &+ a_1\tau + a_2\tau^2 + a_3\tau^3 + a_4\tau^4 + a_5\tau^5\\ &+ a_6\tau^6 + a_7\tau^7 + a_8\tau^8 + a_9\tau^9 + a_{10}\tau^{10}\\ &+ a_{11}\tau^{11} + a_{12}\tau^{12} + a_{13}\tau^{13} + a_{14}\tau^{14} + a_{15}\tau^{15}\\ &+ a_{16}\tau^{16} + a_{17}\tau^{17} + a_{18}\tau^{18} + a_{19}\tau^{19} + a_{20}\tau^{20},\end{aligned} \tag{A.13}$$

$$\begin{aligned}\Gamma_i(\omega) = b_0 &+ b_1\tau + b_2\tau^2 + b_3\tau^3 + b_4\tau^4 + b_5\tau^5\\ &+ b_6\tau^6 + b_7\tau^7 + b_8\tau^8 + b_9\tau^9 + b_{10}\tau^{10}\\ &+ b_{11}\tau^{11} + b_{12}\tau^{12} + b_{13}\tau^{13} + b_{14}\tau^{14} + b_{15}\tau^{15}\\ &+ b_{16}\tau^{16} + b_{17}\tau^{17} + b_{18}\tau^{18} + b_{19}\tau^{19} + b_{20}\tau^{20}\end{aligned} \tag{A.14}$$

and

$$\tau = \log_{10} \mathrm{Re}.$$

This function, seen in Equations (A.12) to (A.14), uses values, experimentally obtained by Green *et.al.* [21] for a_n and b_n, these values can be found in Tables A.1 and A.2.

$$\overline{H} = \frac{h_0}{b_\mathrm{c}} \tag{A.15}$$

The values depend on the ratio $\overline{H}$,the ratio of the separation between the cantilever and the surface (h_0) to the width of the cantilever beam, seen in Equation (A.15). Using Equation (A.11), the Q-factor can be determined.

Table A.1: Coefficients a_n of $\Gamma_r(\omega)$, for variations of $\overline{H}$ [21].

Coefficient	$\overline{H}=0.1$	$\overline{H}=0.2$	$\overline{H}=0.3$	$\overline{H}=0.5$	$\overline{H}=1$
$a_0(\times10^{-1})$	7.5527	6.0895	5.5255	5.1365	5.1711
$a_1(\times10^{-1})$	−2.6135	−2.6693	−2.6899	−2.7059	−2.7351
$a_2(\times10^{-2})$	2.1140	3.1762	3.9445	4.6123	4.9510
$a_3(\times10^{-3})$	16.035	12.848	9.7839	7.1220	−3.6636
$a_4(\times10^{-3})$	4.9104	4.5226	1.1833	1.1513	−7.6334
$a_5(\times10^{-3})$	−3.6684	−3.9971	−2.8825	−2.4522	−0.47742
$a_6(\times10^{-3})$	−1.0236	−1.6638	0.40113	−0.93243	3.8343
$a_7(\times10^{-4})$	4.4735	7.2736	3.7138	−1.7136	5.9373
$a_8(\times10^{-4})$	1.8547	5.8761	−2.2353	2.6990	−9.0752
$a_9(\times10^{-4})$	−0.46932	−1.1135	−0.67274	1.8082	−2.0595
$a_{10}(\times10^{-5})$	−2.0912	−13.423	4.4878	−2.9764	12.360
$a_{11}(\times10^{-5})$	0.49126	1.1295	1.3039	−3.7621	3.6076
$a_{12}(\times10^{-6})$	1.4143	18.730	−4.5050	0.12916	−9.7998
$a_{13}(\times10^{-6})$	−0.46897	−0.61522	−1.5585	4.0217	−3.6271
$a_{14}(\times10^{-7})$	−0.68028	−16.002	2.1963	2.7441	4.0092
$a_{15}(\times10^{-7})$	0.31330	0.11642	1.0401	−2.4224	2.1263
$a_{16}(\times10^{-9})$	3.1539	81.887	−2.8498	−26.540	−3.5162
$a_{17}(\times10^{-9})$	−1.1679	0.28843	−3.6216	7.8073	−6.7705
$a_{18}(\times10^{-10})$	−1.2147	−23.084	−1.4891	10.634	−2.9943
$a_{19}(\times10^{-11})$	1.7914	−1.1380	5.1513	−10.491	9.0577
$a_{20}(\times10^{-12})$	2.1546	27.602	4.4301	−16.211	7.8032

Table A.2: Coefficients b_n of $\Gamma_i(\omega)$, for variations of $\overline{H}$ [21].

Coefficient	$\overline{H}=0.1$	$\overline{H}=0.2$	$\overline{H}=0.3$	$\overline{H}=0.5$	$\overline{H}=1$
$b_0(\times10^{-1})$	26.126	18.379	14.481	10.576	7.3610
$b_1(\times10^{-1})$	−9.9609	−9.8195	−9.6357	−9.1672	−8.2193
$b_2(\times10^{-2})$	0.25151	1.2814	2.3402	4.8949	8.9232
$b_3(\times10^{-2})$	0.17624	0.0068333	1.0713	1.1656	2.9049
$b_4(\times10^{-3})$	1.0613	−2.8251	2.0584	−3.6530	2.5960
$b_5(\times10^{-3})$	−0.64407	4.8823	−2.6861	3.0136	−8.1131
$b_6(\times10^{-3})$	−0.73114	3.9207	−1.0023	6.2433	−4.5414
$b_7(\times10^{-4})$	2.8566	−26.994	13.746	−2.9983	12.639
$b_8(\times10^{-4})$	3.3144	−19.600	7.2786	−25.331	13.671
$b_9(\times10^{-4})$	−0.42741	8.1574	−2.1997	−2.1997	−0.44895
$b_{10}(\times10^{-4})$	−0.78124	5.5755	−1.8264	5.1886	−2.1757
$b_{11}(\times10^{-5})$	−0.10744	−13.351	0.58630	6.5850	−1.7194
$b_{12}(\times10^{-5})$	1.0266	−9.1348	2.1870	−6.3176	1.9995
$b_{13}(\times10^{-6})$	1.1467	12.496	1.9639	−8.2988	3.0821
$b_{14}(\times10^{-7})$	−7.0985	88.408	−13.405	47.700	−10.225
$b_{15}(\times10^{-7})$	−1.3587	−6.7359	−2.3403	5.5350	−2.3243
$b_{16}(\times10^{-8})$	2.1533	−50.125	3.6467	−21.949	2.3257
$b_{17}(\times10^{-9})$	6.5746	19.518	10.491	−19.168	8.5909
$b_{18}(\times10^{-10})$	−0.28485	154.27	−0.45175	56.447	0.69316
$b_{19}(\times10^{-10})$	−1.1696	−2.3605	−1.7327	2.7181	−1.2711
$b_{20}(\times10^{-11})$	−0.82157	−19.935	−1.1795	−6.2262	−0.88792

A.3. Modified Bessel function of the second kind

The modified Bessel function of the second kind, also known as the modified Bessel function of the third kind ($K_n(x)$) is one of the solutions to the modified Bessel differential equation:

$$x^2 \frac{d^2y}{dx^2} + \frac{dy}{dx} - \left(x^2 + n^2\right) y = 0. \tag{A.16}$$

The solution can be written in the following form:

$$y = c_1 I_n(x) + c_2 K_n(x). \tag{A.17}$$

Where c_1 and c_2 are constants, $I_n(x)$ is the modified Bessel function of the first kind and $K_n(x)$ is the modified Bessel function of the second (or third) kind [46]. More on the Bessel functions can be found in "*A Treatise on the Theory of Bessel Functions*" [45]

A.4. Non dispersive infra-red CO_2 sensor

For the gas measurements a Non Dispersive Infra-Red (NDIR) sensor is used. It is the commonly used type of CO_2 sensor and works by directing an infra-red light through a tube filled with the air that needs to be measured, the measurement chamber. Particles in the measurement chamber all absorb a specific wavelength of the infra-red light depending on the size of the particle. At the end of the chamber there is an optical filter, which only allows light with the same wavelength as that is absorbed by CO_2 pass on to the detector behind it (Figure A.3). The light radiated by the source is compared to the light received by the detector. This is then converted into the gas concentration [1].

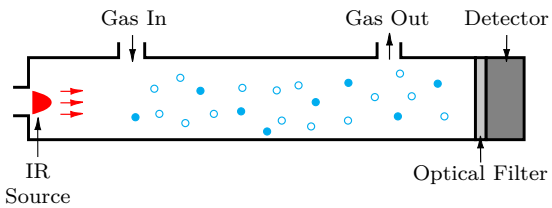

Figure A.3: Gas enters the measurement chamber of the NDIR sensor through the inlet. An infra-red light shines a beam across the chamber, the gas absorbs only a specific wavelength of the emitted light. The amount of remaining light at that wavelength is measured at the detector, this is then converted into a gas concentration[1].

B

Python Code

Two Python scripts are used to model the cantilevers behaviour and analyse the results. These scripts are added in the next pages. An explanation of the techniques used inside these scripts can be found in Chapter 2.

B.1. cantilever_model.py

Python Script B.1: cantilever_model.py

```
# -*- coding: utf-8 -*-
"""
Created on Wed May 10 10:13:21 2017

@author: rswuste
"""
import numpy as np
import sympy as sp
import scipy as sc

#%%
def model_co2(co2_concentration):
    import numpy as np
    co2perc = co2_concentration/100.
    MMn2 = 28.0134 # Molar Mass N2
    MMair= 28.97   # Molar Mass Air
    MMco2= 44.0095 # Molar Mass CO2
    Vn2     = 0.0000174997716 # Viscosity N2
    Vco2    = 0.0000145920975 # Viscosity CO2
    Vair    = 0.0000181329391 # Viscosity Air
    T = 291.15 # Room temperature
    R = 0.08205783 # Gas constant
    mixdn2  = ((1-co2perc)*MMn2 +co2perc*MMco2)/(T*R)
    mixdair = ((1-co2perc)*MMair+co2perc*MMco2)/(T*R)
    mixvn2  = ((1-co2perc)*Vn2 *np.sqrt(MMn2) +(co2perc)*Vco2*np.sqrt(MMco2))/((1-co2perc)*
        np.sqrt(MMn2) +(co2perc)*np.sqrt(MMco2))
    mixvair = ((1-co2perc)*Vair*np.sqrt(MMair)+(co2perc)*Vco2*np.sqrt(MMco2))/((1-co2perc)*
        np.sqrt(MMair)+(co2perc)*np.sqrt(MMco2))
    return(mixdn2,mixvn2,mixdair,mixvair)

#%%
def cantilever_model_free(co2_concentration):

    """ Load External parameters """
    rho_mix_n2, eta_mix_n2, rho_mix_air, eta_mix_air = model_co2(co2_concentration)

    """Parameters"""
    # @ T = 18C p = 1.013 bar
    # www.peacesoftware.de
    rho_c   = 2330.0        # [kg/m3]
    rho_air =    1.214      # [kg/m3]
    rho_liq =  998.6        # [kg/m3]
    rho_co2 =    1.852      # [kg/m3]
#    rho_sf6 =    6.6161      # [kg/m3]

    eta_air = 1.813e-5      # [Pa*s]
    eta_liq = 1.053e-3      # [Pa*s]
    eta_co2 = 1.459e-5      # [Pa*s]
#    eta_sf6 = 1.3771e-5      # [Pa*s]
    rho = rho_air, rho_co2, rho_liq, rho_mix_air, rho_mix_n2
    eta = eta_air, eta_co2, eta_liq, eta_mix_air, eta_mix_n2

    E       = 1.69e11       # [N/m^2]

    lx       = [115*1e-6, 90*1e-6,130*1e-6]
    bx       = [ 38*1e-6, 35*1e-6, 35*1e-6]
    hx       = [1.5*1e-6,2.0*1e-6,2.0*1e-6]


    # Create empty list
    model_solution_free = [0,0,0]
    for k in range (len(lx)):
        l = lx[k]
        b = bx[k]
        h = hx[k]
```

```python

        """Functions"""
        A       = b*h           # [m^2]
        mu      = rho_c*A       # [kg/m]
        I       = b*h**3/12

        """ Eigen Frequencys Higher Eigenmodes (VanEysden2006)"""
        x = sp.Symbol('x')
        f = sp.cos(x)*sp.cosh(x)+1
        bounds = lambda i: (3.14*i, 3.14*(i+1))
        root   = lambda i: sp.solvers.nsolve(f, bounds(i), solver='bisect', verify=False)

        n = 0                                   # n is the mode order
        C= [float(root(n))]                     # Cn is the nth positive root
        n = 1
        C.append(float(root(n)))

        Kappa      = [C_n * b/l for C_n in C]    # Normalized mode numbers
        Gamma_Pade = [(1+0.74273*K+0.14862*K**2)/(1+0.74273*K+0.35004*K**2+0.058364*K**3)
                        for K in Kappa]           # Pade Approximation

        w_vac      = [C_n**2/l**2 * np.sqrt(E*I/mu) for C_n in C]
        w_n        = [[(w_vac[i] *1/(np.sqrt((1+np.pi*rho[j]*b/(4*rho_c*h)*Gamma_Pade[i])))
            )
                        for i in range(len(Gamma_Pade))]for j in range(len(rho))]

        """Analitically found hydrodynamic function (Sader1998)"""
        Re         = [[rho[j]*w_n[j][i]*b**2/(4*eta[j])
                        for i in range(len(w_n[0]))] for j in range(len(w_n))]

        # eq. 18
        Gamma_circ = [[1+(4j* sc.special.kv(1,-1j* np.sqrt(1j*Re[j][i])))/
                      (np.sqrt(1j*Re[j][i]) * sc.special.kv(0,-1j* np.sqrt(1j* Re[j][i])))
                        for i in range(len(Re[0]))]for j in range(len(Re))]

        # eq. 22
        tau = [[np.log10(Re[j][i])
                        for i in range(len(Re[0]))] for j in range(len(Re))]

        # eq. 21
        Omega_r =    [[(0.91324  - 0.48274  *tau[j][i]    + 0.46842   *tau[j][i]**2 -
                                0.12886  *tau[j][i]**3 + 0.044055  *tau[j][i]**4 -
                                0.0035117*tau[j][i]**5 + 0.00069085*tau[j][i]**6)/ \
                       (1        - 0.56964  *tau[j][i]    + 0.48690   *tau[j][i]**2 -
                                0.13444  *tau[j][i]**3 + 0.045155  *tau[j][i]**4 -
                                0.0035862*tau[j][i]**5 + 0.00069085*tau[j][i]**6)
                                for i in range(len(tau[0]))] for j in range(len(tau))]


        Omega_i =    [[(-0.024134 - 0.029256   *tau[j][i]    + 0.016294   *tau[j][i]**2 -
                                 0.00010961 *tau[j][i]**3 + 0.000064577*tau[j][i]**4 -
                                 0.000044510*tau[j][i]**5)/ \
                       ( 1        - 0.59702    *tau[j][i]    + 0.55182    *tau[j][i]**2 -
                                 0.18357    *tau[j][i]**3 + 0.079156   *tau[j][i]**4 -
                                 0.014369   *tau[j][i]**5 + 0.0028361  *tau[j][i]**6)
                                 for i in range(len(tau[0]))] for j in range(len(tau))]

        Omega = [[Omega_r[j][i] + Omega_i[j][i] * 1j
                        for i in range(len(Omega_r[0]))] for j in range (len(Omega_r))]

        # eq. 20
        Gamma_rect = [[Omega[j][i] * Gamma_circ[j][i]
                        for i in range(len(Omega[0]))] for j in range(len(Omega))]

        w    = [[(w_vac[i] *1/(np.sqrt((1+np.pi*rho[j]*b/(4*rho_c*h)*Gamma_rect[j][i]))))
                        for i in range(len(w_vac))] for j in range(len(rho))]

        """ Convert solution """
        f = [[np.real(w[j][i])*0.5*1/np.pi/1000
                        for i in range(len(w[0]))] for j in range(len(w))] #rad/s -> kHz

```

```
        """ Q according to Sader (Sader1998)"""
        Q_sader = [[((4*mu)/(np.pi*rho[j]*b**2))+np.real(Gamma_rect[j][i]))/
                  (np.imag(Gamma_rect[j][i]))
                        for i in range(len(Gamma_rect[0]))] for j in range(len(Gamma_rect))
                            ]

        tc= [Q_sader[j][0]/(np.pi*f[j][0])
                        for j in range(len(f))]

        """ Write found solution to list """
        model_solution_free[k]= [f,Q_sader,tc]

    return(model_solution_free)


#%%
def cantilever_model_near_surface(co2_concentration):

    import numpy as np
    import sympy as sp

    """ Load External parameters """
    rho_mix_n2, eta_mix_n2, rho_mix_air, eta_mix_air = model_co2(co2_concentration)

    """Parameters"""
    # @ T = 18C p = 1.013 bar
    # www.peacesoftware.de
    rho_c   = 2330.0        # [kg/m3]
    rho_air =    1.214      # [kg/m3]
    rho_liq =  998.6        # [kg/m3]
    rho_co2 =    1.852      # [kg/m3]

    eta_air = 1.813e-5      # [Pa*s]
    eta_liq = 1.053e-3      # [Pa*s]
    eta_co2 = 1.459e-5      # [Pa*s]

    rho = rho_air, rho_co2, rho_liq, rho_mix_air, rho_mix_n2
    eta = eta_air, eta_co2, eta_liq, eta_mix_air, eta_mix_n2

    E       = 1.69e11       # [N/m^2]

    lx       = [110*1e-6, 90*1e-6,125*1e-6]
    bx       = [ 35*1e-6, 35*1e-6, 32*1e-6]
    hx       = [2.0*1e-6,2.0*1e-6,1.5*1e-6]

    aH0_1 = 7.5527e-1 , -2.6135e-1 ,  2.1140e-2 , 16.035e-3   ,  4.9104e-3 , -3.6684e-3  \
         , -1.0236e-3 ,  4.4735e-4 ,  1.8547e-4 , -0.46932e-4 , -2.0912e-5 ,  0.49126e-5 \
         ,  1.4143e-6 , -0.46897e-6, -0.68028e-7,  0.31330e-7 ,  3.1539e-9 , -1.1679e-9  \
         , -1.2147e-10,  1.7914e-11,  2.1546e-12

    aH0_2 = 6.0895e-1 , -2.6693e-1 ,  3.1762e-2 , 12.848e-3   ,  4.5226e-3 , -3.9971e-3  \
         , -1.6638e-3 ,  7.2736e-4 ,  5.8761e-4 , -1.1135e-4  ,-13.423e-5  ,  1.1295e-5  \
         , 18.730e-6  , -0.61522e-6,-16.002e-7  ,  0.11642e-7 , 81.887e-9  ,  0.28843e-9 \
         ,-23.084e-10 , -1.1380e-11, 27.602e-12

    aH0_3 = 5.5255e-1 , -2.6899e-1 ,  3.9445e-2 ,  9.7839e-3  ,  1.1833e-3 , -2.8825e-3  \
         ,  0.40113e-3,  3.7138e-4 , -2.2353e-4 , -0.67274e-4 ,  4.4878e-5 ,  1.3039e-5  \
         , -4.5050e-6 , -1.5585e-6 ,  2.1963e-7 ,  1.0401e-7  , -2.8498e-9 , -3.6216e-9  \
         , -1.4891e-10,  5.1513e-11,  4.4301e-12

    aH0_5 = 5.1365e-1 , -2.7059e-1 ,  4.6123e-2 ,  7.1220e-3  ,  1.1513e-3 , -2.4522e-3  \
         , -0.93243e-3, -1.7136e-4 ,  2.6990e-4 ,  1.8082e-4  , -2.9764e-5 , -3.7621e-5  \
         ,  0.12916e-6,  4.0217e-6 ,  2.7441e-7 , -2.4224e-7  ,-26.540e-9  ,  7.8073e-9  \
         , 10.634e-10 ,-10.491e-11 ,-16.211e-12

    aH1   = 5.1711e-1 , -2.7351e-1 ,  4.9510e-2 , -3.6636e-3  , -7.6334e-3 , -0.47742e-3 \
         ,  3.8343e-3 ,  5.9373e-4 , -9.0752e-4 , -2.0595e-4  , 12.360e-5  ,  3.6076e-5  \
         , -9.7998e-6 , -3.6271e-6 ,  4.0092e-7 ,  2.1263e-7  , -3.5162e-9 , -6.7705e-9  \
         , -2.9943e-10,  9.0577e-11,  7.8032e-12

    aH    = aH0_1, aH0_2, aH0_3, aH0_5, aH1
```

```
    bH0_1 = 26.126e-1   , -9.9609e-1 ,  0.25151e-2 ,  0.17624e-2  ,  1.0613e-3  , -0.64407e-3 \
          , -0.73114e-3 ,  2.8566e-4 ,  3.3144e-4  , -0.42741e-4  , -0.78124e-4 , -0.10744e-5 \
          ,  1.0266e-5  ,  1.1467e-6 , -7.0985e-7  , -1.3587e-7   ,  2.1533e-8  ,  6.5746e-9  \
          , -0.28485e-10, -1.1696e-10, -0.82157e-11

    bH0_2 = 18.379e-1   , -9.8195e-1 ,  1.2814e-2  ,  0.0068333e-2, -2.8251e-3  ,  4.8823e-3  \
          ,  3.9707e-3  ,-26.994e-4  ,-19.600e-4   ,  8.1574e-4   ,  5.5755e-4  ,-13.351e-5  \
          , -9.1348e-5  , 12.496e-6  , 88.408e-7   , -6.7359e-7   ,-50.125e-8   , 19.518e-9  \
          ,154.27e-10   , -2.3605e-10,-19.935e-11

    bH0_3 = 14.481e-1   , -9.6357e-1 ,  2.3402e-2  ,  1.0713e-2   ,  2.0584e-3  , -2.6861e-3  \
          , -1.0023e-3  , 13.746e-4  ,  7.2786e-4  , -2.1997e-4   , -1.8264e-4  ,  0.58630e-5 \
          ,  2.1870e-5  ,  1.9639e-6 ,-13.405e-7   , -2.3403e-7   ,  3.6467e-8  , 10.491e-9  \
          , -0.45175e-10, -1.7327e-10, -1.1795e-11

    bH0_5 = 10.576e-1   , -9.1672e-1 ,  4.8949e-2  ,  1.1656e-2   , -3.6530e-3  ,  3.0136e-3  \
          ,  6.2433e-3  , -2.9983e-4 ,-25.331e-4   , -2.1997e-4   ,  5.1886e-4  ,  6.5850e-5  \
          , -6.3176e-5  , -8.2988e-6 , 47.700e-7   ,  5.5350e-7   ,-21.949e-8   ,-19.168e-9  \
          , 56.447e-10  ,  2.7181e-10, -6.2262e-11

    bH1   =  7.3610e-1  , -8.2193e-1 ,  8.9232e-2  ,  2.9049e-2   ,  2.5960e-3  , -8.1131e-3  \
          , -4.4514e-3  , 12.639e-4  , 13.671e-4   , -0.44895e-4  , -2.1757e-4  , -1.7194e-5  \
          ,  1.9995e-5  ,  3.0821e-6 ,-10.225e-7   , -2.3243e-7   ,  2.3257e-8  ,  8.5909e-9  \
          ,  0.69316e-10, -1.2711e-10, -0.88792e-11

    bH      = bH0_1, bH0_2, bH0_3, bH0_5, bH1
    # Create empty list
    model_solution_near_surface = [0,0,0]
    for ii in range (len(lx)):
        l = lx[ii]
        b = bx[ii]
        h = hx[ii]
        # @ T = 18C p = 1.013 bar
        # www.peacesoftware.de

        """Functions"""
        A       = b*h           # [m^2]
        mu      = rho_c*A       # [kg/m]
        I       = b*h**3/12

        """ Eigen Frequencys Higher Eigenmodes (VanEysden2006)"""
        x = sp.Symbol('x')
        f = sp.cos(x)*sp.cosh(x)+1
        bounds = lambda i: (3.14*i, 3.14*(i+1))
        root   = lambda i: sp.solvers.nsolve(f, bounds(i), solver='bisect', verify=False)

        n = 0                                   # n is the mode order
        C= [float(root(n))]                     # Cn is the nth positive root
        n = 1
        C.append(float(root(n)))

        Kappa      = [C_n * b/l for C_n in C]    # Normalized mode numbers
        Gamma_Pade = [(1+0.74273*K+0.14862*K**2)/(1+0.74273*K+0.35004*K**2+0.058364*K**3)
                      for K in Kappa]           # Pade Approximation
```

```
        w_vac       = [C_n**2/l**2 * np.sqrt(E*I/mu) for C_n in C]
        w_n         = [[(w_vac[i] *1/(np.sqrt((1+np.pi*rho[j]*b/(4*rho_c*h)*Gamma_Pade[i])))
            )
                        for i in range(len(Gamma_Pade))]for j in range(len(rho))]

        """Analitically found hydrodynamic function (Sader1998)"""
        Re          = [[rho[j]*w_n[j][i]*b**2/(4*eta[j])
                        for i in range(len(w_n[0]))] for j in range(len(w_n))]

        # eq. 22
        tau = [[np.log10(Re[j][i])
                        for i in range(len(Re[0]))] for j in range(len(Re))]


        Gamma_rect_r =    [[[aH[i][00] +
                            aH[i][ 1]*tau[k][j]** 1 + aH[i][ 2]*tau[k][j]** 2 +
                            aH[i][ 3]*tau[k][j]** 3 + aH[i][ 4]*tau[k][j]** 4 +
                            aH[i][ 5]*tau[k][j]** 5 + aH[i][ 6]*tau[k][j]** 6 +
                            aH[i][ 7]*tau[k][j]** 7 + aH[i][ 8]*tau[k][j]** 8 +
                            aH[i][ 9]*tau[k][j]** 9 + aH[i][10]*tau[k][j]**10 +
                            aH[i][11]*tau[k][j]**11 + aH[i][12]*tau[k][j]**12 +
                            aH[i][13]*tau[k][j]**13 + aH[i][14]*tau[k][j]**14 +
                            aH[i][15]*tau[k][j]**15 + aH[i][16]*tau[k][j]**16 +
                            aH[i][17]*tau[k][j]**17 + aH[i][18]*tau[k][j]**18 +
                            aH[i][19]*tau[k][j]**19 + aH[i][20]*tau[k][j]**20
                          for i in range(len(aH))]
                          for j in range(len(tau[k]))]
                          for k in range(len(tau))]

        Gamma_rect_i =    [[[bH[i][00] +
                            bH[i][ 1]*tau[k][j]** 1 + bH[i][ 2]*tau[k][j]** 2 +
                            bH[i][ 3]*tau[k][j]** 3 + bH[i][ 4]*tau[k][j]** 4 +
                            bH[i][ 5]*tau[k][j]** 5 + bH[i][ 6]*tau[k][j]** 6 +
                            bH[i][ 7]*tau[k][j]** 7 + bH[i][ 8]*tau[k][j]** 8 +
                            bH[i][ 9]*tau[k][j]** 9 + bH[i][10]*tau[k][j]**10 +
                            bH[i][11]*tau[k][j]**11 + bH[i][12]*tau[k][j]**12 +
                            bH[i][13]*tau[k][j]**13 + bH[i][14]*tau[k][j]**14 +
                            bH[i][15]*tau[k][j]**15 + bH[i][16]*tau[k][j]**16 +
                            bH[i][17]*tau[k][j]**17 + bH[i][18]*tau[k][j]**18 +
                            bH[i][19]*tau[k][j]**19 + bH[i][20]*tau[k][j]**20
                          for i in range(len(bH))]
                          for j in range(len(tau[k]))]
                          for k in range(len(tau))]


        Gamma_rect =     [[[Gamma_rect_r[k][i][j] + Gamma_rect_i[k][i][j] * 1j
                          for j in range(len(Gamma_rect_i[k][0]))]
                          for i in range(len(Gamma_rect_i[k]))]
                          for k in range(len(Gamma_rect_i))]

        w     = [[[(w_vac[i] *1/(np.sqrt((1+np.pi*rho[k]*b/(4*rho_c*h)*Gamma_rect[k][i][j]))
            ))
                          for j in range(len(Gamma_rect[k][0]))]
                          for i in range(len(Gamma_rect[k]))]
                          for k in range(len(Gamma_rect))]

        f = [[np.real(w[k][i])*0.5*1/np.pi/1000
            for i in range(len(w[k]))]
            for k in range(len(w))] #rad/s -> kHz

        """ Q according to Sader (Sader1998)"""
        Q_sader = [[[(((4*mu)/(np.pi*rho[k]*b**2))+np.real(Gamma_rect[k][i][j]))/
                    ((np.imag(Gamma_rect[k][i][j])))
                    for j in range(len(Gamma_rect[k][0]))]
                    for i in range(len(Gamma_rect[k]))]
                    for k in range(len(Gamma_rect))]

        tc= [Q_sader[k][0]/(np.pi*f[k][0])
            for k in range(len(f))]
        """ Write found solution to list """
        model_solution_near_surface[ii]= [f,Q_sader,tc]
```

```
    return(model_solution_near_surface)
#%%
def find_nearest(array,value):
    idx = (np.abs(array-value)).argmin()
    return idx
#%%
def error_spread():
    Res_co2_1=[[[0  ,120.295622809, 123.466959591,  114.822326318,  100.045902277,
        116.811478923],
     [50 ,172.975269313,    184.066244631,  144.875389043,  115.352548686,  170.146852324],
     [75 ,124.247033676,    135.596953957,  111.871968029,  91.373871583,   110.840840654],
     [90 ,116.815163622,    110.463485273,  125.276784653,  102.56988139,   107.794360412],
     [95 ,148.837723968,    127.187646749,  149.959725463,  166.455628467,  115.858421952],
     [100,146.865651569,    153.562734874,  144.330415692,  120.399723186,
         131.508034541]],
    [[0  ,169.839684535,    171.345626632,  127.67314695,   174.083758074,  156.775987934],
     [50 ,207.037939316,    198.077597837,  178.688638408,  204.836238225,  200.640725489],
     [75 ,196.868301678,    170.862167085,  134.319559804,  178.752377608,  197.31361203],
     [90 ,190.832772872,    136.863293235,  151.236688102,  190.25651204,   185.838691412],
     [97 ,200.729652653,    161.315831341,  187.622205279,  217.538644364,  184.602515261],
     [100,183.142507334,    178.271233331,  186.855338409,  177.763905622,
         190.232784141]],
    [[0  , 95.2947005312, 99.379562964,  87.5265442787, 72.5452364614, 88.1807180896],
     [30 , 99.8001761898, 91.7432610419,100.474440923,  106.276642051,   81.9071591909],
     [50 ,137.439579717,    112.319643697,1058.00820042,    212.804768613,  150.981972163],
     [75 ,154.300433204, 138.56113602,  116.027343808,  88.5317058927,123.077747246],
     [95 , 95.1594700457, 96.6448724359, 94.7335034497, 93.3864130742, 89.4025026889],
     [100, 99.401354358,  99.8035149052,100.856749834, 111.399368268,  88.6912324833]]]
    Dif_A=np.zeros([3,6,4])
    X_data_tot = [[]]
    Y_data_tot = [[]]
    Y_max_tot = [[]]
    Y_min_tot = [[]]
    for j in range(len(Res_co2_1)):
        Y_max=[]
        Y_min=[]
        X_data=[]
        Y_data=[]
        for i in range(len(Res_co2_1[j])):

            Dif_A[j][i]=[Res_co2_1[j][i][2]-Res_co2_1[j][i][1],Res_co2_1[j][i][3]-Res_co2_1
                [j][i][1],Res_co2_1[j][i][4]-Res_co2_1[j][i][1],Res_co2_1[j][i][5]-
                Res_co2_1[j][i][1]]
            if Dif_A[j][i].max() <= 0:
                Y_max.append(0)
            else:
                Y_max.append(Dif_A[j][i].max())
            Y_min.append(abs(Dif_A[j][i].min()))
            X_data.append(Res_co2_1[j][i][0])
            Y_data.append(Res_co2_1[j][i][1])
        if j == 0:
            X_data_tot[0]=X_data
            Y_data_tot[0]=Y_data
            Y_max_tot[0]=Y_max
            Y_min_tot[0]=Y_min
        else:
            X_data_tot.append(X_data)
            Y_data_tot.append(Y_data)
            Y_max_tot.append(Y_max)
            Y_min_tot.append(Y_min)

    Res_co2_2=[[[0  ,158.967232848  ,157.810549112  ,164.022112006  ,167.0204407
        ,149.040908953],
    [2  ,162.429926356  ,178.189746107  ,143.043845405  ,164.712618544  ,173.992881447],
    [12 ,161.141647976  ,168.970073842  ,165.214623893  ,160.135146482  ,151.983236144],
    [21 ,156.610875081  ,157.4608092    ,150.587864771  ,153.685566568  ,167.123122543],
    [30 ,157.556793277  ,154.596120332  ,153.098371014  ,155.364023753  ,168.407881082],
    [50 ,155.684643502  ,163.056285486  ,157.051913991  ,151.38983572   ,151.952365603],
    [60 ,148.645814382  ,144.846485006  ,142.753655845  ,152.560388738  ,155.035110094],
    [77 ,151.449850691  ,158.951537843  ,157.612999624  ,146.261944782  ,145.255395677],
```

```
    [85 ,153.92443319   ,154.983500708  ,153.445659883  ,157.788558724  ,153.154375338],
    [90 ,147.271699428  ,147.428290758  ,153.04578639   ,142.128335619  ,146.949826631],
    [100    ,160.541484297  ,164.694093836  ,158.076345848  ,157.417338366
        ,162.085257358]],
    [[0,    139.075863012   ,147.142313733  ,140.041904334  ,130.167982038
        ,139.780813922],
    [14,    150.302506281   ,151.985486465  ,155.755712403  ,144.542346757
        ,148.772112796],
    [22,    144.438066418   ,139.270458869  ,139.088311871  ,153.253020264
        ,148.309849191],
    [30, 146.451701363  ,150.280997139  ,143.890818037  ,143.419297812  ,149.105377572],
    [40,    151.91514118    ,158.50735685   ,150.381638088  ,145.214822249
        ,154.273810785],
    [53,    140.392092509   ,138.837221364  ,133.648035275  ,141.511294664
        ,147.798453987],
    [62,    32.3562603805   ,34.2486980813  ,32.6100064291  ,29.9677747451
        ,33.8675683063],
    [70,    26.1176668089   ,27.8327836777  ,22.5023557625  ,24.8601837223
        ,30.0602804682],
    [80,    24.2281497892   ,23.1719000329  ,21.8948165478  ,26.6184120859
        ,25.6475835771],
    [90,    21.2423328579   ,15.8811095851  ,13.3344320422  ,28.2413255869
        ,26.1678941562],
    [98,    21.7410113003   ,25.6549148646  ,19.9351657648  ,19.130607513
        ,22.4194656513],
    [100    ,25.2438459642  ,20.3908632253  ,303.015319405  ,499.195966421
        ,21.2094812878],
    [100    ,34.6754422763  ,254.40563334   ,28.5113044682  ,27.9922130084
        ,474.421109933]]]
    Dif_A_2=np.zeros([2,13,4])
    X_data_tot_2 = [[]]
    Y_data_tot_2 = [[]]
    Y_max_tot_2 = [[]]
    Y_min_tot_2 = [[]]
    for j in range(len(Res_co2_2)):
        Y_max=[]
        Y_min=[]
        X_data=[]
        Y_data=[]
        for i in range(len(Res_co2_2[j])):

            Dif_A_2[j][i]=[Res_co2_2[j][i][2]-Res_co2_2[j][i][1],Res_co2_2[j][i][3]-
                Res_co2_2[j][i][1],Res_co2_2[j][i][4]-Res_co2_2[j][i][1],Res_co2_2[j][i
                ][5]-Res_co2_2[j][i][1]]
            if Dif_A_2[j][i].max() <= 0:
                Y_max.append(0)
            else:
                Y_max.append(Dif_A_2[j][i].max())
            Y_min.append(abs(Dif_A_2[j][i].min()))
            X_data.append(Res_co2_2[j][i][0])
            Y_data.append(Res_co2_2[j][i][1])
        if j == 0:
            X_data_tot_2[0]=X_data
            Y_data_tot_2[0]=Y_data
            Y_max_tot_2[0]=Y_max
            Y_min_tot_2[0]=Y_min
        else:
            X_data_tot_2.append(X_data)
            Y_data_tot_2.append(Y_data)
            Y_max_tot_2.append(Y_max)
            Y_min_tot_2.append(Y_min)
    return([[X_data_tot,Y_data_tot,Y_min_tot,Y_max_tot],[X_data_tot_2,Y_data_tot_2,
        Y_min_tot_2,Y_max_tot_2]])
```

B.2. Data_analysis.py

Python Script B.2: Data_analysis.py

```
# -*- coding: utf-8 -*-
"""
Created on Tue May 09 13:01:25 2017

@author: Rolf
"""

#%%
""" Initialize """
import cantilever_model as model
import numpy as np
import scipy.signal
import scipy as sc
import ast
import pickle as pl

import os
#import copy
import glob2  # Help localizing files
from scipy.optimize import curve_fit
import matplotlib.pyplot as plt
from matplotlib import interactive
interactive(True)
plt.close()

def Es(x,amp,f0 ,Q, noise):
    return amp * f0**4 / ( (x**2 - f0**2)**2 + (x*f0/Q)**2 ) + noise

#%%
""" Set Parameters """
# Set ask for parameters, or accept given

# CO2 Concentration model
co2_concentration = np.linspace(0,100,11) # 0...100 in 11 steps

# Colors
color_tu = '#00a6d6'
color_bl = '#000000'
color_gr = '#a4a4a4'
color_rd = '#ff0000'
color_1_4= '#ff8000'
color_2_4= '#ff00ff'
color_3_4= '#0000ff'
color_4_4= '#00ff00'

# Set region to analyze
Search_lowerbound_preset = 75.    # kHz
Search_upperbound_preset = 300.   # kHz
Search_meankernel = 3     # Size of the smoothing kernel
Search_toppercent = 0.2   # Precent to show around the top

# Measurement file extention
ext_txt = 'txt'
ext_bb  = 'BB'

# Select Output
Run_Model  = 1
Run_Exp    = 0
Dev_Mode   = 0
Dev_Resume = 0
Dev_BB     = 0
Show_error = 0
SaveVar    = 0
MakeTable  = 0
MakePDF    = 0
```

```
MakePGF     = 0
MakeOverv   = 0

# Higher Harmonics
hh = 2 #[1,2,3]
Measurement_files_marked=[]
#%% Set Mode Model or Experiment
""" Model """

if Run_Model == 1:
    # Find Q-factor in free air
    model_output_free = model.cantilever_model_free(co2_concentration)
    # Output [Cantilever][Output(f,Q,tc)][Medium(Air,CO2,Liq,mixair,mixn2)][Mode(1,2)]
    # Find Q-factor near surface
    model_output_near_surface = model.cantilever_model_near_surface(co2_concentration)
    # Output [Cantilever][Output(f,Q,tc)][Medium(Air,CO2,Liq,mixair,mixn2)][Mode(1,2)][dist]

#%%
""" Experiment """
if Run_Exp ==1:

    Measurement_maps     = glob2.glob("../*")[0:-3]
    print '\n'.join(Measurement_maps)
    if Dev_Mode == 1:
        Selected_map_number = 3
    else:
        Selected_map_number = raw_input('Choose data set [1-'+
                                        str(len(Measurement_maps))+']')
    Selected_map         = Measurement_maps[int(Selected_map_number)-1]
    if Dev_BB == 1:
        ext = ext_bb
    else:
        ext = ext_txt

    Measurement_files    = [os.path.basename(x)
            for x in glob2.glob(str(Selected_map)+"/**"+str(ext))]
    #Filename_files_no_ext     = Measurement_files[0][:-4]
    #Filename_full             = Measurement_files[0]

    # Open Log file
    if Dev_Resume != 1:
        h = open("..\\Data Overview\\"+str(Selected_map[3:])+".dat","w")
        h.writelines(str(Selected_map[3:])+"\n \n")
        h.close()
        Resume_loop = 0
    else:
        Resume_loop = i

    for i in range (len(Measurement_files[Resume_loop:])):
        Filename_files_no_ext     = Measurement_files[Resume_loop+i][:-4]
        Filename_full             = Measurement_files[Resume_loop+i]

        print str(i+1)+" of "+str(len(Measurement_files[Resume_loop:]))
        print (Filename_files_no_ext)
        if Dev_BB == 1:
            Measurement_data = np.genfromtxt(str(Selected_map)+
                                        '/'+str(Filename_full) ,comments='%', delimiter="\t")
            Measurement_data_kfreq = Measurement_data[:,0]
        else:
            Measurement_data = np.genfromtxt(str(Selected_map)+
                                        '/'+str(Filename_full) ,comments='%', delimiter=";")
            Measurement_data_freq     = Measurement_data[:,0]
            Measurement_data_kfreq    = Measurement_data_freq/1e3

        Measurement_data_V        = Measurement_data[:,1]
        Measurement_data_uV       = Measurement_data_V*1e6
        Search_upperbound = Search_upperbound_preset
        Search_lowerbound = Search_lowerbound_preset
```

```
        if Measurement_data_kfreq.max() <= Search_upperbound:
            Search_upperbound = Measurement_data_kfreq.max()
        if Measurement_data_kfreq.min() >= Search_lowerbound:
            Search_lowerbound = Measurement_data_kfreq.min()

        """ Finding Peaks """
        Search_smooth       = sc.signal.medfilt(Measurement_data_uV, Search_meankernel)
        Search_cutoff_low   = np.where(Measurement_data_kfreq<=Search_lowerbound)[0]
        Search_cutoff_high  = np.where(Measurement_data_kfreq>=Search_upperbound)[0]
        Search_searchdom    = np.where(Search_smooth==Search_smooth
                                [Search_cutoff_low[-1]:Search_cutoff_high[0]].max())[0]
        Search_lowsearch    = int(Search_searchdom[0]*(1-Search_toppercent))
        Search_highsearch   = int(Search_searchdom[-1]*(1+Search_toppercent))

        """ Fitting data """
        Fit_full_Vmax       = Measurement_data_uV[Search_searchdom].max()
        Fit_full_Fcal       = Measurement_data_kfreq[Search_searchdom].max()
        Fit_full_Vhalf      = Fit_full_Vmax / np.sqrt(2)
        Fit_full_Vhalf_index= (Search_smooth[Search_lowsearch:Search_highsearch]>
                                Fit_full_Vhalf).nonzero()
        Fit_full_Vhalf_max  = Fit_full_Vhalf_index[0].max()
        Fit_full_Vhalf_min  = Fit_full_Vhalf_index[0].min()
        Fit_full_freqminmax = (Measurement_data_kfreq
                                    [Search_lowsearch:Search_highsearch]
                                    [Fit_full_Vhalf_max]-
                                    Measurement_data_kfreq
                                    [Search_lowsearch:Search_highsearch]
                                    [Fit_full_Vhalf_min])
        Fit_full_Qcal       = Fit_full_Fcal/Fit_full_freqminmax
        Fit_full_baseline   = Measurement_data_uV.min()
        Fit_full_p0         = np.array([Fit_full_Vmax/Fit_full_Qcal**2,
                                        Fit_full_Fcal,
                                        Fit_full_Qcal,
                                        Fit_full_baseline],
                                        dtype=np.double)
        Plot_Xlim = [Measurement_data_kfreq[Search_lowsearch], Measurement_data_kfreq[
            Search_highsearch]]
        Plot_Ylim = [0,Fit_full_Vmax+20]
        Fit_full_good = 'N'
        while Fit_full_good != 'Y' and Fit_full_good != 'y':
            Search_lowsearch = model.find_nearest(Measurement_data_kfreq,Plot_Xlim[0])
            Search_highsearch= model.find_nearest(Measurement_data_kfreq,Plot_Xlim[1])
            Fit_full_popt, Fit_full_pcov  = curve_fit(Es,
                            Measurement_data_kfreq[Search_lowsearch:Search_highsearch],
                            Measurement_data_uV[Search_lowsearch:Search_highsearch],
                            p0       = Fit_full_p0,
                            maxfev   = 200000,
                            bounds =(0,[np.inf,np.inf,np.inf,np.inf]))
            Fit_full_freqspace = np.linspace(Measurement_data_kfreq[Search_lowsearch],
                                             Measurement_data_kfreq[Search_highsearch],
                                             3000)
            Fit_full_eq_opt = Es(Fit_full_freqspace,
                            Fit_full_popt[0],
                            Fit_full_popt[1],
                            Fit_full_popt[2],
                            Fit_full_popt[3])
            Fit_full_eq_p0 = Es(Fit_full_freqspace,
                            Fit_full_p0[0],
                            Fit_full_p0[1],
                            Fit_full_p0[2],
                            Fit_full_p0[3])
            Fit_full_eq_optfull =  Es(Measurement_data_kfreq,
                            Fit_full_popt[0],
                            Fit_full_popt[1],
                            Fit_full_popt[2],
                            Fit_full_popt[3])


            print 'p0  =',Fit_full_p0,'\npopt=',Fit_full_popt
            Plot_full = plt.figure()
            plt.subplot(2,1,1)
```

```
            plt.grid(which='major')
            plt.plot(Measurement_data_kfreq,
                     Measurement_data_uV,
                     '-',
                     color = color_bl,
                     alpha=1,
                     linewidth=0.5,
            #         markersize = 3,
                     label='Measured Data')

            plt.plot(Measurement_data_kfreq,
                     Fit_full_eq_optfull,
                     '-',
                     color = color_tu,
                     alpha=1,
                     linewidth=1,
                     label='Fitted Data')

            plt.xlabel("Frequency (kHz)")
            plt.xlim([Measurement_data_kfreq.min(), Measurement_data_kfreq.max()])
            plt.ylim([0,Fit_full_Vmax+20])
            plt.ylabel("Amplitude (uV)")
            plt.legend(loc=1)

            plt.subplot(2,1,2)
            plt.grid(which='major')
            plt.plot(Fit_full_freqspace,
                     Fit_full_eq_p0,
                     '--',
                     color = color_rd,
                     alpha=1,
                     linewidth=2,
                     label='Initial guess')
            plt.plot(Fit_full_freqspace,
                     Fit_full_eq_opt,
                     '-',
                     color = color_tu,
                     alpha=1,
                     linewidth=2,
                     label='Fitted Data')
            plt.plot(Measurement_data_kfreq[Search_lowsearch:Search_highsearch],
                     Measurement_data_uV[Search_lowsearch:Search_highsearch],
                     '.',
                     color = color_bl,
                     alpha=1,
                     markersize = 3,
                     label='Measured Data')
            plt.xlim(Plot_Xlim)
            plt.ylim(Plot_Ylim)
            plt.xlabel("Frequency (kHz)")
            plt.ylabel("Amplitude (uV)")
            plt.legend(loc=1)
            plt.pause(1)
            Plot_settings = raw_input('press return to continue [s,m]')
            if Plot_settings =='S' or Plot_settings=='s':
                Plot_Xlim = ast.literal_eval(raw_input('X-lim[min,max]') or str(Plot_Xlim))
                Plot_Ylim = ast.literal_eval(raw_input('Y-lim[min,max]') or str(Plot_Ylim))
            elif  Plot_settings =='M' or Plot_settings=='m':
                Measurement_files_marked.append(str(Filename_full))
            if Dev_Mode == 1:
                Fit_full_good = 'Y'
                plt.close()
            else:
                Fit_full_good    = raw_input('Good? [Y-N]') or 'Y'
                if Fit_full_good!= 'Y' and Fit_full_good !='y':
                    plt.close()
                    Fit_full_p0_t    = raw_input('Set new P0'+str(Fit_full_p0)) or ('['+
                    str(Fit_full_p0[0])+','+str(Fit_full_p0[1])+','+
                    str(Fit_full_p0[2])+','+str(Fit_full_p0[3])+']')
                    Fit_full_p0 = np.array(ast.literal_eval(Fit_full_p0_t))
                else:
```

```
                    if MakePDF == 1:
                        plt.savefig(str(Selected_map)+"\\Data Overview\\"+
                                    str(Filename_files_no_ext)+"-Full.pdf",bbox_inches='tight')
                    pl.dump(Plot_full,file(str(Selected_map)+"\\Data Overview\\"+
                                           str(Filename_files_no_ext)+"-Full.pickle","w"))
                    plt.close()

        Fit_1_4_popt, Fit_full_pcov  = curve_fit(Es,
                        Measurement_data_kfreq[Search_lowsearch:Search_highsearch][0::4],
                        Measurement_data_uV[Search_lowsearch:Search_highsearch][0::4],
                        p0       = Fit_full_popt,
                        maxfev   = 200000,
                        bounds =(0,[np.inf,np.inf,np.inf,np.inf]))
        Fit_2_4_popt, Fit_full_pcov  = curve_fit(Es,
                        Measurement_data_kfreq[Search_lowsearch:Search_highsearch][1::4],
                        Measurement_data_uV[Search_lowsearch:Search_highsearch][1::4],
                        p0       = Fit_full_popt,
                        maxfev   = 200000,
                        bounds =(0,[np.inf,np.inf,np.inf,np.inf]))
        Fit_3_4_popt, Fit_full_pcov  = curve_fit(Es,
                        Measurement_data_kfreq[Search_lowsearch:Search_highsearch][2::4],
                        Measurement_data_uV[Search_lowsearch:Search_highsearch][2::4],
                        p0       = Fit_full_popt,
                        maxfev   = 200000,
                        bounds =(0,[np.inf,np.inf,np.inf,np.inf]))
        Fit_4_4_popt, Fit_full_pcov  = curve_fit(Es,
                        Measurement_data_kfreq[Search_lowsearch:Search_highsearch][3::4],
                        Measurement_data_uV[Search_lowsearch:Search_highsearch][3::4],
                        p0       = Fit_full_popt,
                        maxfev   = 200000,
                        bounds =(0,[np.inf,np.inf,np.inf,np.inf]))

        Fit_1_4_eq_opt = Es(Fit_full_freqspace,
                        Fit_1_4_popt[0],
                        Fit_1_4_popt[1],
                        Fit_1_4_popt[2],
                        Fit_1_4_popt[3])
        Fit_2_4_eq_opt = Es(Fit_full_freqspace,
                        Fit_2_4_popt[0],
                        Fit_2_4_popt[1],
                        Fit_2_4_popt[2],
                        Fit_2_4_popt[3])
        Fit_3_4_eq_opt = Es(Fit_full_freqspace,
                        Fit_3_4_popt[0],
                        Fit_3_4_popt[1],
                        Fit_3_4_popt[2],
                        Fit_3_4_popt[3])
        Fit_4_4_eq_opt = Es(Fit_full_freqspace,
                        Fit_4_4_popt[0],
                        Fit_4_4_popt[1],
                        Fit_4_4_popt[2],
                        Fit_4_4_popt[3])

        print '1 popt=',Fit_1_4_popt,' \n2 popt=',Fit_2_4_popt,' \n3 popt=',Fit_3_4_popt,' \n4 popt=',Fit_4_4_popt

        Plot_4 = plt.figure()

        plt.grid(which='major')

        plt.plot(Fit_full_freqspace,
                 Fit_1_4_eq_opt,
                 '-',
                 color = color_1_4,
                 alpha=0.5,
                 linewidth=1,
                 label='Fitted 1/4')
        plt.plot(Fit_full_freqspace,
                 Fit_2_4_eq_opt,
                 '-',
```

```
                color = color_2_4,
                alpha=0.5,
                linewidth=1,
                label='Fitted 2/4')
        plt.plot(Fit_full_freqspace,
                Fit_3_4_eq_opt,
                '-',
                color = color_3_4,
                alpha=0.5,
                linewidth=1,
                label='Fitted 3/4')
        plt.plot(Fit_full_freqspace,
                Fit_4_4_eq_opt,
                '-',
                color = color_4_4,
                alpha=0.5,
                linewidth=1,
                label='Fitted 4/4')
        plt.plot(Fit_full_freqspace,
                Fit_full_eq_opt,
                '-',
                color = color_tu,
                alpha=1,
                linewidth=2,
                label='Fitted Data')
        plt.plot(Measurement_data_kfreq[Search_lowsearch:Search_highsearch],
                Measurement_data_uV[Search_lowsearch:Search_highsearch],
                '-',
                color = color_bl,
                alpha=1,
                linewidth= 0.5,#    markersize = 3,
                label='Measured Data')
        plt.xlabel("Frequency (kHz)")
        plt.xlim(Plot_Xlim)
        plt.ylim(Plot_Ylim)
        plt.ylabel("Amplitude (uV)")
        plt.legend(loc=1)
        plt.pause(1)
        Plot_4_check = raw_input('press return to continue[m]')
        if  Plot_4_check =='M' or Plot_4_check=='m':
            Measurement_files_marked.append(str(Filename_full))
        if MakePDF == 1:
            plt.savefig(str(Selected_map)+"\\Data Overview\\"+
                        str(Filename_files_no_ext)+"-Parts.pdf",bbox_inches='tight')
        pl.dump(Plot_4,file(str(Selected_map)+"\\Data Overview\\"+
                            str(Filename_files_no_ext)+"-Parts.pickle","w"))
        plt.close()
        Plot_zoom = plt.figure(1,figsize=(9,4.0))
        plt.title("Termal Spectrum")
        plt.grid(which='major')
        plt.plot(Fit_full_freqspace,
                Fit_full_eq_p0,
                '--',
                color = color_rd,
                alpha=1,
                linewidth=2,
                label='Initial guess')
        plt.plot(Fit_full_freqspace,
                Fit_full_eq_opt,
                '-',
                color = color_tu,
                alpha=1,
                linewidth=2,
                label='Fitted Data')
        plt.plot(Measurement_data_kfreq[Search_lowsearch:Search_highsearch],
                Measurement_data_uV[Search_lowsearch:Search_highsearch],
                '.',
                color = color_bl,
                alpha=1,
                markersize = 3,
                label='Measured Data')
```

```
        plt.xlabel("Frequency (kHz)")
        plt.xlim(Plot_Xlim)
        plt.ylim(Plot_Ylim)
        plt.ylabel("Amplitude (uV)")
        plt.legend(loc=1)
        plt.pause(1)
        Plot_zoom_check = raw_input('press return to continue[m]')
        if  Plot_zoom_check =='M' or Plot_zoom_check=='m':
                    Measurement_files_marked.append(str(Filename_full))
        if MakePDF == 1:
            plt.savefig(str(Selected_map)+"\\Data Overview\\"+
                        str(Filename_files_no_ext)+"-Zoom.pdf",bbox_inches='tight')
        pl.dump(Plot_zoom,file(str(Selected_map)+"\\Data Overview\\"+
                               str(Filename_files_no_ext)+"-Zoom.pickle","w"))
        plt.close()

        # Write data to file
        g = open(str(Selected_map)+"\\Data Overview\\"+str(Filename_files_no_ext)+".dat","w")
        g.writelines(str(Filename_files_no_ext)+"\n \n")
        g.writelines("\n")
        g.writelines("Full Data set\n")
        g.writelines("p0: \t"+ str(Fit_full_p0)+"\n")
        g.writelines("popt: \t"+str(Fit_full_popt)+"\n")
        g.writelines("\n")
        g.writelines("popt 1: \t"+str(Fit_1_4_popt)+"\n")
        g.writelines("popt 2: \t"+str(Fit_2_4_popt)+"\n")
        g.writelines("popt 3: \t"+str(Fit_3_4_popt)+"\n")
        g.writelines("popt 4: \t"+str(Fit_4_4_popt)+"\n\n")
        g.writelines("Q f: \t"+str(Fit_full_popt[2])+" F:\t"+str(Fit_full_popt[1])+"\n")
        g.writelines("Q 1: \t"+str(Fit_1_4_popt[2])+" F:\t"+str(Fit_1_4_popt[1])+"\n")
        g.writelines("Q 2: \t"+str(Fit_2_4_popt[2])+" F:\t"+str(Fit_2_4_popt[1])+"\n")
        g.writelines("Q 3: \t"+str(Fit_3_4_popt[2])+" F:\t"+str(Fit_3_4_popt[1])+"\n")
        g.writelines("Q 4: \t"+str(Fit_4_4_popt[2])+" F:\t"+str(Fit_4_4_popt[1])+"\n")
        g.close()

        h = open("..\\Data Overview\\"+str(Selected_map[3:])+".dat","a")
        h.writelines(str(Filename_full)+"\n")
        h.writelines("\t f \t \t 1 \t \t 2 \t \t 3 \t \t 4\n")
        h.writelines("Q:\t"+str(Fit_full_popt[2])+"\t"+str(Fit_1_4_popt[2])+"\t"+str(Fit_2_4_popt[2])+
                "\t"+str(Fit_3_4_popt[2])+"\t"+str(Fit_4_4_popt[2])+"\n")
        h.writelines("F:\t"+str(Fit_full_popt[1])+"\t"+str(Fit_1_4_popt[1])+"\t"+str(Fit_2_4_popt[1])+
                "\t"+str(Fit_3_4_popt[1])+"\t"+str(Fit_4_4_popt[1])+"\n\n")
        h.close()

    print 'done!'

#%%
""" Data Output """

# Data model
if Run_Model == 1:
    # Find Q-factor in free air
    model_output_free
    # Output [Cantilever][Output(f,Q,tc)][Medium(Air,CO2,Liq,mixair,mixn2)][Mode(1,2)][co2]

    model_output_near_surface
    # Output [Cantilever][Output(f,Q,tc)][Medium(Air,CO2,Liq,mixair,mixn2)][Mode(1,2)][dist][co2]
    #    Fitdata = '#00a6d6'
    plt.show()
    plt.figure(figsize=(9,5))
    plt.title('test')
    plt.grid(which='major')
    plt.plot(co2_concentration,model_output_free[0][1][4][0], '-',color = color_bl, alpha=1, linewidth=0.5, label='CO2 concentration')
    plt.plot(co2_concentration,model_output_near_surface[0][1][4][0][0], '-',color = color_bl, alpha=1, linewidth=0.5, label='H0.1')
```

```
    plt.plot(co2_concentration,model_output_near_surface[0][1][4][0][1], '-',color = color_bl, alpha=1, linewidth=0.5, label='H0.2')
    plt.plot(co2_concentration,model_output_near_surface[0][1][4][0][2], '-',color = color_bl, alpha=1, linewidth=0.5, label='H0.3')
    plt.plot(co2_concentration,model_output_near_surface[0][1][4][0][3], '-',color = color_bl, alpha=1, linewidth=0.5, label='H=0.5')
    plt.plot(co2_concentration,model_output_near_surface[0][1][4][0][4], '-',color = color_bl, alpha=1, linewidth=0.5, label='H=1')
    plt.xlabel("CO2 concentration")
    plt.xlim([0,100])
    plt.ylim([0,200])
    plt.ylabel("Q Factor")
    plt.legend(loc=1)

if Show_error ==1:
    Exp_co2_1,Exp_co2_2 = model.error_spread()
    X_data_1,Y_data_1,Y_data_min_1,Y_data_max_1 = Exp_co2_1
    X_data_2,Y_data_2,Y_data_min_2,Y_data_max_2 = Exp_co2_2

    plt.show()
    Plot_error_1 = plt.figure(figsize=(9,5))
    plt.title('test')
    plt.grid(which='major')
    plt.errorbar(X_data_1[0],Y_data_1[0],[Y_data_min_1[0],Y_data_max_1[0]], color = color_bl,label = 'A')
    plt.errorbar(X_data_1[1],Y_data_1[1],[Y_data_min_1[1],Y_data_max_1[1]], color = color_rd,label = 'B')
    plt.errorbar(X_data_1[2],Y_data_1[2],[Y_data_min_1[2],Y_data_max_1[2]], color = color_tu,label = 'C')


    plt.xlabel("CO2 concentration")
    plt.xlim([0,100])
    plt.ylim([50,300])
    plt.ylabel("Q Factor")
    plt.legend(loc=1)
    plt.pause(1)
    raw_input("Press enter to continue...")
    if MakePDF == 1:
        plt.savefig("..\\Data Overview\\errorplot_1.pdf",bbox_inches='tight')
        pl.dump(Plot_error_1,file("..\\Data Overview\\errorplot_1.pickle","w"))
    plt.close()
    plt.show()

    Plot_error_2 = plt.figure(figsize=(9,5))
    plt.title('test')
    plt.grid(which='major')
    plt.errorbar(X_data_2[0],Y_data_2[0],[Y_data_min_2[0],Y_data_max_2[0]],fmt='.', color = color_tu,label = 'Free')
    plt.errorbar(X_data_2[1],Y_data_2[1],[Y_data_min_2[1],Y_data_max_2[1]],fmt='.', color = color_bl,label = 'On Surface')


    plt.xlabel("CO2 concentration")
    plt.xlim([0,100])
    plt.ylim([140,175])
    plt.ylabel("Q Factor")
    plt.legend(loc=3)
    plt.pause(1)
    raw_input("Press enter to continue...")
    if MakePDF == 1:
        plt.savefig("..\\Data Overview\\errorplot_2.pdf",bbox_inches='tight')
        pl.dump(Plot_error_1,file("..\\Data Overview\\errorplot_2.pickle","w"))
    plt.close()
```

C

Specifications

The measurements performed in this thesis require a lot of equipment. The specifications of this equipment is, where possible and/or relevant, added in this Appendix. The supplied information comes directly from the manufacturers.

C.1. Anfatec AFM

The Anfatec Level AFM – a short description

Atomic Force Microscopy - approved devices for affordable prices

Our system is complete for almost all typical applications. It provides all basic modes as:

- high resolution contact mode
- high resolution dynamic mode (non-contact mode) with simultaneous phase acquisition
- lateral force mode (friction mode)

but also some more enhanced experiments like

- force spectroscopy
- Magnetic Force Microscopy (2nd trace imaging) – without special cantilevers & samples
- Electrical Force Microscopy (2nd trace imaging) – without special cantilevers & samples
- Nano-Lithography with script-language
- Elastic Force Microscopy (Force Modulation Mode)

and can be ordered with options for EFM (2nd 6-phase lock-in amplifier) and conduction AFM.

The instrument is a complete working AFM with full support and service!
It is as easy to handle, as a laser deflection AFM can be. We provide a fast, cost effective and uncomplicated support for our systems. With all systems, we give a personal 8 h introduction. The operation modes are demonstrated at your samples to make the start-up easy for you.

System parameters:

lateral resolution:	< 1 nm (practical resolution) technical resolution: 0.19 nm (18 bit achieved technical resolution) mathematical resolution: 32 Bit (< 0.1 pm)
height resolution:	< 150 pm noise floor in DNC (atomic steps and layers) technical resolution: 0.026 nm (18 bit achieved technical resolution)
maximum scan range:	50 µm (standard, others possible on request), z-range: 6 µm
maximum sample size:	4 cm x 6 cm
manual positioning range:	5 mm x 5 mm
accessories:	15 cantilevers; 1 calibration grating UMG01 20 sample holders; 2 sample boxes, tweezers

The system consists of:

- a base plate made from stone with wiring
- vibration isolation
- microscope base:
  - ☑ 3 integrated miniaturized stepper motors for head levelling
  - ☑ lateral coarse positioning with 6 mm travel range
  - ☑ self-adjustable grooves (head always in same position)
  - ☑ calibrated scanner (about 30 µm range)
  - ☑ electrical contact to sample (can be used for Electrical Force Microscopy)
- standard AFM-head
  - ☑ laser diode maximum 3 mW, 670 nm with lens system
  - ☑ laser adjustment in <u>three</u> axis
  - ☑ integrated 4-quadrant photo-detector with amplifier electronics

- ☑ adjustment of the laser beam onto the photo detector in two directions (X, Y)
- ☑ built-in dither piezo for acoustical excitation in dynamic mode
- ☑ integrated illumination
- ☑ color-camera with microscope optic with a direct view onto the cantilever
- ☑ uncomplicated mounting of the cantilever chips

- control electronics consisting of:
  - ☑ low-noise high voltage amplifier V45E (1 pm noise floor)
  - ☑ dual DSP controlling system incl. DS4L-Module with Interface to the AMU 2.x
  - ☑ control of the level station
  - ☑ 8 x 24-bit D/A and 8 x 24-bit A/D channels
  - ☑ switchable laser power
- control computer:
  - ☑ typically: up-to-date AMD-processor based modern system
  - ☑ TFT monitor(s)
  - ☑ USB video camera
  - ☑ installed software: Windows XP Prof.,
    Anfatec Scan with GNU GPL, Anfatec Present, Curve, Acrobat, OpenOffice
- Anfatec Measurement Interface **AMU 2.x** (PCI bus board with integrated LockIn amplifier)
- tools: 1 calibration grating UMG01, 1 start-up set of cantilevers (15 pcs.), connection cables
- English or German manual, certain tutorials for NC AFM, contact AFM, Force Spectroscopy, LFM, Scanner calibration
- Special features:
  - ➢ software- or hardware-linearisation and calibration of the scanner
  - ➢ mixed frequency board AMU2.x with better signal to noise ratio
  - ➢ 2nd trace imaging for MFM
  - ➢ 2nd internal LockIn amplifier for integrated Kelvin feedback and EFM imaging

Microscope Mechanics

The mechanics consists of three main parts: the base plate, the “body” and the “head”.
The head holds the cantilever simply by a spring loaded mechanism. It needs no glue or cantilever holder and can work with all commercially available cantilevers, even high-frequency cantilevers. All electronic components for laser and photo diode, a specialized lens and mirror system and fine mechanics are integrated in the head.

Additionally, a small CCD camera with top-view onto the tip is mounted on the head. The camera image shows directly the cantilever from the top. LED light, whose intensity is adjustable, illuminates the tip and the sample.

The base plate provides the electrical connections and allows to bring the whole system under a vacuum bell jar. This can minimize acoustical coupling from the environment and enables to work under protection gas.

The body is heavy and hangs vibration damped above the base plate. It includes all tools for coarse positioning and the scanner in 5 mm by 5 mm range. Usually, the x and y coarse movement is done manually with a travel range of 5 mm. Three stepper motors allow to position the head in three degrees of freedom.

Sample holder and Scanner

The scanner is a tripod-type and scans the sample, while the tip is mounted in the head. The sample is mounted on a steel plate on three small magnets. Possible samples sizes are up to 2 cm by 2 cm, however, bigger samples are possible, too. There are two new linearisation modes for the scanners available: a software-mode and a hardware mode. The maximum scan range is 50 µm.

Applications

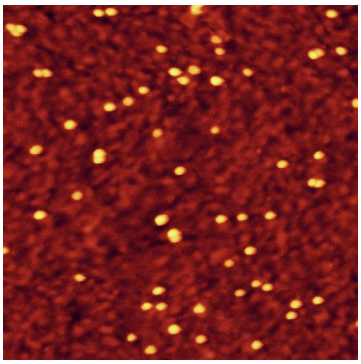

← 30 nm gold clusters on a gold surface
Scan range: 2 µm. Height scale: 36 nm.
Sample: University of Karlsruhe, Dr. U. Plutowski

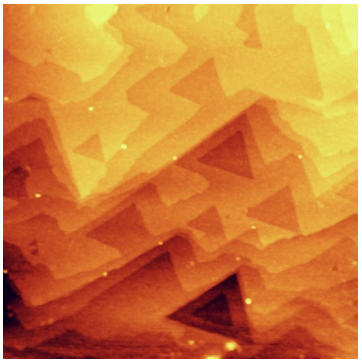

atomic steps on a hydrogen passivated Si(111)-surface →
Image range: 1 µm x 1 µm; height scale: 2.6 nm
Sample: Hahn-Meitner Insitute Berlin, Dr. H. Angermann

Control System

- up-to-date PC with Windows XP UK English Professional Edition
- high-quality and high-speed LockIn-amplifier on PCI-board
- dual DSP control with a fast data interface to the SPM-control unit

Electronic control

The system is provided with a HV amplifier V45E and a high performance SPM control unit:

- 8 channel – 24 Bit A/D (4 used for AFM, 2 additional used for hardware linearisation option)
- 8 channel – 24 Bit D/A (4 pre-specified for AFM)
- motor control
- head control
- fast digital interface to the PC

SOFTWARE

The Software works under NT based Windows systems (typically: multilingual Windows XP).

- Image Acquisition Software "Anfatec Scan" (GPL licence)
- Image Evaluation Software "Anfatec Present"

Anfatec Scan

- ☑ Simultaneous acquisition of up to 8 external channels + height image + LockIn channels + 8 external channels from a second basis module
- ☑ forward-trace images, backward trace images and 2nd trace images
- ☑ software feedback (PI type) with 6 different feedback modes
- ☑ free parameter input during scan
- ☑ images saved in Anfatec file format (read by Anfatec Present and SPIP[1]) and unscaled as Bitmap
- ☑ distance spectroscopy / voltage spectroscopy
- ☑ coarse positioning
- ☑ automatic approach
- ☑ switching between dynamic mode and contact mode
- ☑ adaptable to almost every hardware due to
  - ☑ free scalability of all channels in physical units
  - ☑ software offset correction
  - ☑ invert-channel-option
- ☑ user settings are saved in an initialization file

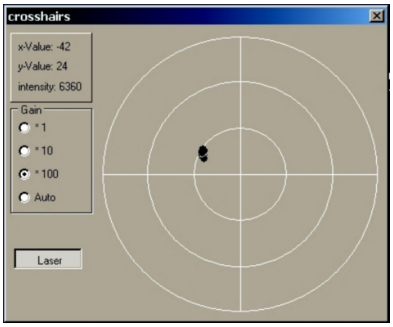

All functions are easy to select by menu buttons. A time-scaled oscilloscope provides observation of all input channels. A *Crosshairs* window (see figure) makes the adjustment of the laser for AFM easy.

Anfatec Present

- diverse filter functions (high pass, low pass, Fourier, noise, ..)
- enhanced line and plane correction with various selection options
- data import and export
- shows scan information
- histogram for brightness & contrast
- variable colour palettes
- **3D view**

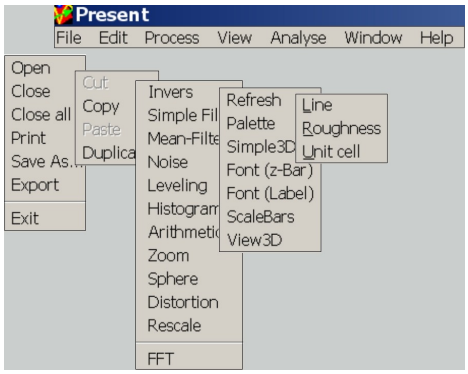

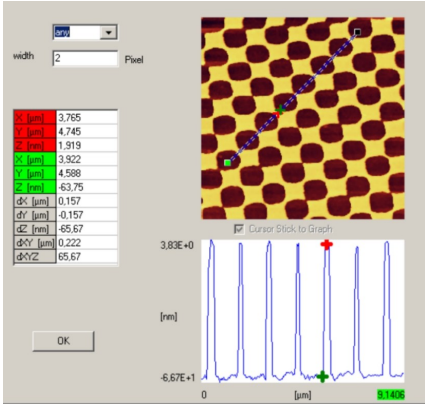

- line and **roughness analysis**
- automated unit cell detection and averaging
- copy and save functions to other programs

Lock-In-Amplifier on the AMU2.x

Signal Input

Voltage Input	SMB
Input Impedance	1 MΩ
Damage Threshold	> +/- 12 V
Bandwidth	dc to > 1 MHz (3 dB bandwidth)
Full Scale Sensitivity	7 V, 0.7 V, 70 mV
Input Noise:	
@ 100 kHz, high dynamic	< 2 $\mu V/\sqrt{Hz}$
@ 100 kHz, normal dynamic	< 0,4 $\mu V/\sqrt{Hz}$
@ 100 kHz, low dynamic	< 10 $nV/\sqrt{Hz}$

Reference Output

Internal Oscillator	3 mHz .. 1 MHz
Frequency Resolution	3 mHz
Frequency Accuracy	+/- 50 ppm from 0°C to 70 °C
Reference Output Voltage	< 1 mVpp ... max. 20 Vpp
Output Noise @ 100 kHz for 7 V_{rms} output	160 $nV/\sqrt{Hz}$

Scanner:

Maximum range in z-direction:	6 µm +/- 0.3 µm / 150V
Maximum range in x- and y-direction:	50 µm
technical resolution in x- und y-direction:	0,9 nm
technical resolution in z-direction:	0,034 nm
achieved resolution:	about 5 nm
achieved resolution z-direction:	< 0.2 nm

Optional features (not necessary for standard applications):

- Vibration isolation table under the microscope
- Hardware scanner linearisation
- Glass bell jar for acoustic protection
- Additional cantilever packages and gratings
- enhanced LFM mode sensitivity due to a spot-like laser diode
- additional LockIn amplifier for dynamic EFM or MFM
- implemented Kelvin feedback
- current amplifier for conductance AFM incl. power supply
- SPIP – Scanning Probe Image Processor - with all costumer specific modules from Imaging Metrology
- 2nd TFT monitor

C.2. Bruker Dimension FastScan AFM

Dimension FastScan Specifications

Parameter	Icon AFM Scanner	FastScan AFM Scanner
X-Y scan range	90µm x 90µm typical, 85µm minimum	35µm x 35µm typical, 30µm minimum
Z range	10µm typical in imaging and force curve modes, 9.5µm minimum	≥3µm
Vertical noise floor	<30pm RMS, height in appropriate environment, typical imaging BW (up to 625Hz)	<40pm RMS, sensor in appropriate environment (up to 625Hz)
X-Y tip-velocity max. (1% tracking error)	—	>2mm/Sec
Z tip-velocity max.	—	12mm/Sec
X-Y position noise (closed-loop)	≤0.15nm RMS typical imaging BW (up to 625Hz)	≤0.20nm RMS typical imaging BW (up to 2.5kHz in Adaptive)
Z sensor noise level	35pm RMS typical imaging BW (up to 625Hz); 50pm RMS force curve BW (0.1Hz to 5kHz)	30pm RMS typical imaging BW (up to 625Hz)
X-Y flatness (30µm range)	—	≤3nm
Integral nonlinearity (X-Y-Z)	<0.50%	≤0.50%
Sample size/holder	210mm vacuum chuck for samples ≤210mm in diameter, ≤15mm thick	
Motorized position stage: X & Y axis	150mm × 180mm inspectable area with rotating chuck; 2µm repeatability, unidirectional; 3µm repeatability, bidirectional	
Microscope optics	5MP digital camera; 180µm to 1465µm viewing area; digital zoom and motorized focus	5MP digital camera; 130µm to 1040µm viewing area; digital zoom and motorized focus
Controller/Software	NanoScope V/ NanoScope v8.15 and later	
Workstation	Integrates NanoScope V, Stage Controller, HV Amplifiers, computer and provides an ergonomic design with immediate physical and visual access	
Vibration and Acoustic isolation	Integrated, refer to installation requirements for additional information	
AFM Modes	**Standard:** ScanAsyst, TappingMode (air), Contact Mode, Lateral Force Microscopy, PhaseImaging, Lift Mode, MFM, Force Spectroscopy, Force Volume, EFM, Surface Potential, Piezoresponse Microscopy, Force Spectroscopy **Optional:** PeakForce QNM, PeakForce Tuna, HarmoniX, Nanoindentation, Nanomanipulation, Nanolithograpy, Force Modulation (air/fluid), TappingMode (fluid), Torsional Resonance Mode, Dark Lift, STM, SCM, C-AFM, SSRM, TUNA, TR-TUNA, VITA	**Standard:** ScanAsyst, Nanomechanical Mapping, TappingMode (air), TappingMode (fluid), PhaseImaging, Contact Mode, Lateral Force Microscopy, Lift Mode, MFM, EFM, Force Spectroscopy, Force Volume **Optional:** Nanoindentation, Nanomanipulation, Nanolithograpy, Surface Potential, Piezoresponse Microscopy
EH&S compliance	CE certified	

© 2011 Bruker Corporation. B077, Rev. A2

Cover images
Foreground: Dimension FastScan AFM.
Background: (left) Phase image and (right) Topography of Closed-loop 4µm AFM survey scan of SPP-PEO, 60Hz scan rate and 256x256 pixel density.

Bruker Nano Surfaces Division is continually improving its products and reserves the right to change specifications without notice. Broadband, Dimension, FastScan, Icon, PhaseImaging, TappingMode, LiftMode, HarmoniX, ScanAsyst, PeakForce QNM and NanoScope are trademarks of Bruker Corporation. All other trademarks are the property of their respective companies.

Bruker Nano Surfaces Division
Santa Barbara, CA USA
Phone +1.805.967.1400/800.873.9750
productinfo@bruker-nano.com

www.bruker.com

C.3. Zurich Instruments UHFLI Lock-in Amplifier

UHFLI
Lock-in Amplifier

Zurich Instruments

2 Input Channel, 2 Generator,
600 MHz Digital Lock-in Amplifier

Product Specification
Release date: May 2015

Key Features

- 600 MHz operation frequency
- 2 independent lock-in units
- 2 high-performance signal generators
- 4 independent harmonics per lock-in unit
- High-resolution 12-bit scope with 65k samples
- FRA frequency response analyzer
- FFT spectrum analyzer with 5 MHz span
- LabOne support for Windows and Linux

Summary

The Zurich Instruments UHFLI is a completely digital lock-in amplifier with 1.8 GSa/s sampling rate at its signal inputs and signal generators. It operates in the frequency range up to 600 MHz, features the lowest time constant in the market and consequently provides unmatched performance for the most demanding applications.

The UHFLI combines 2 lock-in amplifiers, 2 signal generators, 1 oscilloscope, 1 frequency response analyzer and a powerful FFT spectrum analyzer in 1 box. Moreover, the instrument also supports sweeping of several internal parameters. This unprecedented integration is capable of replacing a full set of instruments, thus simplifying ever more complex instrumentation setups.

With the increasing requirements of research applications, the UHFLI has the capability to become the most desired multi-functional instrument in any research laboratory. The wide frequency range, the ultra-wide demodulation bandwidth and the best-in-class dynamic reserve make this instrument a new standard in the test and measurement market.

Zurich Instruments equips all its instruments with extended platform programmability: virtually any programming language can be used for remote control, including LabVIEW, MATLAB, C, and Python. Linux and any Windows version later than XP are supported.

Description

High-precision Inputs

Operating in single ended mode, the 2 signal inputs of the UHFLI provide excellent noise specifications. It is possible to work with high impedance for low frequency and with 50 Ω impedance for high-speed applications. 2 input and 2 bidirectional connectors enable the external reference mode and precise triggering on external events. Dual internal and dual-auto reference modes are also supported.

Signal Generators

The UHFLI generates 2 low-distortion sinusoid outputs ideally capable to drive the device under test or most modulating devices. With the UHF-MF multi-frequency option 6 additional oscillators are provided, and it is possible to generate a linear combination of up to 8 independent sinusoids.

Additional connectors on the front panel carry demodulated samples, square wave references or signal to trigger external hardware.

Demodulators and Filters

Eight dual-phase demodulators for simultaneous measurement at 4 harmonic frequencies per signal input are provided. Each demodulator can be configured with its own filter properties and phase shift and demodulated samples are streamed in real-time to the host computer.

Specifications

General

dimensions	45 x 35 x 10 cm (19” rack) 17.7 x 13.6 x 3.9 inch
weight	6.4 kg
power supply	100-240 V, 50/60 Hz
connectors	BNC on front panel SMA on back panel

UHF signal inputs

frequency range	DC - 600 MHz
input impedance	50 Ω or 1 MΩ || 18 pF
input voltage noise	4 nV/√Hz (> 100 kHz)
dynamic reserve	100 dB
input full range sensitivity	1 nV to 1.5 V
A/D conversion	12 bit, 1.8 GSa/s

UHF signal generators

frequency range	DC - 600 MHz
output ranges	±150 mV, ±1.5 V (high-Z) -12.5 dBm, 7.5 dBm (50 Ω)
D/A conversion	14 bit, 1.8 GSa/s

Demodulators and reference

number of demodulators	8 dual-phase
output sample rate	1GbE: 1.6 MSa/s (max) USB: 400 kSa/s (max) Aux outputs: 28 MSa/s
time constant	30 ns to 76 s
measurement bandwidth	80 µHz to 5 MHz
filter slope (dB/Oct)	6, 12, 18, 24, 30, 36, 42, 48
reference phase res.	1.0 µ°
reference frequency res.	6 µHz
reference and trigger	2 bidirectional, 2 input, 2 output connectors

Auxiliary and others

auxiliary outputs	4 channels, ±10 V, amplitude, phase, X, Y, frequency, value
auxiliary inputs	2 channels, ±10 V
PC connectivity	10GbE optical (option) 1GbE USB 2.0 480 MBit
clock	10 MHz input and output
digital I/O	32 bit, bidirectional

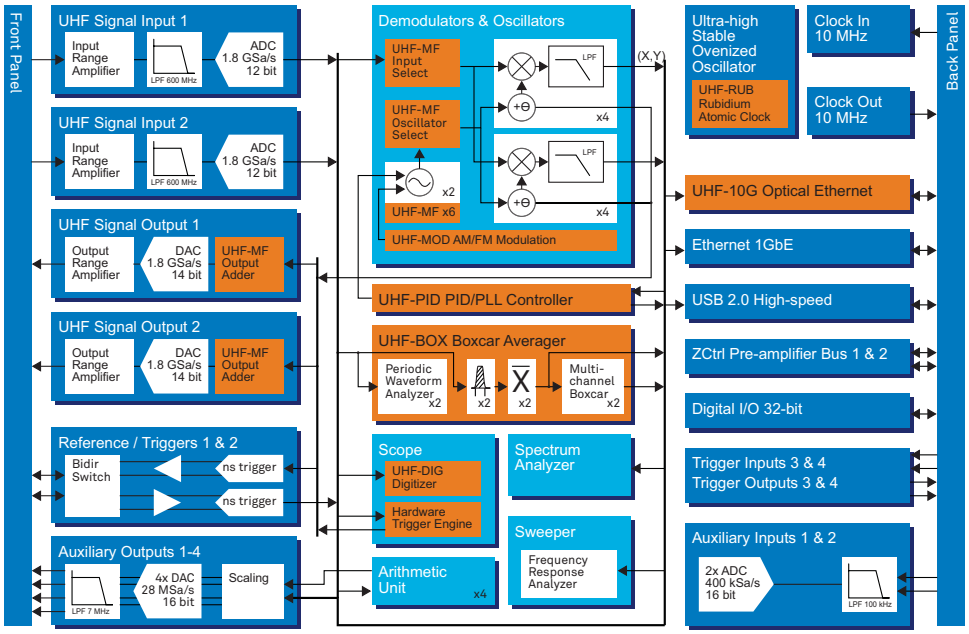

Zurich Instruments
Technoparkstrasse 1
CH-8005 Zurich
Switzerland

Phone +41-44-5150410
Email info@zhinst.com
Web www.zhinst.com

About Zurich Instruments
Zurich Instruments makes lock-in amplifiers, boxcar averagers, phase-locked loops, and impedance spectroscopes that have revolutionized instrumentation in the high-frequency (HF) and ultra-high-frequency (UHF) ranges by combining frequency-domain tools and time-domain tools within each product. This reduces the complexity of laboratory setups, removes sources of problems and provides new measurement approaches that support the progress of research.

Disclaimer
The contents of this document are provided by Zurich Instruments, 'as is'. ZI makes no representations nor warranties with respect to the accuracy or completeness of the contents of this publication and reserves the right to make changes to the specification at any time without notice. All trademarks are the property of their respective owners.

C.4. HQ:NSC35 Cr-Au BS

REGULAR

HQ: NSC, CSC & XSC

Noncontact (NSC), Contact (CSC) and 4 - Lever (XSC) silicon probes

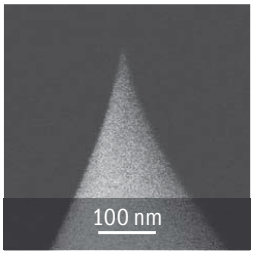

SEM image of the regular silicon tip

Pyramidal silicon etched probes* are characterized by high tip sharpness and narrow resonance peaks, making them very suitable for topography imaging in dynamic AFM modes and compositional mapping. These probes are available in a wide range of resonance frequencies and spring constants.

Tip properties:

Tip radius . . . . . ~ **8 nm**

Tip material . . . . . silicon

Back side coating:

Al BS . . . . . Al 30 nm

no Al . . . . . none

Cr-Au BS . . Au 30 nm on Cr 20 nm sublayer

Cantilever Series	Available Coatings	Length l, ± 5 µm	Width w, ± 3 µm	Thickness ± 0.5 µm	Resonance Frequency kHz (typical)	Resonance Frequency kHz (range)	Force Constant N/m (typical)	Force Constant N/m (range)
▼	▼	▼	▼	▼	▼	▼	▼	▼
HQ:NSC14	/No Al, /Al BS	125	25	2.1	**160**	110 - 220	**5.0**	1.8 - 13
HQ:NSC15	/No Al, /Al BS, /Cr-Au BS	125	30	4.0	**325**	265 - 410	**40**	20 - 80
HQ:NSC16	/No Al, /Al BS	225	37.5	7.0	**190**	170 - 210	**45**	30 - 70
HQ:CSC17	/No Al, /Al BS	450	50	2.0	**13**	10 - 17	**0.18**	0.06 - 0.40
HQ:NSC18	/No Al, /Al BS, /Cr-Au BS	225	27.5	3.0	**75**	60 - 90	**2.8**	1.2 - 5.5
HQ:NSC19	/No Al, /Al BS	125	22.5	1.0	**65**	25 - 120	**0.5**	0.05 - 2.3
HQ:NSC35								
lever A	/No Al, /Al BS, /Cr-Au BS	110	35	2.0	**205**	130 - 290	**8.9**	2.7 - 24
lever B		90	35	2.0	**300**	185 - 430	**16**	4.8 - 44
lever C		130	35	2.0	**150**	95 - 205	**5.4**	1.7 - 14
HQ:NSC36								
lever A	/No Al, /Al BS, /Cr-Au BS	110	32.5	1.0	**90**	30 - 160	**1.0**	0.1 - 4.6
lever B		90	32.5	1.0	**130**	45 - 240	**2**	0.2 - 9
lever C		130	32.5	1.0	**65**	25 - 115	**0.6**	0.06 - 2.7
HQ:CSC37								
lever A	/No Al, /Al BS	250	35	2.0	**40**	30 - 55	**0.8**	0.3 - 2
lever B		350	35	2.0	**20**	15 - 30	**0.3**	0.1 - 0.6
lever C		300	35	2.0	**30**	20 - 40	**0.4**	0.1 - 1
HQ:CSC38								
lever A	/No Al, /Al BS	250	32.5	1.0	**20**	8 - 32	**0.09**	0.01 - 0.36
lever B		350	32.5	1.0	**10**	5 - 17	**0.03**	0.003 - 0.13
lever C		300	32.5	1.0	**14**	6 - 23	**0.05**	0.005 - 0.21
HQ:XSC11								
lever A	/No Al, /Al BS	500	30	2.7	**15**	12 - 18	**0.2**	0.1 - 0.4
lever B		210	30	2.7	**80**	60 - 100	**2.7**	1.1 - 5.6
lever C		150	30	2.7	**155**	115 - 200	**7**	3 - 16
lever D		100	50	2.7	**350**	250 - 465	**42**	17 - 90

* See specifications on page 5

C.5. COZIR Wide range CO_2 Sensor

COZIR™

Ultra Low Power Carbon Dioxide Sensor

COZIR is an ultra low power (3.5mW[4]), high performance CO_2 sensor, ideally suited for battery operation and portable instruments. Based on patented IR LED and Detector technology and innovative optical designs, COZIR is the lowest power NDIR sensor available. Optional temperature and humidity sensing are available. COZIR is a third generation product from Gas Sensing Solutions Ltd – leaders in IR LED CO_2 sensing.

With measurement ranges of 0-5%, 0-20%, 0-60% and 0-100%, COZIR **Wide Range** sensors are suited for process control applications such as diving, industrial safety and automotive.

- Ultra-low Power 3.5mW
- Measurement ranges from 0 to 100%
- 3.3V supply.
- Peak current only 33mA.
- Optional Temperature and Humidity Output

COZIR™ Wide Range Sensor

Specifications

General Performance	
Warm-up Time	< 10s
Operating Conditions	0°C to 50°C (Standard) -25°C to 55°C (Extended range) 0 to 95% RH, non-condensing
Recommended Storage	-30°C to +70°C
CO2 Measurement	
Sensing Method	Non-dispersive infrared (NDIR) absorption Patented Gold-plated optics Patented Solid-state source and detector
Sample Method	Diffusion
Measurement Range	0-5%,0-20%,0-60%,0-100%
Accuracy	±70 ppm +/- 5% of reading[1] (100% Range ±300 ppm +/- 5% of reading[1])
Non Linearity	< 1% of FS
Pressure Dependence	0.13% of reading per mm Hg in normal atmospheric conditions.
Operating Pressure Range	950 mbar to 10 bar[2]
Response Time	4 secs to 2 mins (user Configurable)[3] Reading refreshed twice per second.[3]

Information supplied by GSS Ltd is believed to be accurate and reliable. However no responsibility is assumed by GSS Ltd for its use.

© GSS Ltd 2012

C.6. CO_2 cartridge

iSi Components GmbH Kürschnergasse 6a 1217 Vienna T +43 (1) 250 99-803 ico@isi.com

CO_2

Kohlendioxid
carbon dioxide

Geruch (odour)

leicht säuerlich
slightly pungent

Feuchtigkeit* (moisture*)

< 20 ppm v/v

Geschmack (taste)

leicht säuerlich
slightly pungent

Löslichkeit in Wasser (solubility in water)

0.851 l/kg

Reinheit* (purity*)

3.5 = 99.95%

Masse im Vergleich zu Luft (mass compared to breathing air)

schwerer
heavier

Kritische Temperatur (critical temperature)

31.06 °C
304.21 °K
87.91 °F

Kritischer Druck (critical pressure) - 1 bar = 14.5 PSI

73.83 bar

Gasausbeute (1g Gas = x Liter expandiertes Volumen):
gas yield (1g of gas = x liter of expanded volume):

bei 30°C / 1 bar (at 30°C / 1 bar)	0.570 l
bei 15°C / 1 bar (at 15°C / 1 bar)	0.541 l
bei 0°C / 1 bar (at 0°C / 1 bar)	0.513 l
bei -15°C / 1 bar (at -15°C / 1 bar)	0.484 l

Beispiel 21ml Zylinder mit typischer Gasfüllung: Gasausbeute bei 15°C / 1 bar
(example 21ml cylinder with typical gas fill: gas yield at 15°C / 1 bar)

16g = 8.66 l

Auftrieb / buoyancy (Richtwerte / guide values)

expandiertes Volumen (expanded gas yield) in liters x g** = Auftrieb (buoyancy) in N

* Maximalwert gemäß iSi Components Einkaufsspezifikation (maximum according to iSi Components purchasing specification)
** g=9.81

Quellen / Sources: iSi Components Einkaufsspezifikation (iSi Components purchasing specification), AGA Gas Handbook

D

Custom holder design

At the start of this research, only one AFM was available, the Anfatec AFM (Figure D.1). Since this AFM has no native support for measurements in liquid, a special holder needed to be created to enable this.

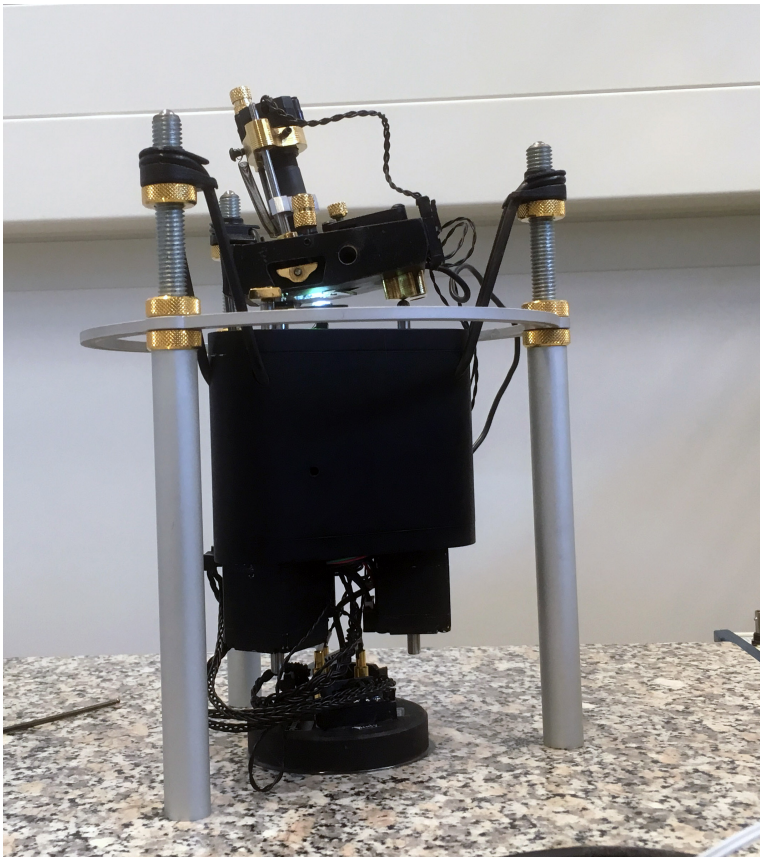

Figure D.1: Anfatec AFM. The base is suspended by three large rubber bands, on top of the base rests the scan head, on three contact points.

Van Es *et.al.*[43] created a holder for this AFM. While a few measurements where completed using this holder, it was difficult to install, and hard to operate. When the holder needed to be installed, the AFM had to be dismantled but the most difficult part was aligning the OBD's laser onto the cantilever and back to the sensor. Alignment could be achieved without the liquid, but even then, everything was at its limits. When liquid was added, the laser beam was deflected in such a way that alignment became almost impossible. The original cantilever holder is shown in Figure D.2.

(a) Original cantilever holder for liquid measurements inside the AFM scan head.

(b) The original cantilever holder for measurements in liquid.

Figure D.2: The original cantilever holder as created by van Es *et.al.*[43]. To insert the holder into the scanhead, the holding bridge had to be dismounted and the whole holder needed to be greased up, in order to contain the liquid drop onto the glass plate.

To overcome this problem, a new cantilever holder needed to be designed. With the help of the Applied Labs at Industrial Design, a series of different holders were designed and created using rapid prototyping. A selective laser melting 3D printer created these models relatively fast and cheap, creating an opportunity to experiment with the design. The end result was an easy to use holder which allowed for rapid installation. Special grease slots helped to waterproof the design. The laser alignment remained a big problem, even after experimenting with different cantilever angles. The second main problem was the stress on the cantilever holding bridge. This stress caused the different parts to snap. These problems where eventually solved, but at that time the Bruker AFM became available, and the whole holder became obsolete. The new version of the cantilever holder can be seen in Figure D.3.

(a) Improved cantilever holder for liquid measurements inside the AFM scan head.

(b) Improved version of the cantilever holder for liquid applications.

Figure D.3: The improved version of the cantilever holder, it contains a groove to apply a hydrophobic material, to contain the liquid. To insert the new holder into the scanhead, the holding bridge does not have to be removed any more.

E

Results

To keep the report readable, only a necessary selection of data is given. The full dataset is displayed here, beginning with the results of the model, followed by the graphs created from the data measured in the experiments. An explanation of the used models and measurement settings can be found in Chapter 2.

E.1. Models

The results from the model are listed below, starting with the near surface results in the first five columns, and concluded with the results of the free vibration.

Table E.1: HQ:NSC35-A Calculated resonance frequencies for different distances from surface.

NSC35 - A		$\overline{H} = 0.1$	$\overline{H} = 0.2$	$\overline{H} = 0.3$	$\overline{H} = 0.5$	$\overline{H} = 1$	Free Vibration
Air	1st	227.02	227.14	227.18	227.22	227.24	226.13
	2nd	1423.08	1423.84	1424.16	1424.43	1424.56	1418.76
Liquid	1st	103.82	136.42	118.06	103.02	96.82	77.49
	2nd	755.38	589.37	512.96	466.42	470.81	517.36
Gas	1st	226.82	227.00	227.07	227.12	227.15	225.65
	2nd	1422.03	1423.18	1423.66	1424.06	1424.26	1415.93

Table E.2: HQ:NSC35-A Calculated Q-factors and response times for different distances from surface.

NSC35 - A		$\overline{H} = 0.1$	$\overline{H} = 0.2$	$\overline{H} = 0.3$	$\overline{H} = 0.5$	$\overline{H} = 1$	Free Vibration
Air	Q	120	317	1127	1147	595	257
	τ_c	0.16871	0.44440	1.57849	1.60713	0.83284	0.36131
Liquid	Q	1	2	1	1	0	6
	τ_c	0.00385	0.00560	0.00247	0.00175	0.00151	0.02508
Gas	Q	103	467	1050	319	242	234
	τ_c	0.14415	0.65442	1.47138	0.44682	0.33975	0.33026

Table E.3: HQ:NSC35-B Calculated resonance frequencies for different distances from surface.

NSC35 - B		$\overline{H} = 0.1$	$\overline{H} = 0.2$	$\overline{H} = 0.3$	$\overline{H} = 0.5$	$\overline{H} = 1$	Free Vibration
Air	1st	339.15	339.33	339.40	339.45	339.48	337.92
	2nd	2125.91	2127.08	2127.57	2127.96	2128.15	2119.68
Liquid	1st	171.78	188.01	160.81	141.67	134.91	117.89
	2nd	1055.71	825.75	721.15	657.67	679.55	779.35
Gas	1st	338.87	339.14	339.24	339.32	339.37	337.21
	2nd	2124.39	2126.13	2126.87	2127.46	2127.76	2115.51

Table E.4: HQ:NSC35-B Calculated Q-factors and response times for different distances from surface.

NSC35 - B		$\overline{H} = 0.1$	$\overline{H} = 0.2$	$\overline{H} = 0.3$	$\overline{H} = 0.5$	$\overline{H} = 1$	Free Vibration
Air	Q	141	489	12030	612	429	315
	τ_c	0.13215	0.45885	11.28262	0.57387	0.40201	0.29708
Liquid	Q	2	1	1	0	0	7
	τ_c	0.00358	0.00232	0.00138	0.00103	0.00090	0.01942
Gas	Q	126	1825	440	239	197	286
	τ_c	0.11863	1.71330	0.41324	0.22413	0.18499	0.26959

Table E.5: HQ:NSC35-C Calculated resonance frequencies for different distances from surface.

NSC35 - C		$\overline{H} = 0.1$	$\overline{H} = 0.2$	$\overline{H} = 0.3$	$\overline{H} = 0.5$	$\overline{H} = 1$	Free Vibration
Air	1st	162.53	162.62	162.65	162.67	162.68	161.85
	2nd	1018.85	1019.40	1019.62	1019.80	1019.90	1015.65
Liquid	1st	68.02	101.40	91.50	79.39	73.93	54.50
	2nd	564.05	447.94	388.38	351.17	348.87	367.40
Gas	1st	162.38	162.51	162.56	162.60	162.61	161.50
	2nd	1018.08	1018.90	1019.23	1019.52	1019.67	1013.61

Table E.6: HQ:NSC35-C Calculated Q-factors and response times for different distances from surface.

NSC35 - C		$\overline{H} = 0.1$	$\overline{H} = 0.2$	$\overline{H} = 0.3$	$\overline{H} = 0.5$	$\overline{H} = 1$	Free Vibration
Air	Q	107	244	576	5227	889	215
	τ_c	0.21009	0.47790	1.12697	10.22737	1.74025	0.42364
Liquid	Q	1	7	1	1	1	5
	τ_c	0.00457	0.02087	0.00428	0.00278	0.00235	0.03118
Gas	Q	89	284	4440	452	302	198
	τ_c	0.17410	0.55622	8.69484	0.88396	0.59045	0.38985

E.2. Measurements

The measurements are split up into three parts, the liquid measurements, the gas measurements and the revised gas measurements. Each set of measurements starts with a reference measurement in air.

E.2.1. Liquid measurements

Reference measurement air - Cantilever A - 'Free vibration', $Q = 181,\ f_c = 145.2\,\text{kHz}$

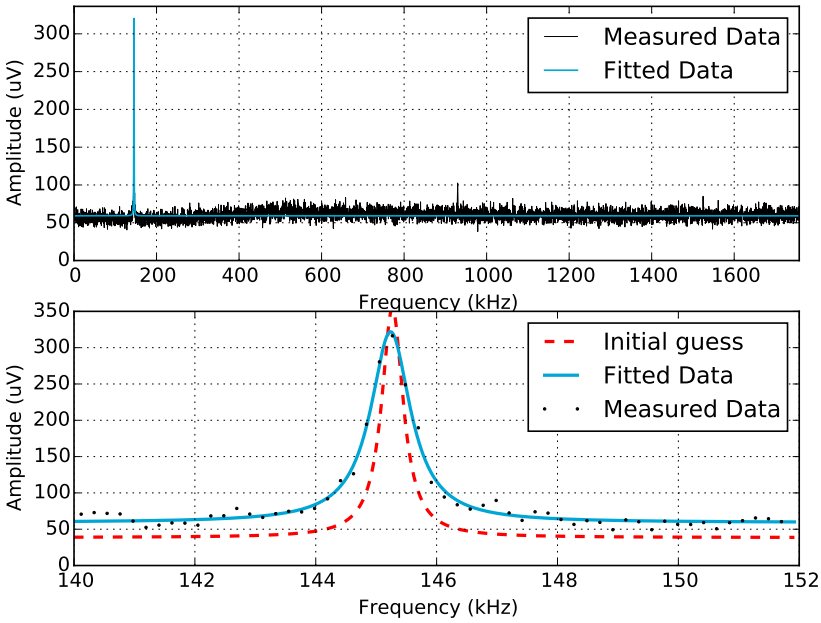

Figure E.1: Reference measurement in air, using cantilever A, away from the surface.

Measurement liquid - Cantilever A - 'Free vibration', $Q = 4,\ f_c = 67.29\,\text{kHz}$

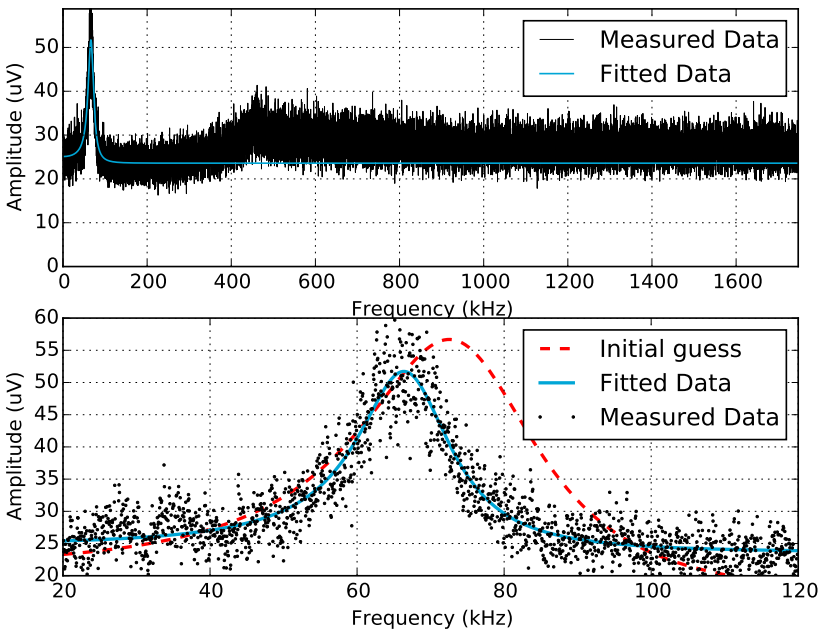

Figure E.2: Measurement in liquid, using cantilever A, away from the surface.

Reference measurement air - Cantilever A - 'Near surface', $Q = 50,\ f_c = 143.6\,\mathrm{kHz}$

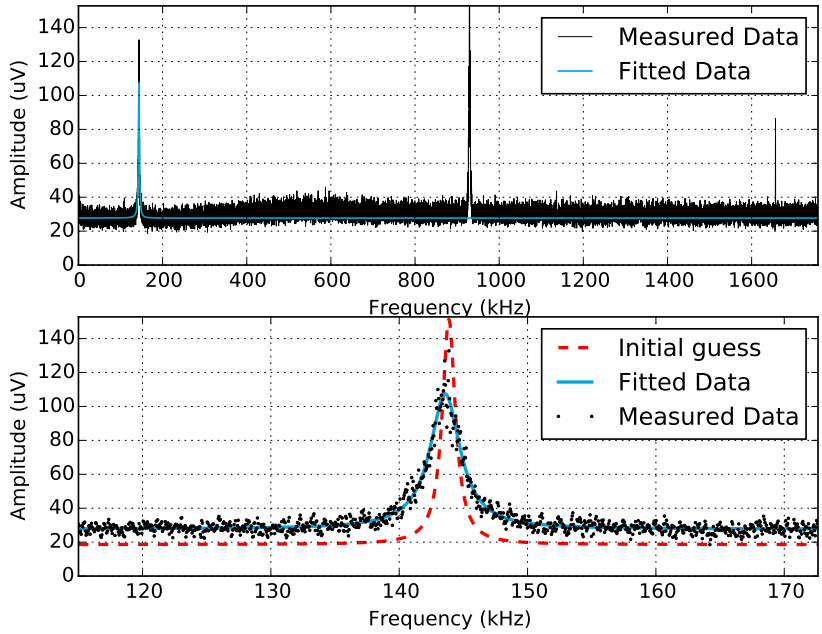

Figure E.3: Reference measurement in air, using cantilever A, near the surface.

Measurement liquid - Cantilever A - 'Near surface', $Q = 2,\ f_c = 95.42\,\mathrm{kHz}$

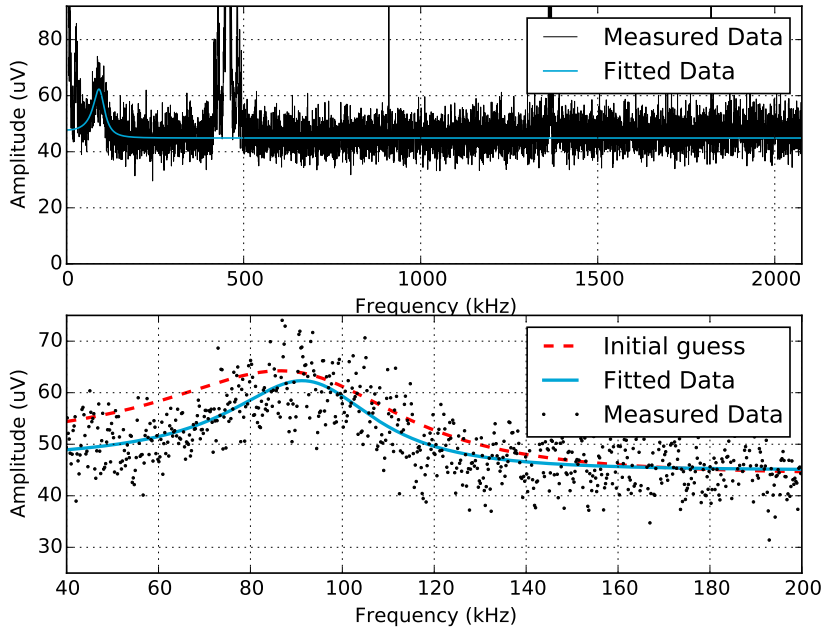

Figure E.4: Measurement in liquid, using cantilever A, near the surface.

Reference measurement air - Cantilever b - 'Free vibration', $Q = 255,\ f_c = 214.8\,\mathrm{kHz}$

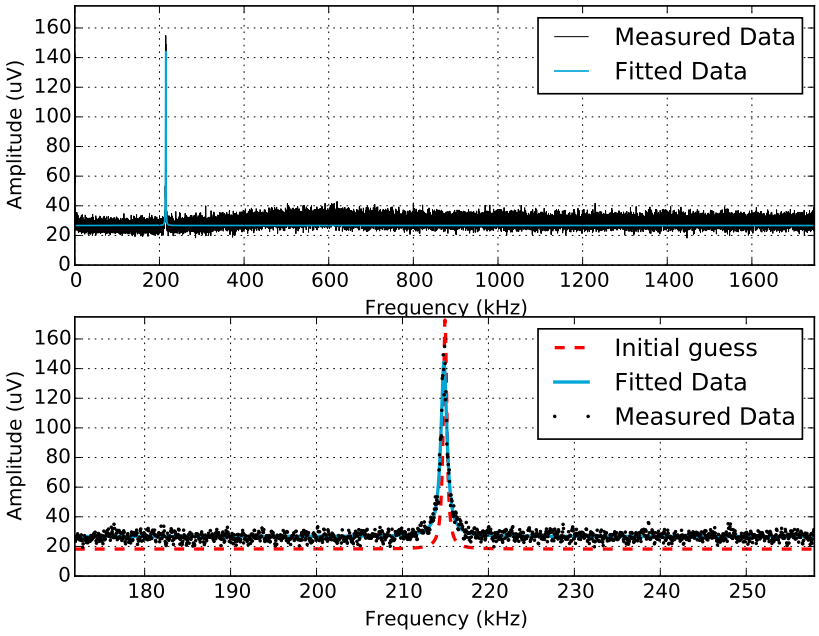

Figure E.5: Reference measurement in air, using cantilever B, away from the surface.

Measurement liquid - Cantilever B - 'Free vibration',$Q = 6,\ f_c = 105.0\,\mathrm{kHz}$

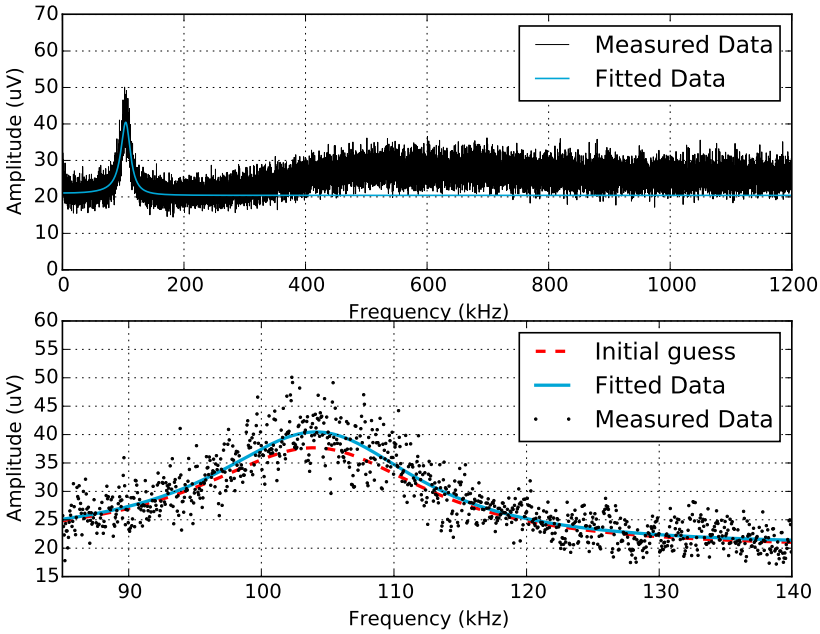

Figure E.6: Measurement in liquid, using cantilever B, away from the surface.

Reference measurement air - Cantilever B - 'Near surface', $Q = 43,\ f_c = 212.1\,\mathrm{kHz}$

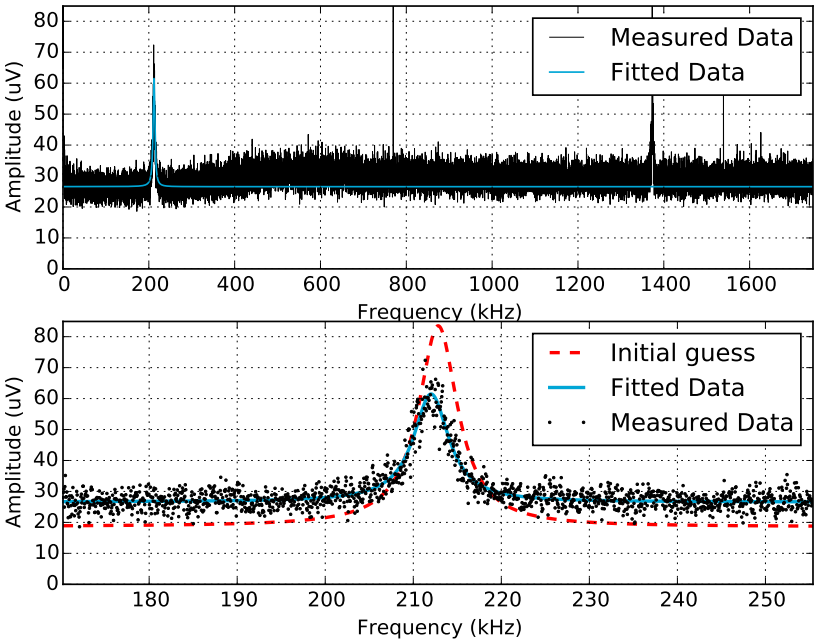

Figure E.7: Reference measurement in air, using cantilever B, near the surface.

Measurement liquid - Cantilever B - 'Near surface', $Q = 3,\ f_c = 127.9\,\mathrm{kHz}$

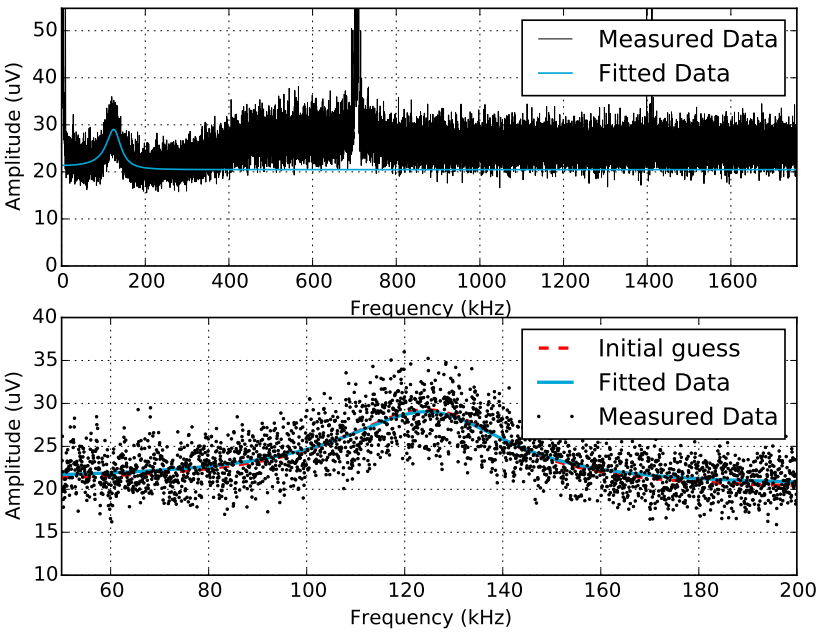

Figure E.8: Measurement in liquid, using cantilever B, near the surface.

Reference measurement air - Cantilever C - 'Free vibration', $Q = 158,\ f_c = 107.0\,\mathrm{kHz}$

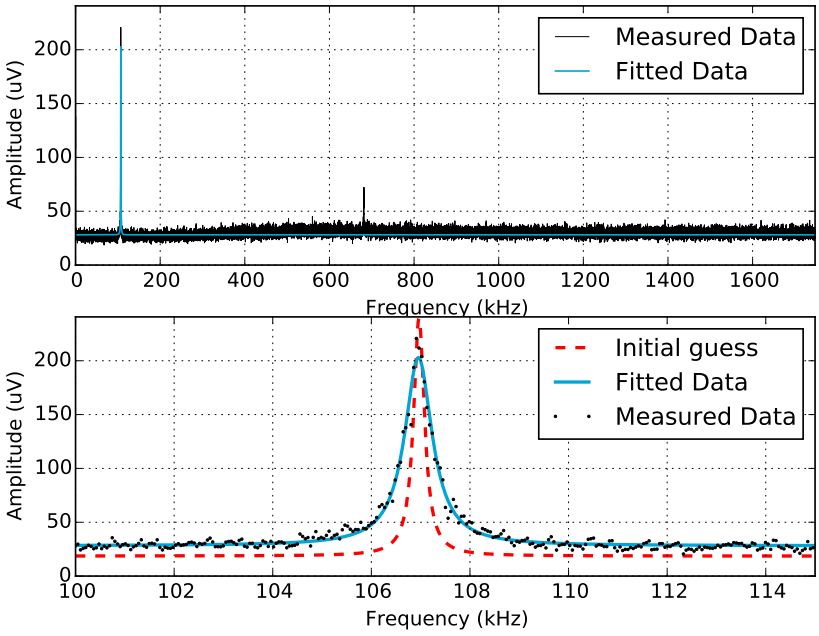

Figure E.9: Reference measurement in air, using cantilever C, away from the surface.

Measurement liquid - Cantilever C - 'Free vibration',$Q = 3,\ f_c = 47.64\,\mathrm{kHz}$

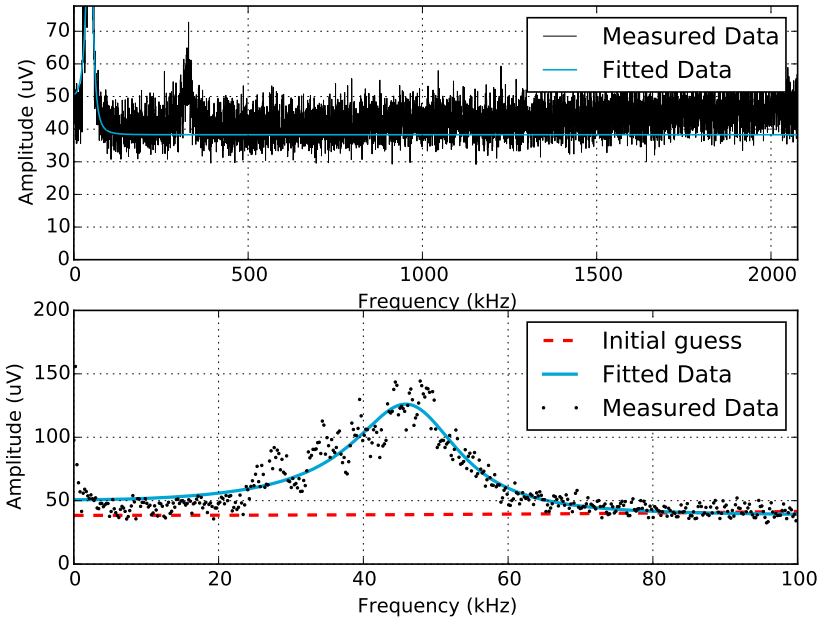

Figure E.10: Measurement in liquid, using cantilever C, away from the surface.

Reference measurement air - Cantilever C - 'Near surface', $Q = 51,\ f_c = 106.7\,\mathrm{kHz}$

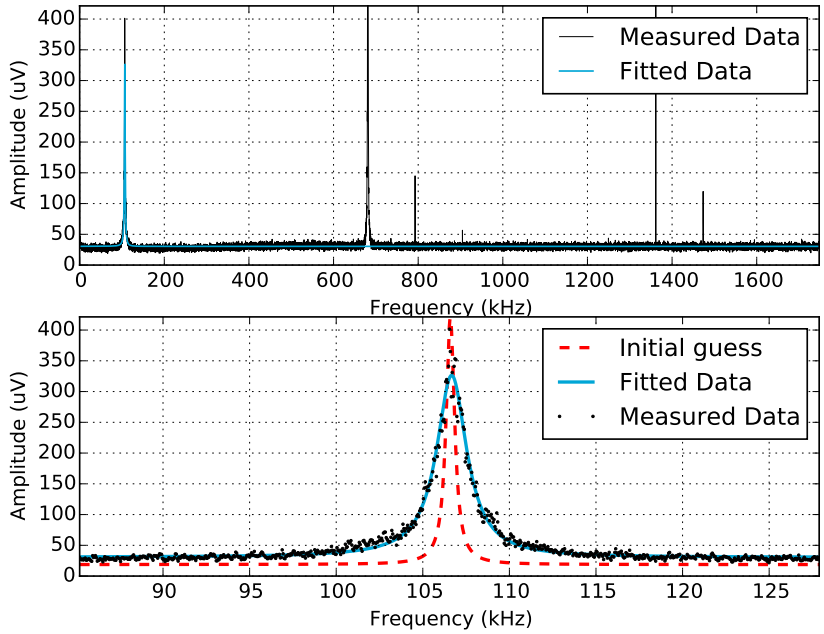

Figure E.11: Reference measurement in air, using cantilever C, near the surface.

Measurement liquid - Cantilever C - 'Near surface',$Q = 2,\ f_c = 55.39\,\mathrm{kHz}$

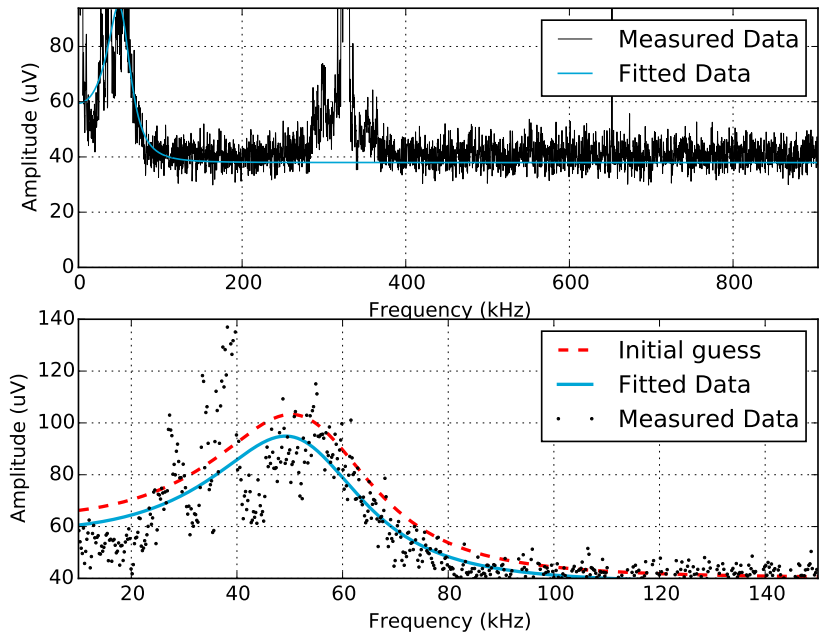

Figure E.12: Measurement in liquid, using cantilever C, near the surface.

E.2.2. Gas measurements

Reference measurement air - Cantilever A - 'Free vibration', $Q = 120$, $f_c = 141.3\,\text{kHz}$

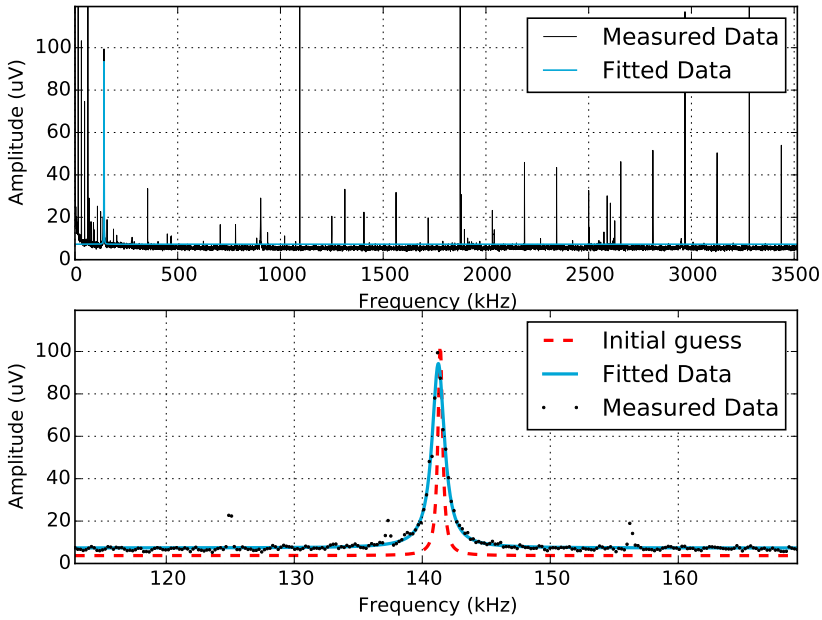

Figure E.13: Reference measurement in air, using cantilever A, away from the surface.

Measurement gas - 50% - Cantilever A - 'Free vibration', $Q = 173$, $f_c = 141.2\,\text{kHz}$

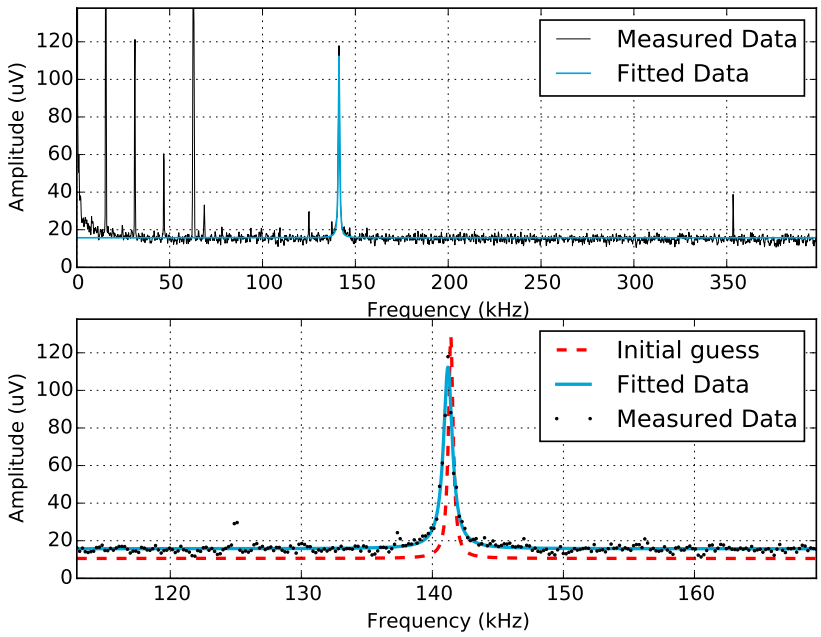

Figure E.14: Measurement in 50% CO_2, using cantilever A, away from the surface.

Measurement gas - 75% - Cantilever A - 'Free vibration', $Q = 124$, $f_c = 141.2\,\mathrm{kHz}$

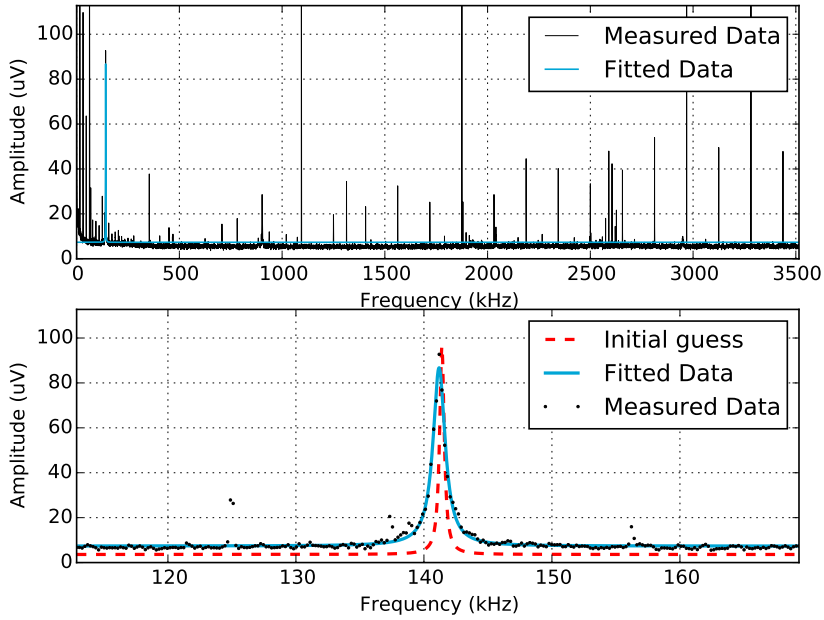

Figure E.15: Measurement in 75% CO_2, using cantilever A, away from the surface.

Measurement gas - 90% - Cantilever A - 'Free vibration', $Q = 117$, $f_c = 141.2\,\mathrm{kHz}$

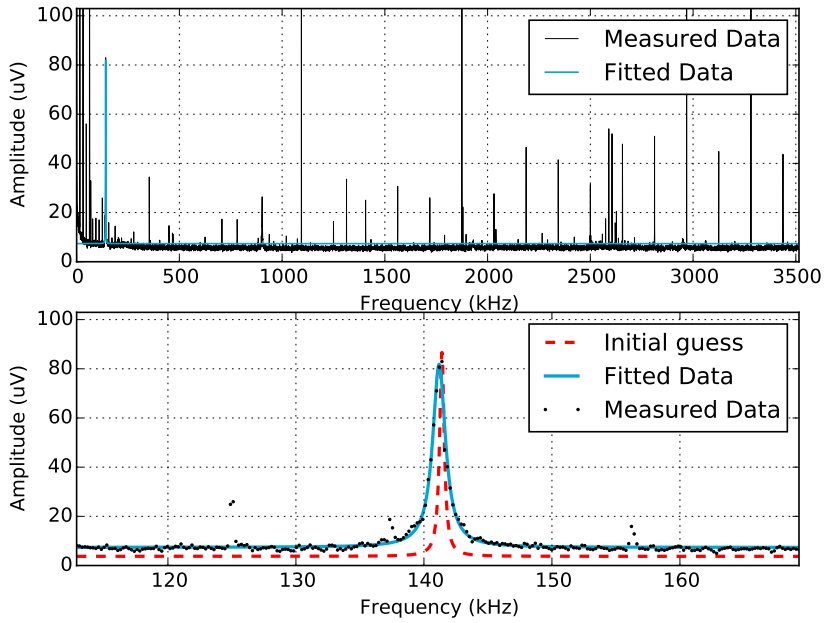

Figure E.16: Measurement in 90% CO_2, using cantilever A, away from the surface.

Measurement gas - 95% - Cantilever A - 'Free vibration', $Q = 149$, $f_c = 141.1\,\mathrm{kHz}$

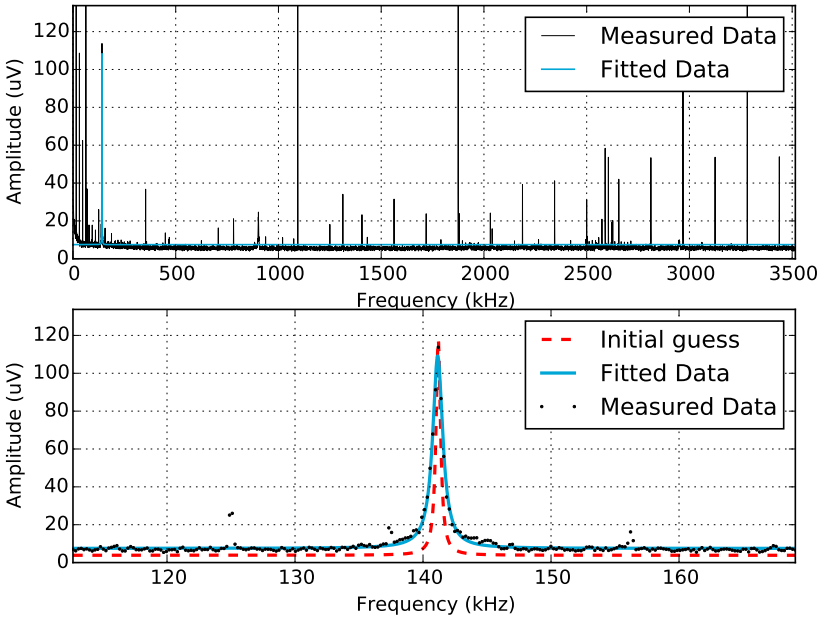

Figure E.17: Measurement in 95% CO_2, using cantilever A, away from the surface.

Measurement gas - 100% - Cantilever A - 'Free vibration', $Q = 147$, $f_c = 141.2\,\mathrm{kHz}$

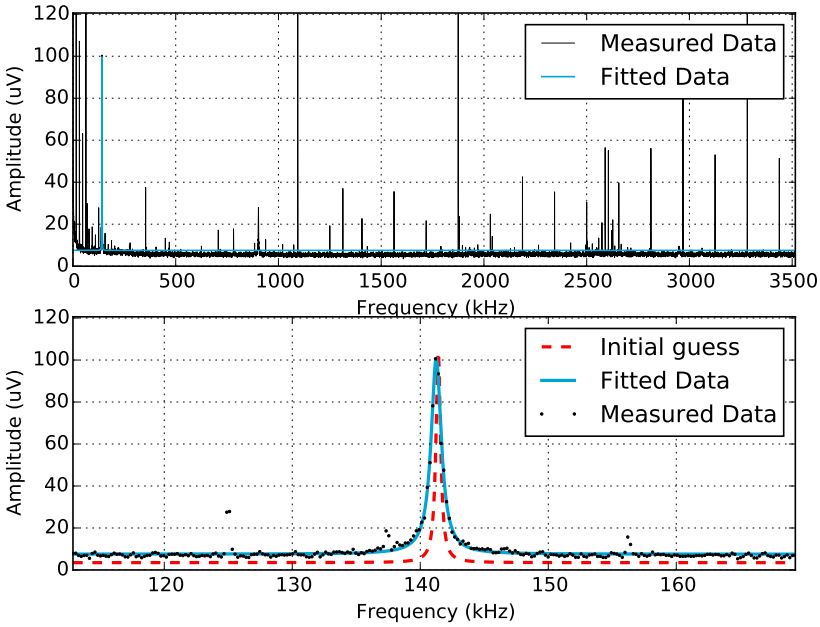

Figure E.18: Measurement in 100% CO_2, using cantilever A, away from the surface.

Reference measurement air - Cantilever A - 'Near surface', $Q = 26,\ f_c = 136.9\,\mathrm{kHz}$

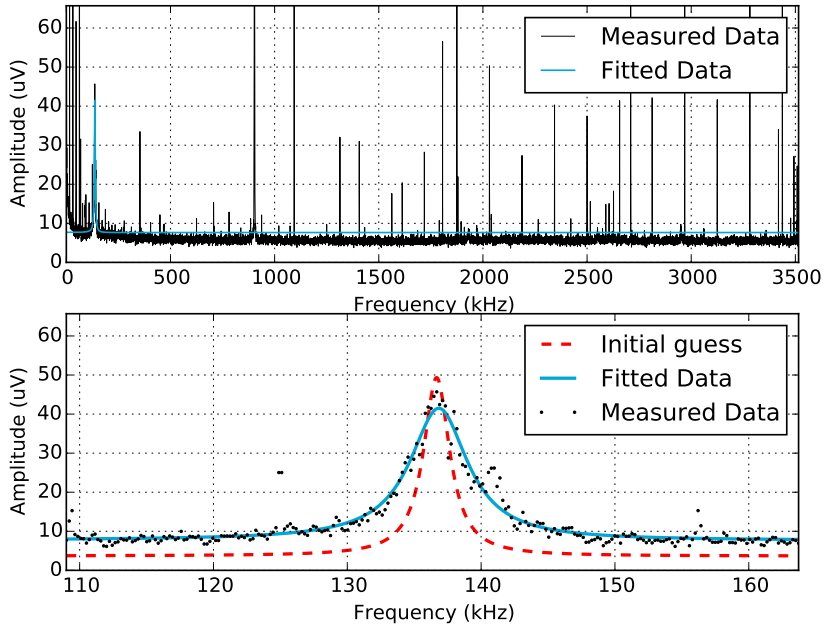

Figure E.19: Reference measurement in air, using cantilever A, near the surface.

Measurement gas - 100% - Cantilever A - 'Near surface', $Q = 11,\ f_c = 133.1\,\mathrm{kHz}$

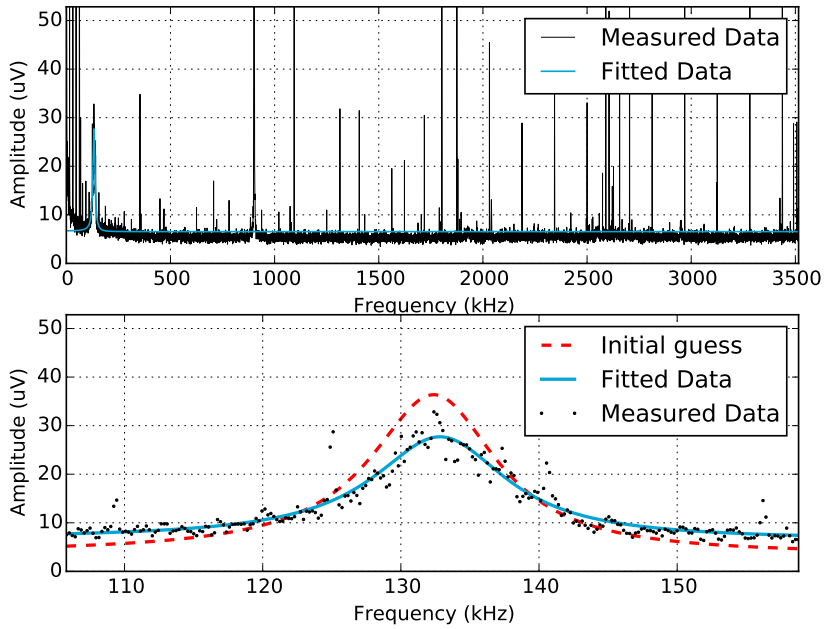

Figure E.20: Measurement in 100% CO_2, using cantilever A, near the surface.

Reference measurement air - Cantilever B - 'Free vibration', $Q = 180,\ f_c = 208.1\,\mathrm{kHz}$

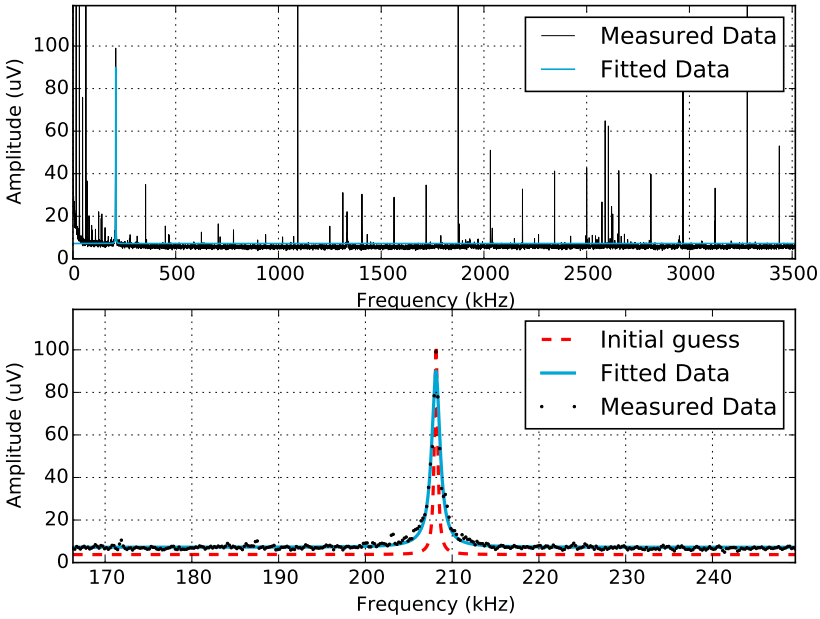

Figure E.21: Reference measurement in air, using cantilever B, away from the surface.

Measurement gas - 50% - Cantilever B - 'Free vibration', $Q = 207,\ f_c = 208.1\,\mathrm{kHz}$

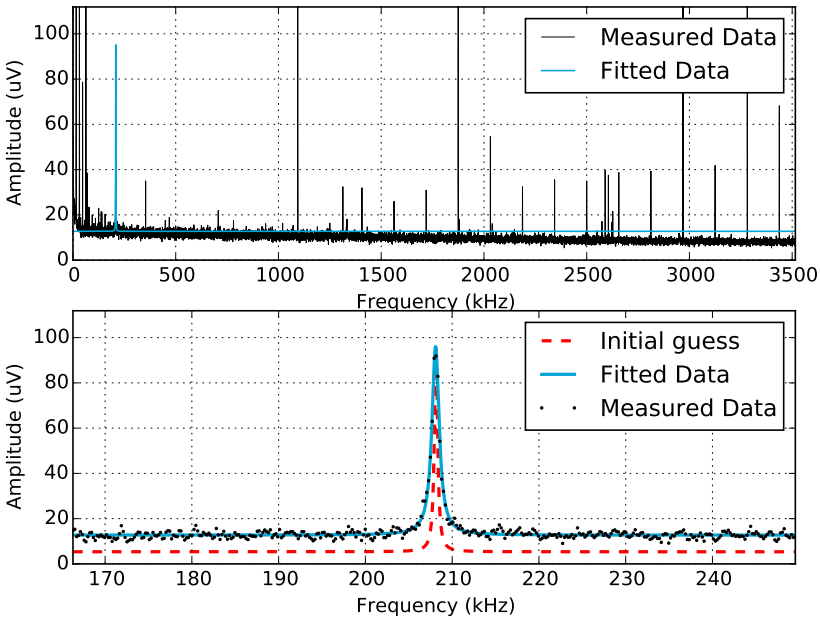

Figure E.22: Measurement in 50% CO_2, using cantilever B, away from the surface.

Measurement gas - 75% - Cantilever B - 'Free vibration', $Q = 197$, $f_c = 208.1\,\mathrm{kHz}$

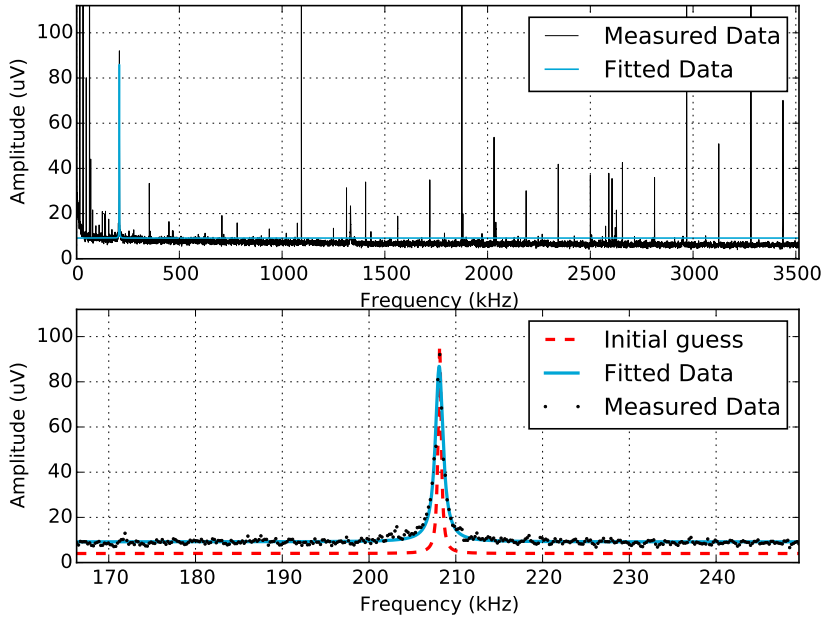

Figure E.23: Measurement in 75% CO_2, using cantilever B, away from the surface.

Measurement gas - 90% - Cantilever B - 'Free vibration', $Q = 191$, $f_c = 208.0\,\mathrm{kHz}$

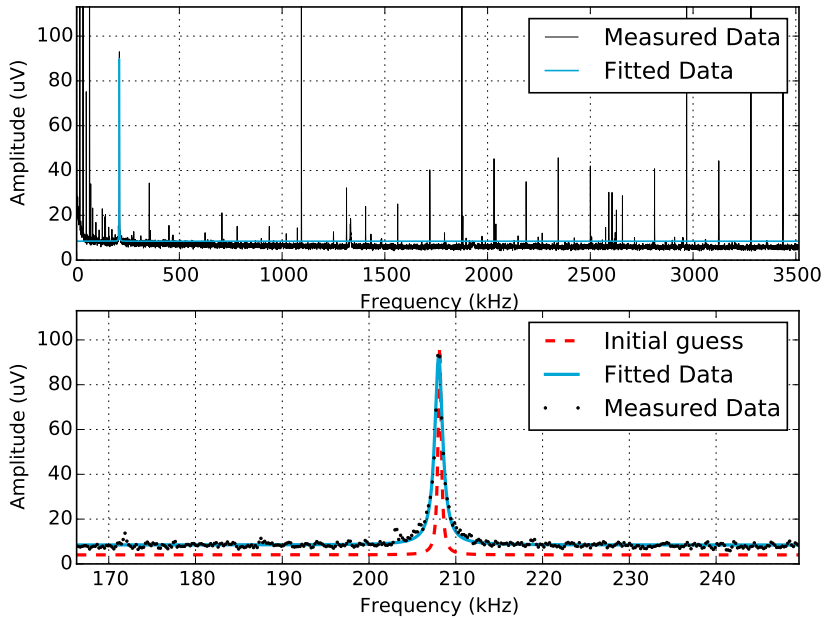

Figure E.24: Measurement in 90% CO_2, using cantilever B, away from the surface.

Measurement gas - 97% - Cantilever B - 'Free vibration', $Q = 201$, $f_c = 208.0\,\mathrm{kHz}$

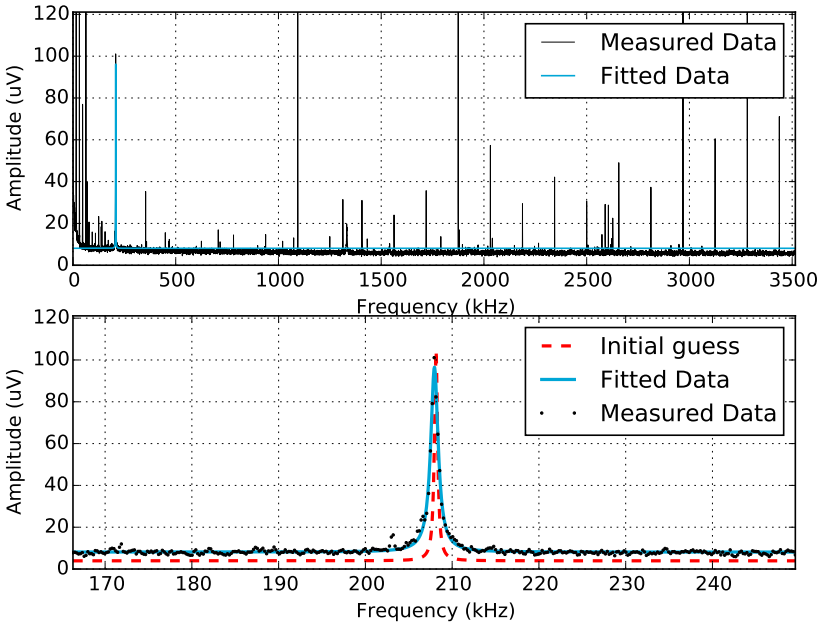

Figure E.25: Measurement in 97% CO_2, using cantilever B, away from the surface.

Measurement gas - 100% - Cantilever B - 'Free vibration', $Q = 183$, $f_c = 208.0\,\mathrm{kHz}$

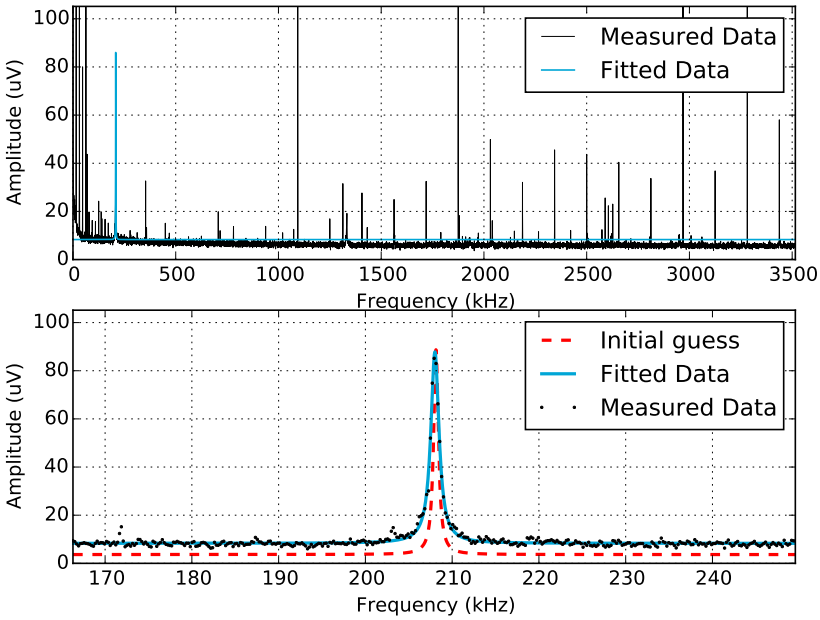

Figure E.26: Measurement in 100% CO_2, using cantilever B, away from the surface.

Reference measurement air - Cantilever B - 'Near surface', $Q = 35,\ f_c = 208.3\,\mathrm{kHz}$

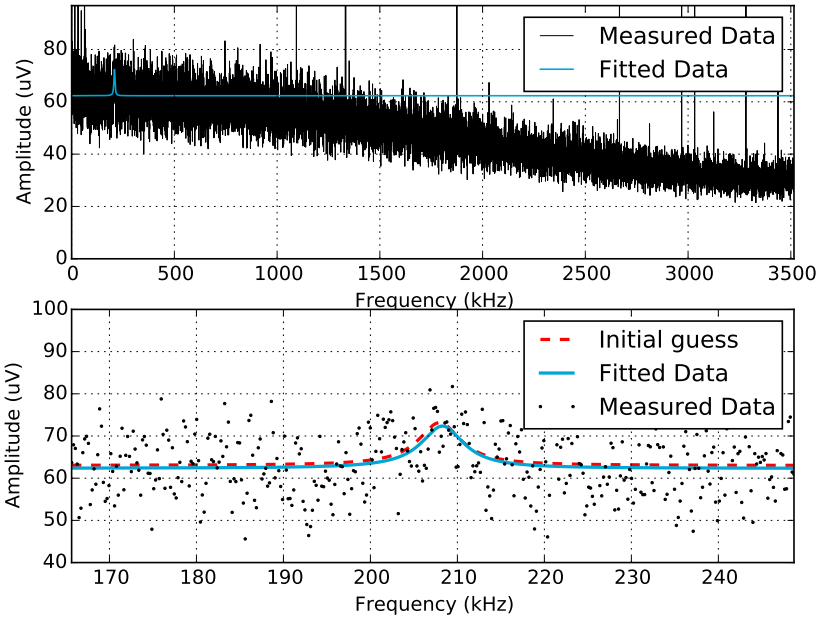

Figure E.27: Reference measurement in air, using cantilever B, near the surface.

Measurement gas - 100% - Cantilever B - 'Near surface', $Q = 29,\ f_c = 202.4\,\mathrm{kHz}$

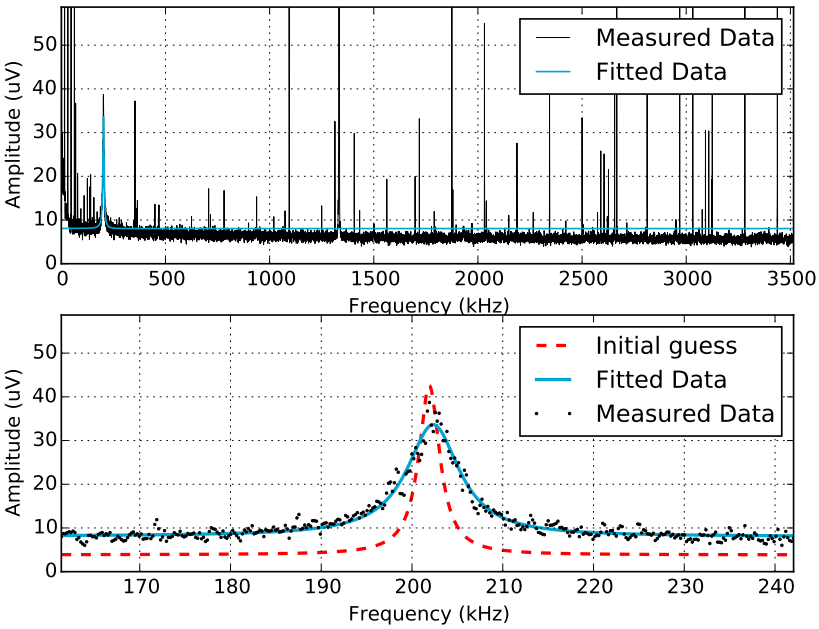

Figure E.28: Measurement in 100% CO_2, using cantilever B, near the surface.

Reference measurement air - Cantilever C - 'Free vibration', $Q = 125,\ f_c = 102.7\,\mathrm{kHz}$

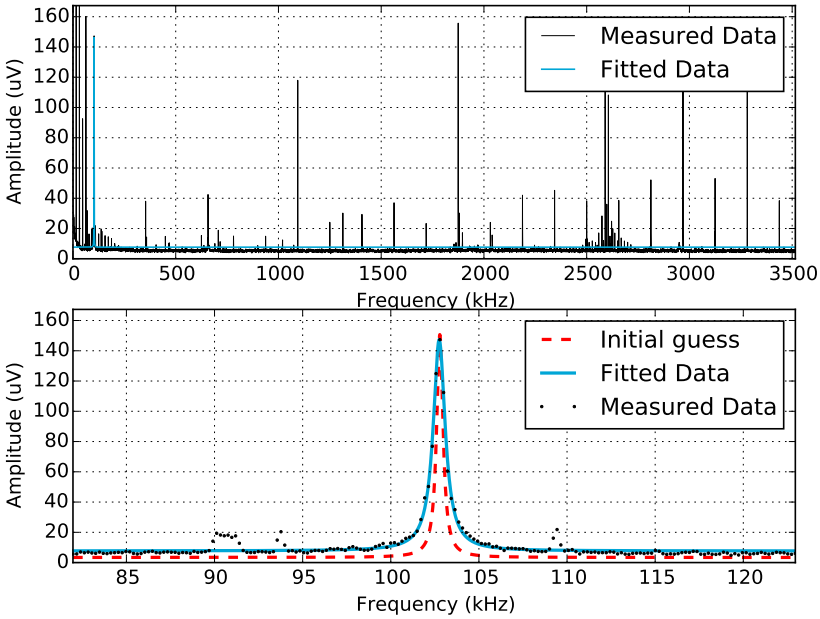

Figure E.29: Reference measurement in air, using cantilever C, away from the surface.

Measurement gas - 0% - Cantilever C - 'Free vibration', $Q = 95,\ f_c = 102.8\,\mathrm{kHz}$

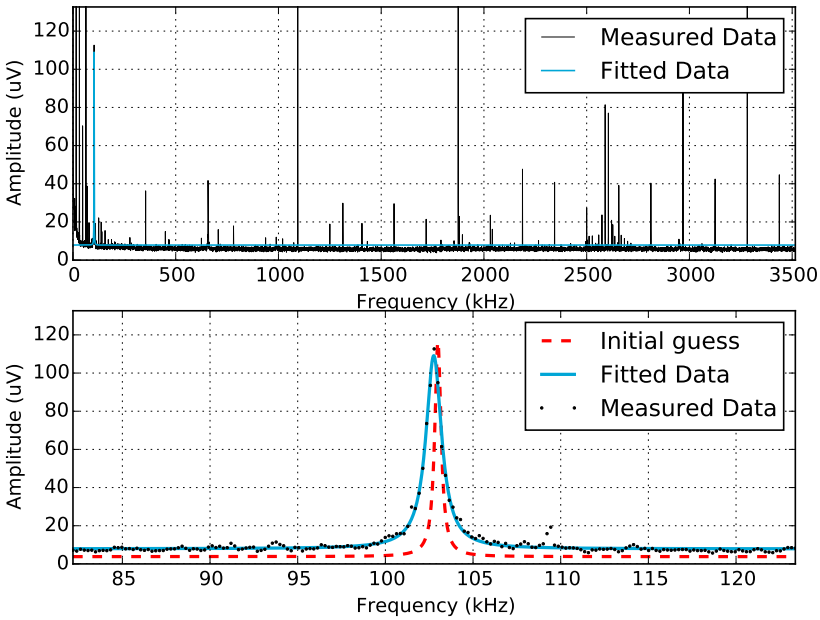

Figure E.30: Measurement in 0% CO_2, using cantilever C, away from the surface. The 0% is achieved by flushing the system with N_2.

Measurement gas - 30% - Cantilever C - 'Free vibration', $Q = 100,\ f_c = 102.7\,\text{kHz}$

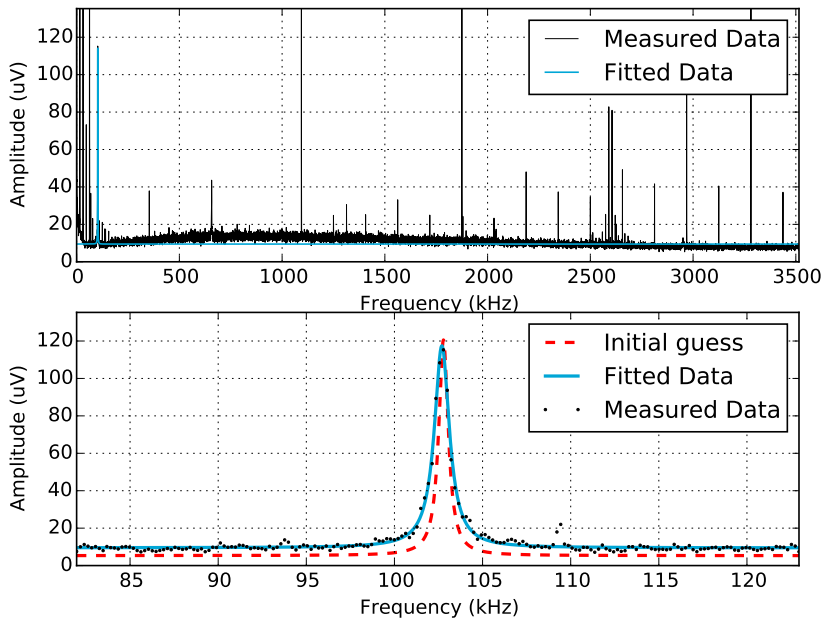

Figure E.31: Measurement in 30% CO_2, using cantilever C, away from the surface.

Measurement gas - 50% - Cantilever C - 'Free vibration', $Q = 137,\ f_c = 102.7\,\text{kHz}$

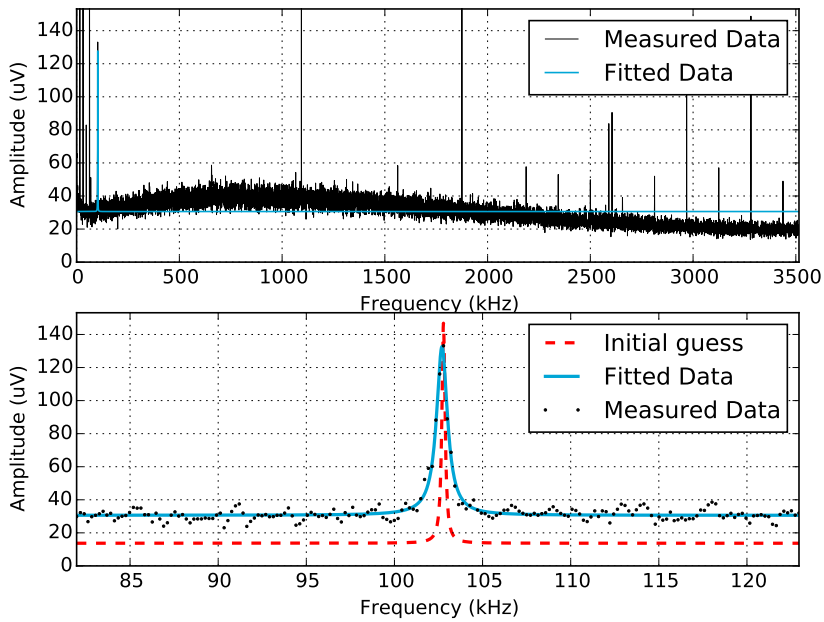

Figure E.32: Measurement in 50% CO_2, using cantilever C, away from the surface.

Measurement gas - 75% - Cantilever C - 'Free vibration', $Q = 154$, $f_c = 102.6\,\mathrm{kHz}$

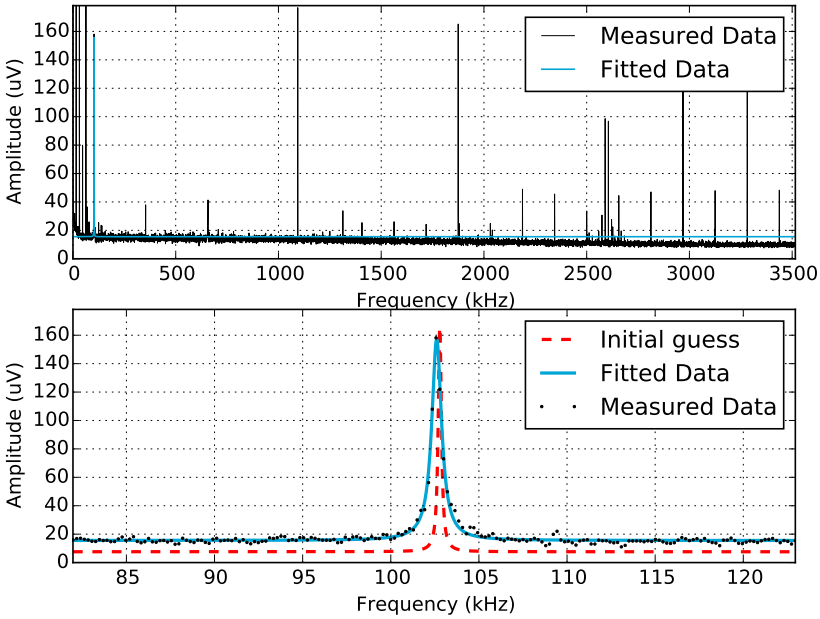

Figure E.33: Measurement in 75% CO_2, using cantilever C, away from the surface.

Measurement gas - 95% - Cantilever C - 'Free vibration', $Q = 95$, $f_c = 102.6\,\mathrm{kHz}$

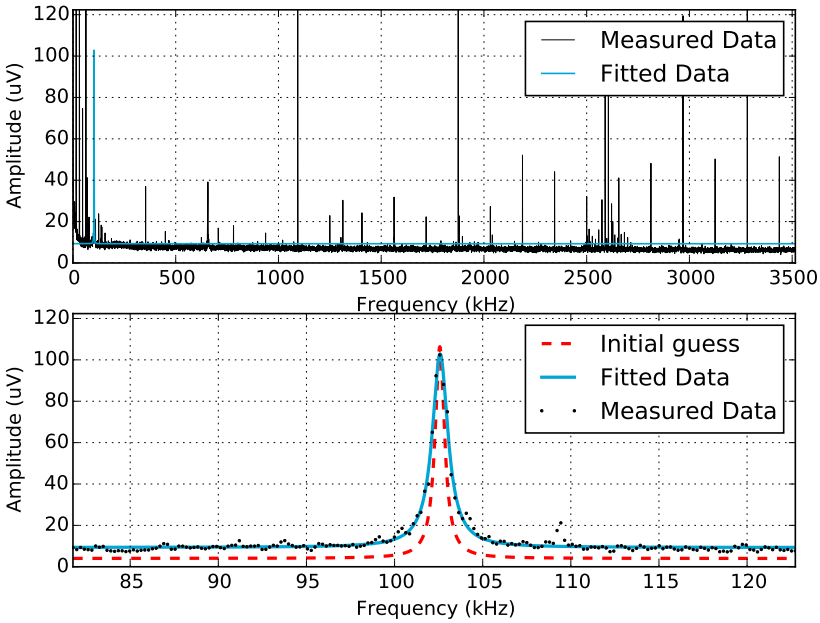

Figure E.34: Measurement in 95% CO_2, using cantilever C, away from the surface.

Measurement gas - 100% - Cantilever C - 'Free vibration', $Q = 99,\ f_c = 102.6\,\mathrm{kHz}$

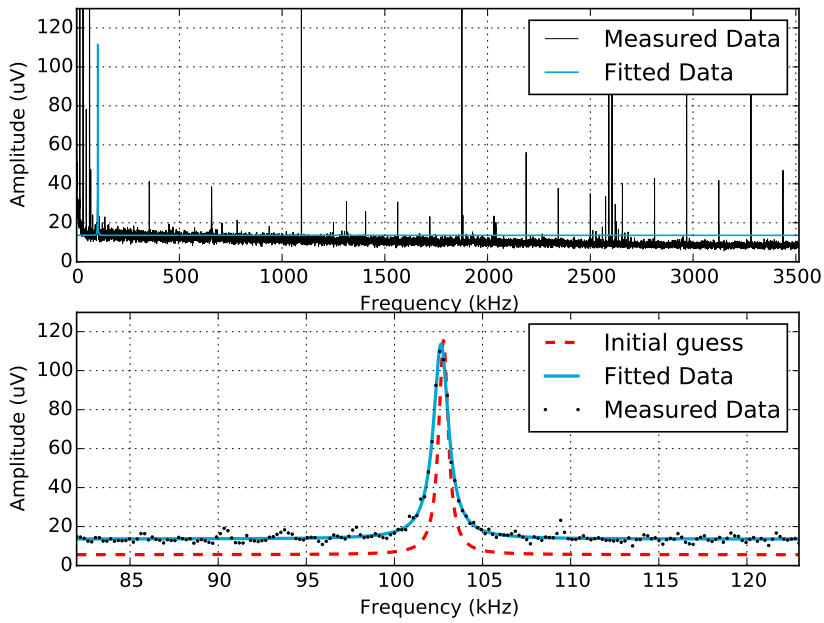

Figure E.35: Measurement in 100% CO_2, using cantilever C, away from the surface.

Reference measurement air - Cantilever C - 'Near surface', $Q = 7,\ f_c = 101.1\,\mathrm{kHz}$

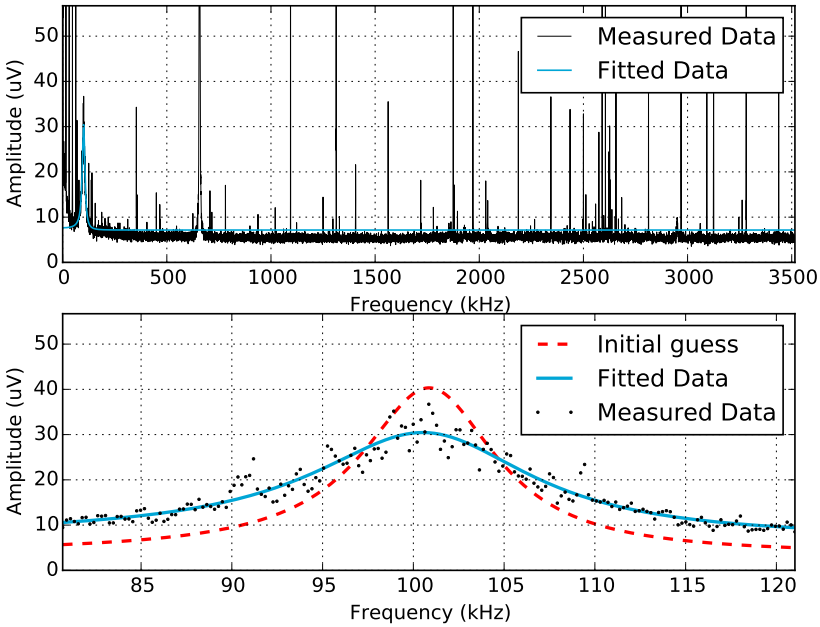

Figure E.36: Reference measurement in air, using cantilever C, near the surface.

Measurement gas - 100% - Cantilever C - 'Near surface', $Q = 20,\ f_c = 99.15\,\mathrm{kHz}$

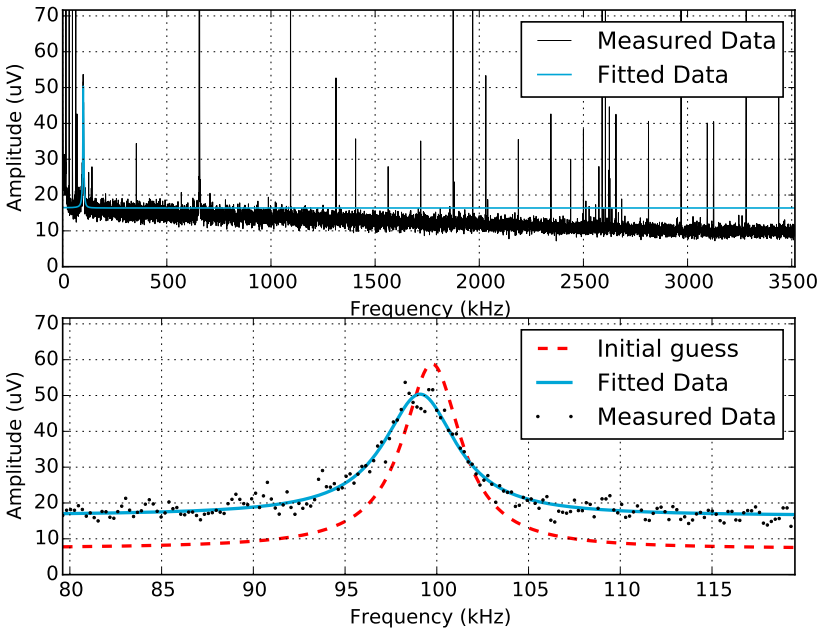

Figure E.37: Measurement in 100% CO_2, using cantilever C, near the surface.

E.2.3. Revised gas measurements

Reference measurement air - Cantilever C - 'Free vibration', $Q = 156,\ f_c = 103.3\,\mathrm{kHz}$

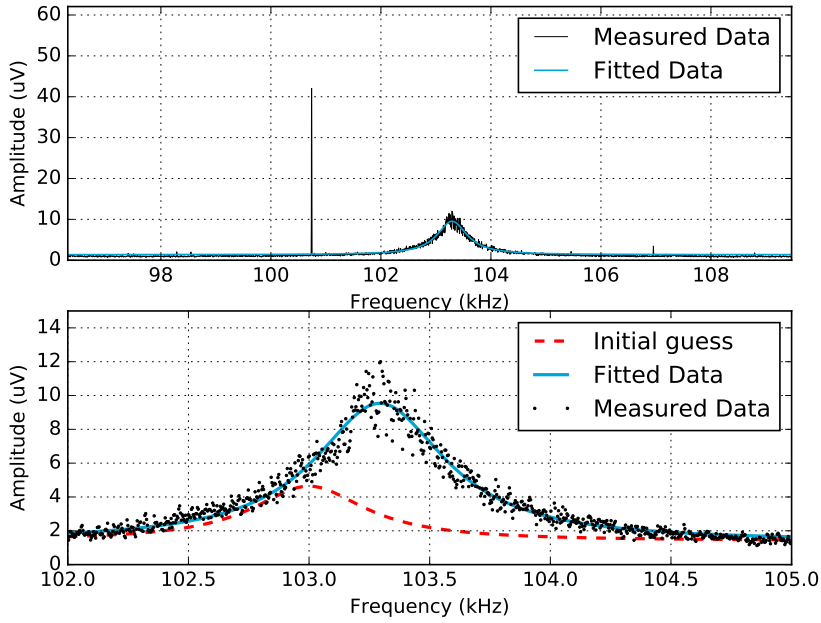

Figure E.38: Reference measurement in air, using cantilever C, away from the surface.

Measurement gas - 0% - Cantilever C - 'Free vibration', $Q = 159,\ f_c = 103.3\,\mathrm{kHz}$

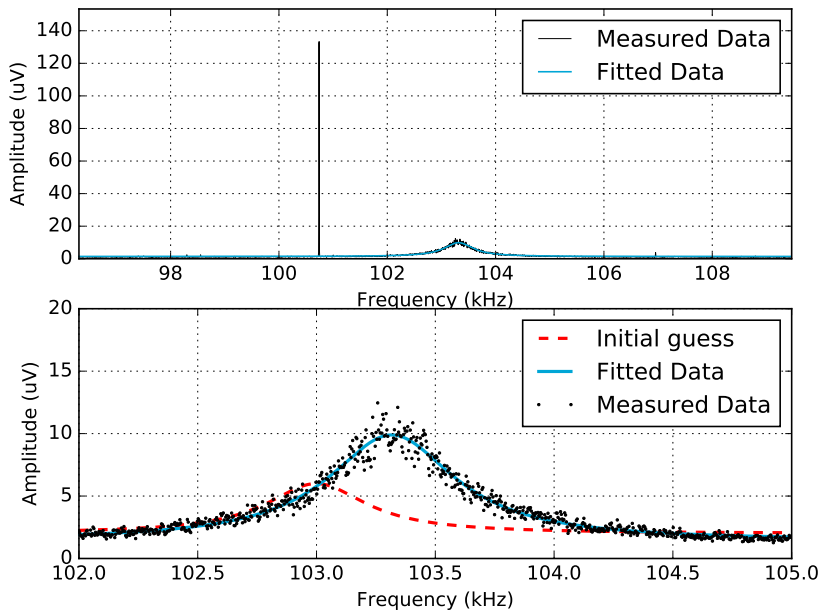

Figure E.39: Measurement in 0% CO_2, using cantilever C, away from the surface.

Measurement gas - 2% - Cantilever C - 'Free vibration', $Q = 162,\ f_c = 103.3\,\mathrm{kHz}$

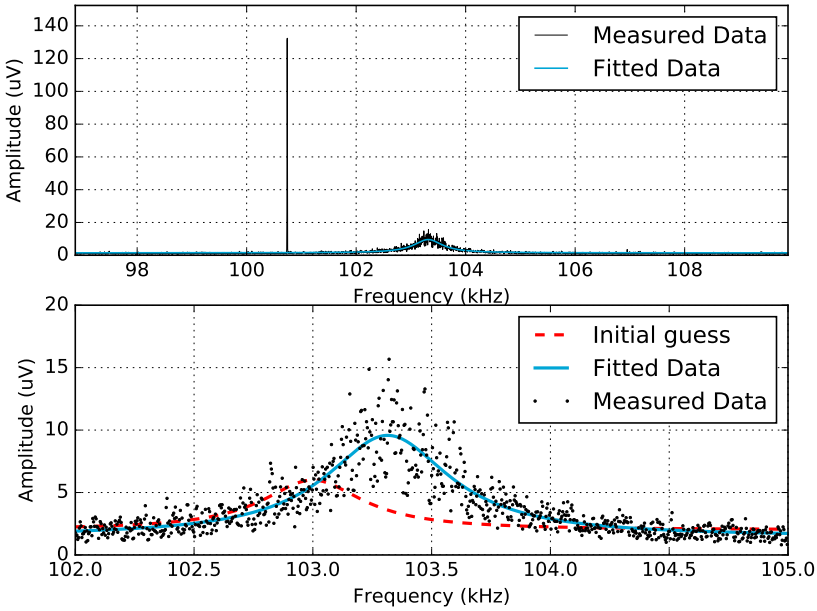

Figure E.40: Measurement in 2% CO_2, using cantilever C, away from the surface.

Measurement gas - 12% - Cantilever C - 'Free vibration', $Q = 161,\ f_c = 103.3\,\mathrm{kHz}$

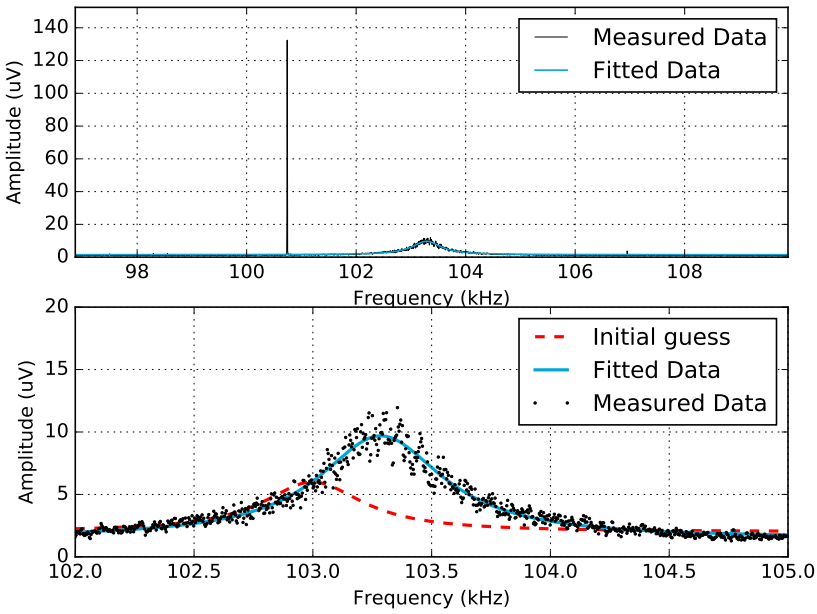

Figure E.41: Measurement in 12% CO_2, using cantilever C, away from the surface.

Measurement gas - 21% - Cantilever C - 'Free vibration', $Q = 157,\ f_c = 103.3\,\mathrm{kHz}$

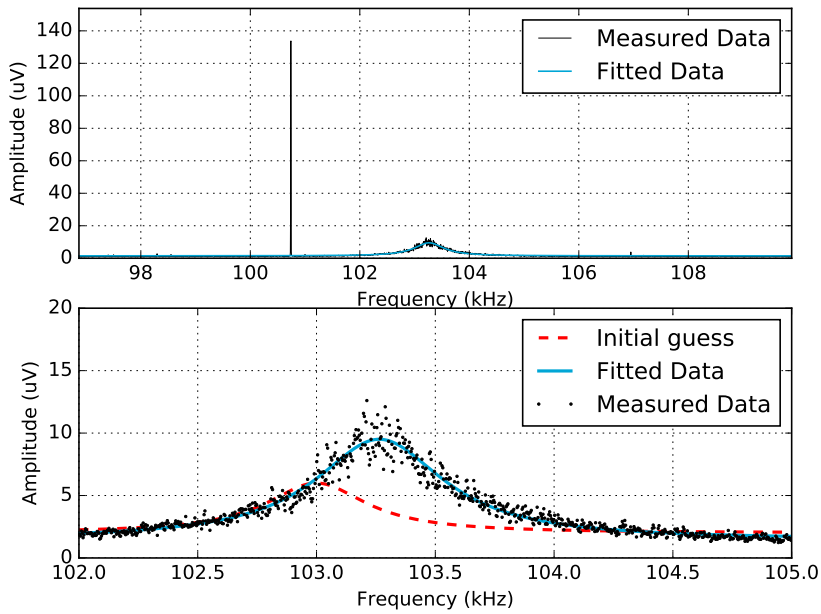

Figure E.42: Measurement in 21% CO_2, using cantilever C, away from the surface.

Measurement gas - 30% - Cantilever C - 'Free vibration', $Q = 158,\ f_c = 103.3\,\mathrm{kHz}$

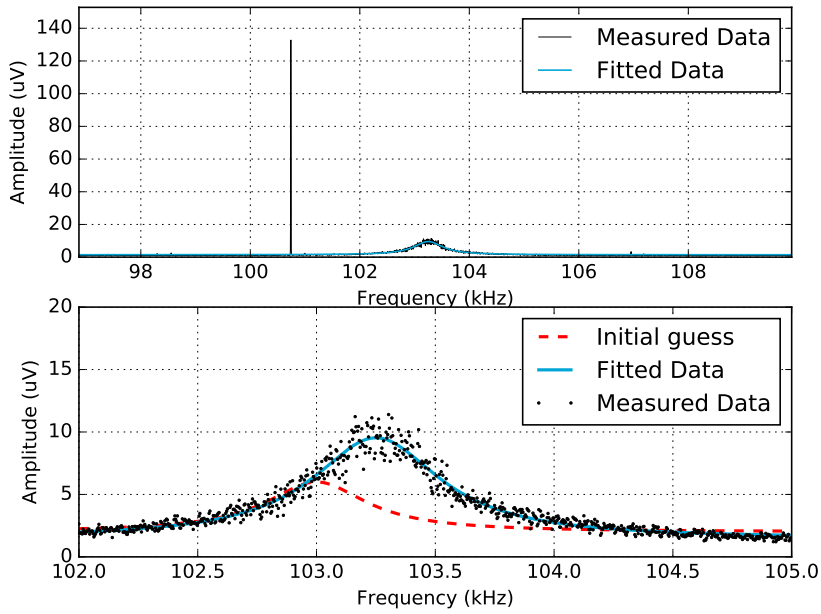

Figure E.43: Measurement in 30% CO_2, using cantilever C, away from the surface.

Measurement gas - 50% - Cantilever C - 'Free vibration', $Q = 156$, $f_c = 103.2\,\mathrm{kHz}$

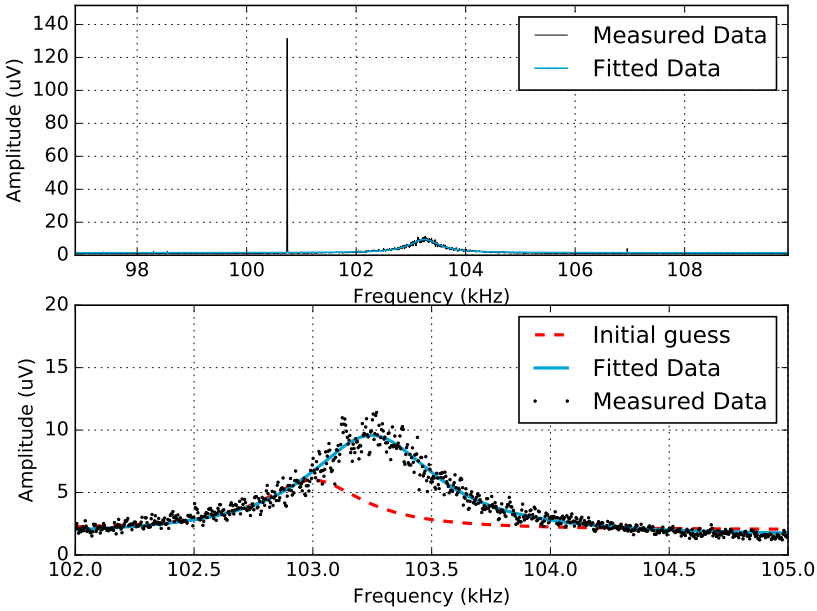

Figure E.44: Measurement in 50% CO_2, using cantilever C, away from the surface.

Measurement gas - 60% - Cantilever C - 'Free vibration', $Q = 149$, $f_c = 103.2\,\mathrm{kHz}$

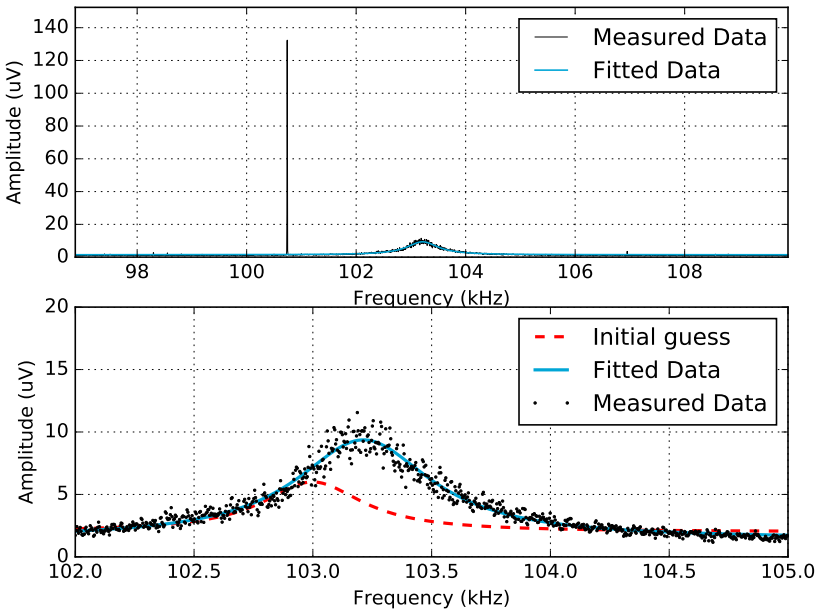

Figure E.45: Measurement in 60% CO_2, using cantilever C, away from the surface.

Measurement gas - 77% - Cantilever C - 'Free vibration', $Q = 151,\ f_c = 103.2\,\mathrm{kHz}$

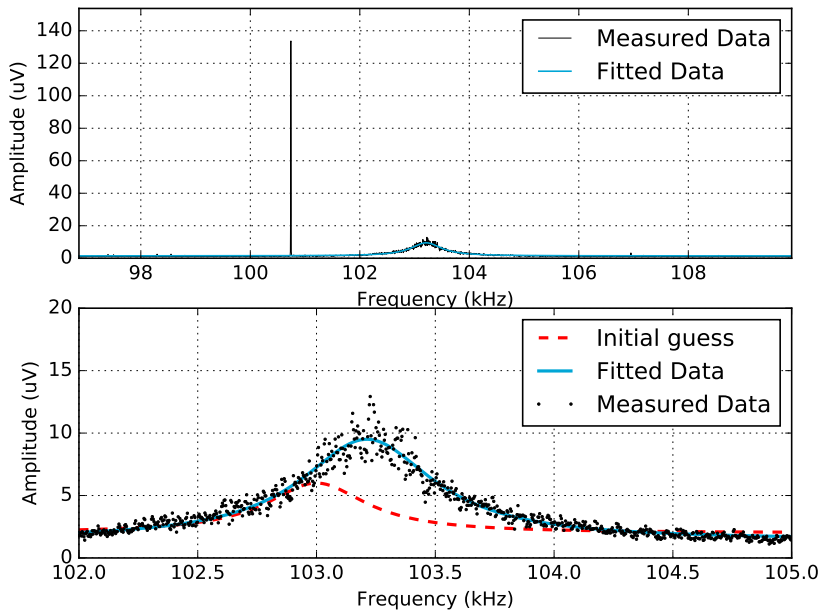

Figure E.46: Measurement in 77% CO_2, using cantilever C, away from the surface.

Measurement gas - 85% - Cantilever C - 'Free vibration', $Q = 154,\ f_c = 103.2\,\mathrm{kHz}$

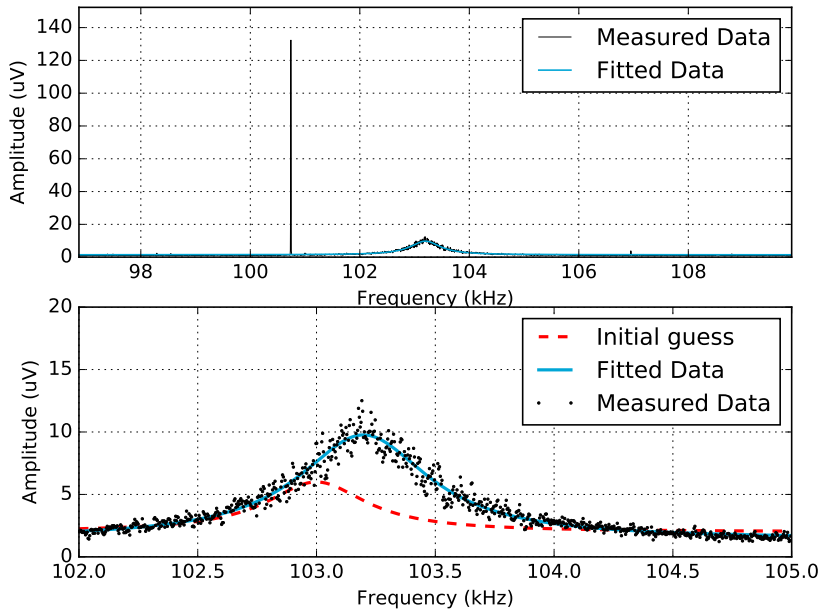

Figure E.47: Measurement in 85% CO_2, using cantilever C, away from the surface.

Measurement gas - 90% - Cantilever C - 'Free vibration', $Q = 147,\ f_c = 103.2\,\mathrm{kHz}$

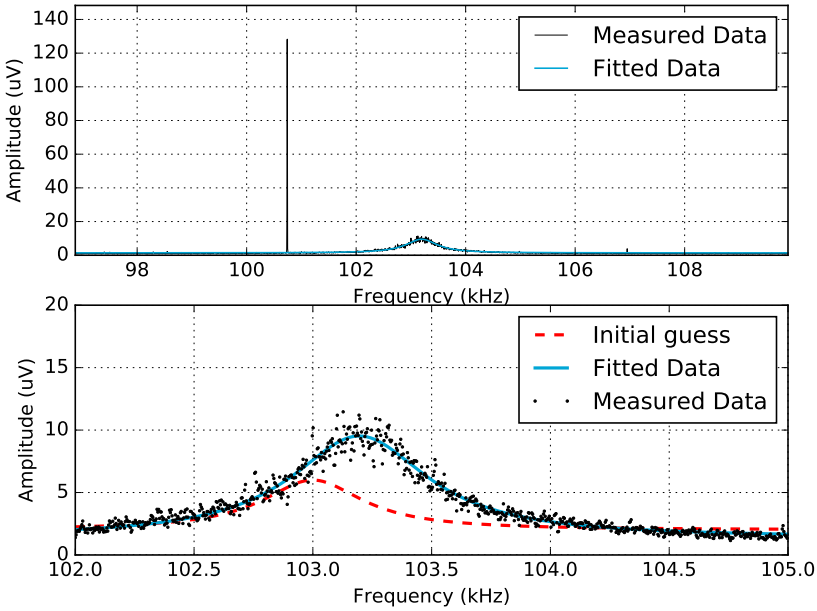

Figure E.48: Measurement in 90% CO_2, using cantilever C, away from the surface.

Measurement gas - 100% - Cantilever C - 'Free vibration', $Q = 161,\ f_c = 103.2\,\mathrm{kHz}$

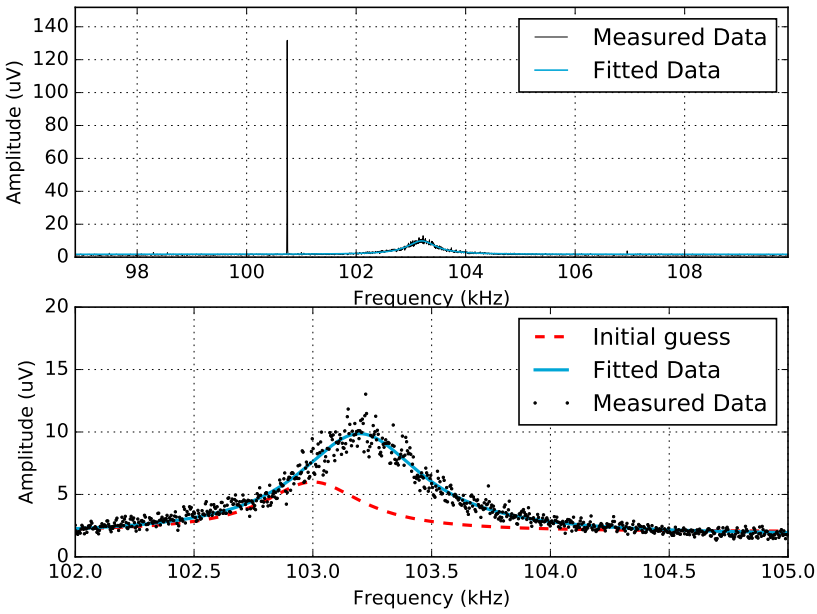

Figure E.49: Measurement in 100% CO_2, using cantilever C, away from the surface.

Reference measurement air - Cantilever C - 'Near surface', $Q = 66,\ f_c = 101.7\,\text{kHz}$

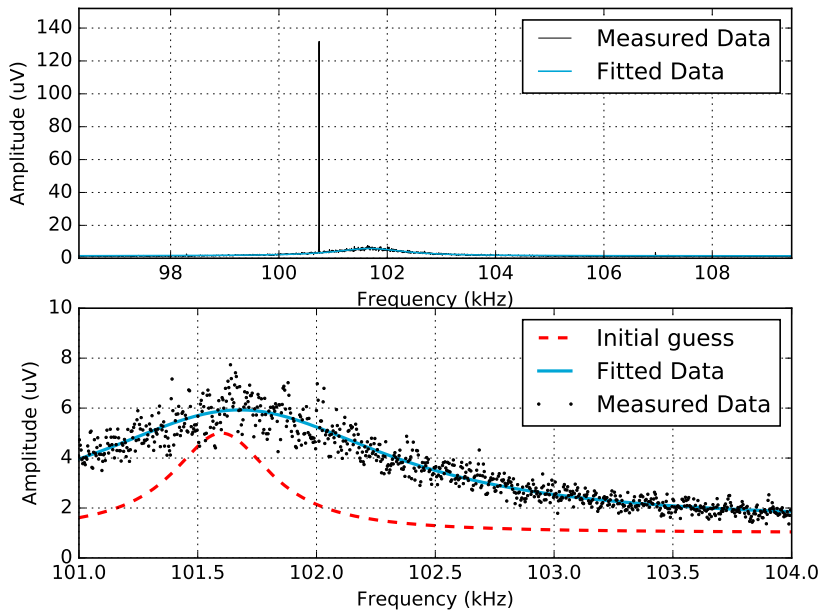

Figure E.50: Reference measurement in air, using cantilever C, near the surface.

Measurement gas - 100% - Cantilever C - 'Near surface', $Q = 35,\ f_c = 101.3\,\text{kHz}$

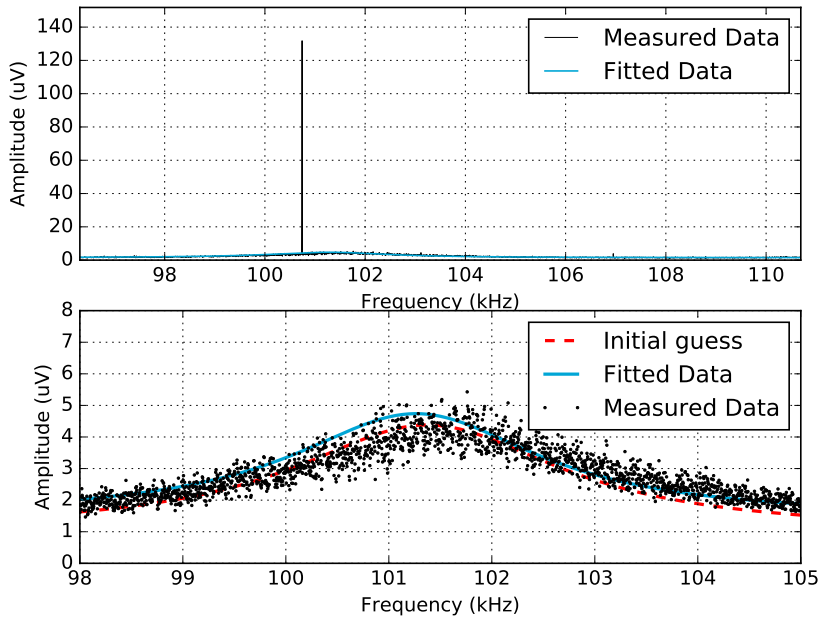

Figure E.51: Measurement in 100% CO_2, using cantilever C, near the surface. This measurement is the first gas measurement near the surface, before the jar is washed with N_2, in the report referred to as 'the red point'.

Measurement gas - 0% - Cantilever C - 'Near surface', $Q = 139,\ f_c = 103.3\,\mathrm{kHz}$

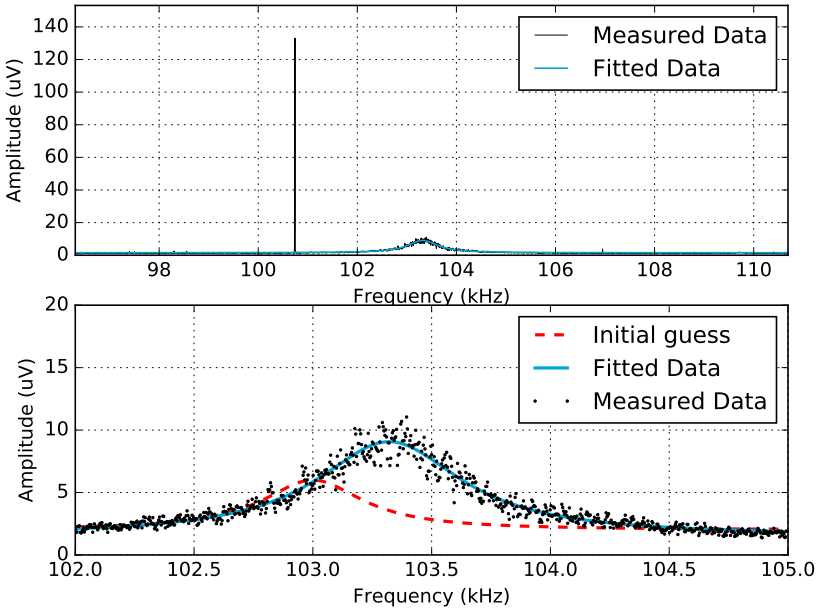

Figure E.52: Measurement in 0% CO_2, using cantilever C, near the surface.

Measurement gas - 14% - Cantilever C - 'Near surface', $Q = 150,\ f_c = 103.3\,\mathrm{kHz}$

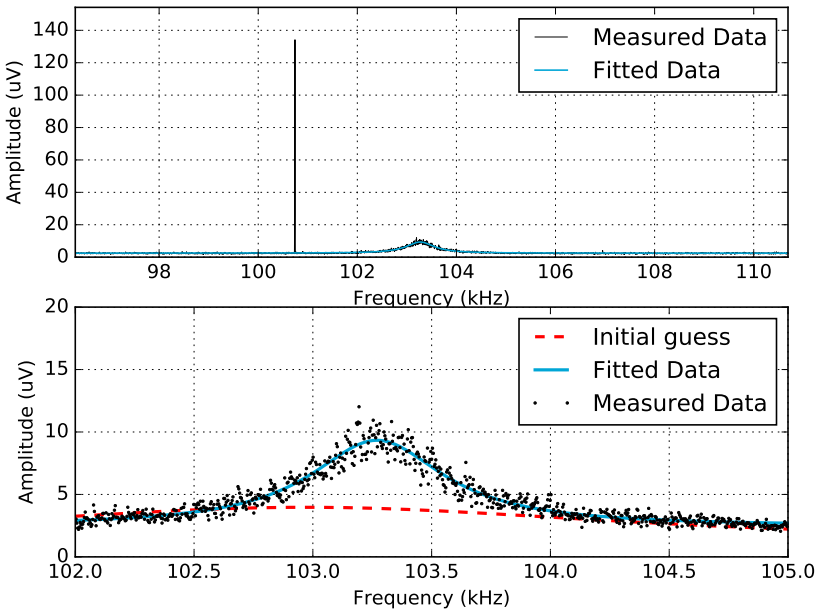

Figure E.53: Measurement in 14% CO_2, using cantilever C, near the surface.

Measurement gas - 22% - Cantilever C - 'Near surface', $Q = 144$, $f_c = 103.3\,\mathrm{kHz}$

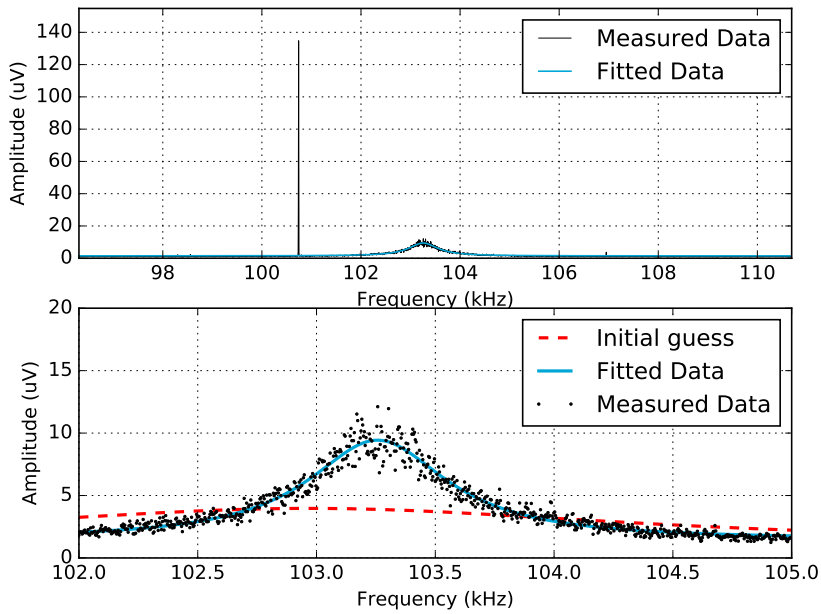

Figure E.54: Measurement in 22% CO_2, using cantilever C, near the surface.

Measurement gas - 30% - Cantilever C - 'Near surface', $Q = 146$, $f_c = 103.2\,\mathrm{kHz}$

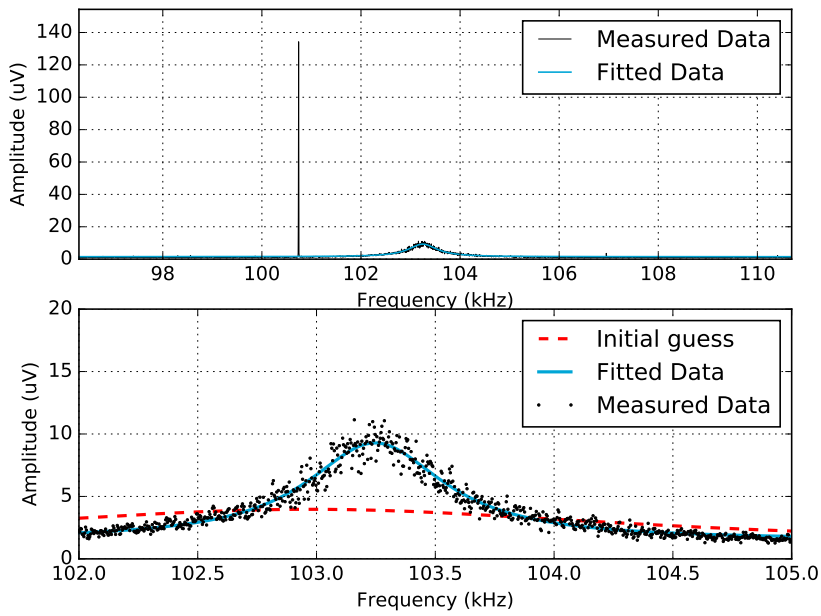

Figure E.55: Measurement in 30% CO_2, using cantilever C, near the surface.

Measurement gas - 40% - Cantilever C - 'Near surface', $Q = 152,\ f_c = 103.2\,\text{kHz}$

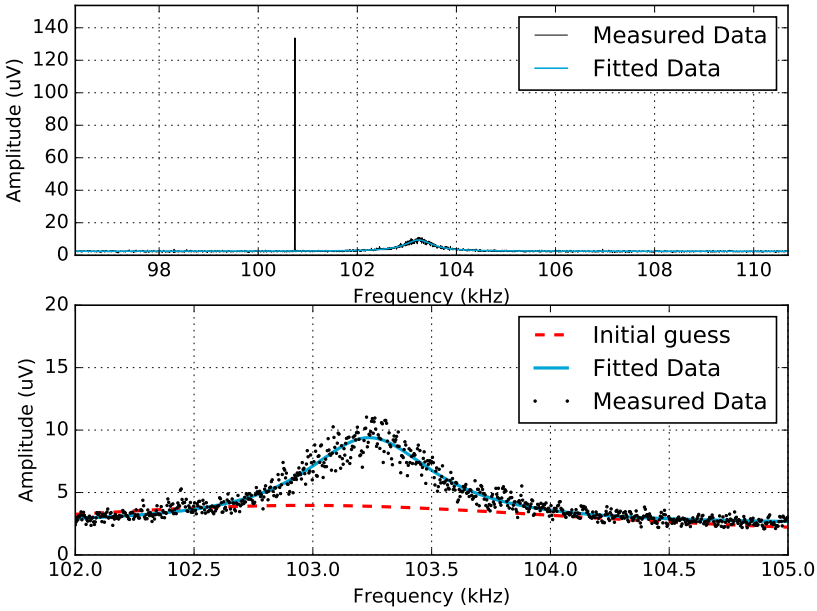

Figure E.56: Measurement in 40% CO_2, using cantilever C, near the surface.

Measurement gas - 53% - Cantilever C - 'Near surface', $Q = 140,\ f_c = 103.2\,\text{kHz}$

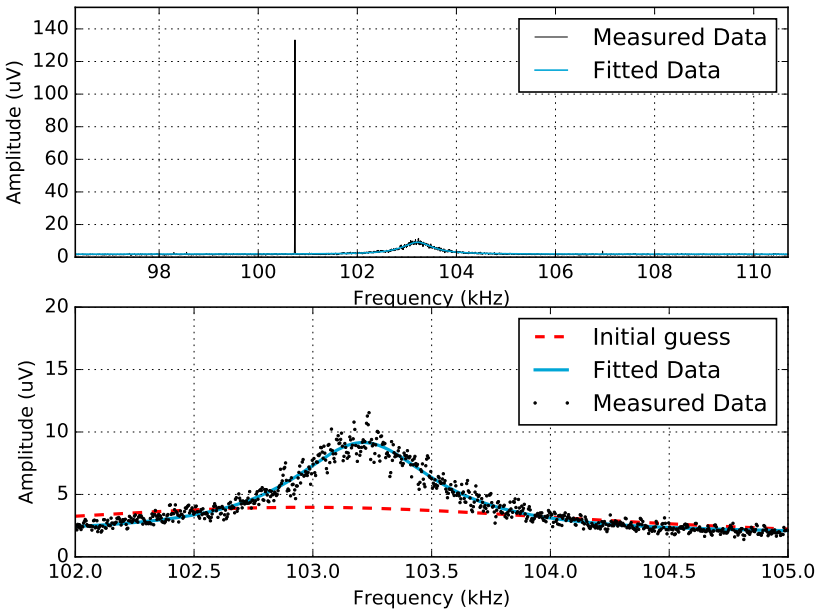

Figure E.57: Measurement in 53% CO_2, using cantilever C, near the surface.

Measurement gas - 62% - Cantilever C - 'Near surface', $Q = 32,\ f_c = 98.09\,\text{kHz}$

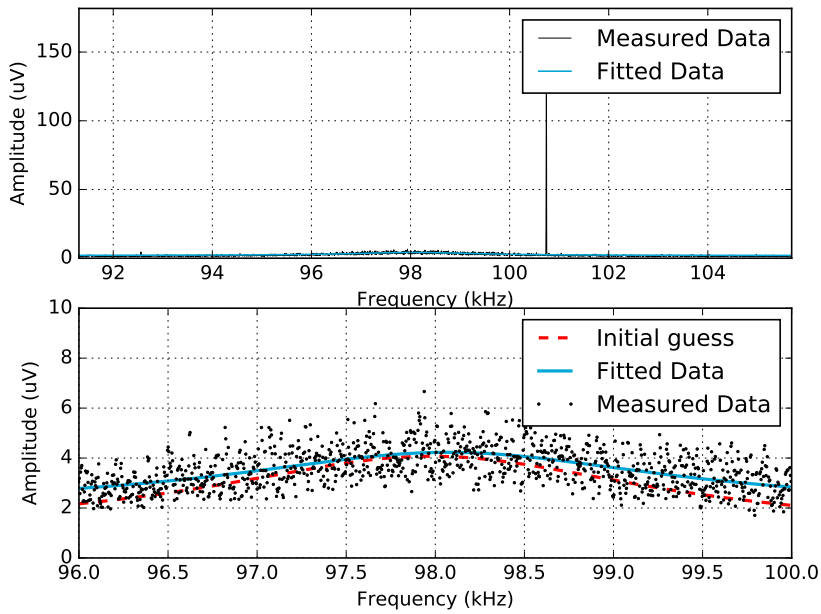

Figure E.58: Measurement in 62% CO_2, using cantilever C, near the surface.

Measurement gas - 70% - Cantilever C - 'Near surface', $Q = 26,\ f_c = 98.07\,\text{kHz}$

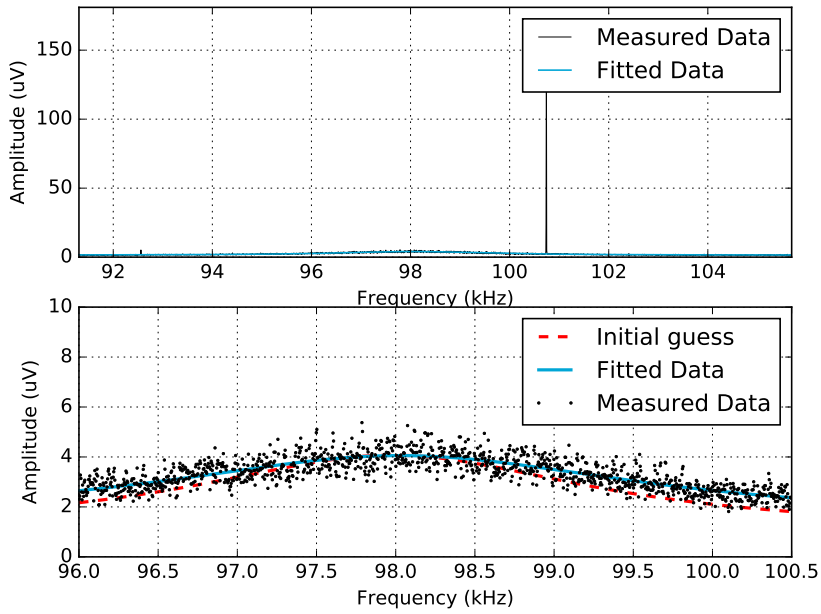

Figure E.59: Measurement in 70% CO_2, using cantilever C, near the surface.

Measurement gas - 80% - Cantilever C - 'Near surface', $Q = 24,\ f_c = 97.95\,\text{kHz}$

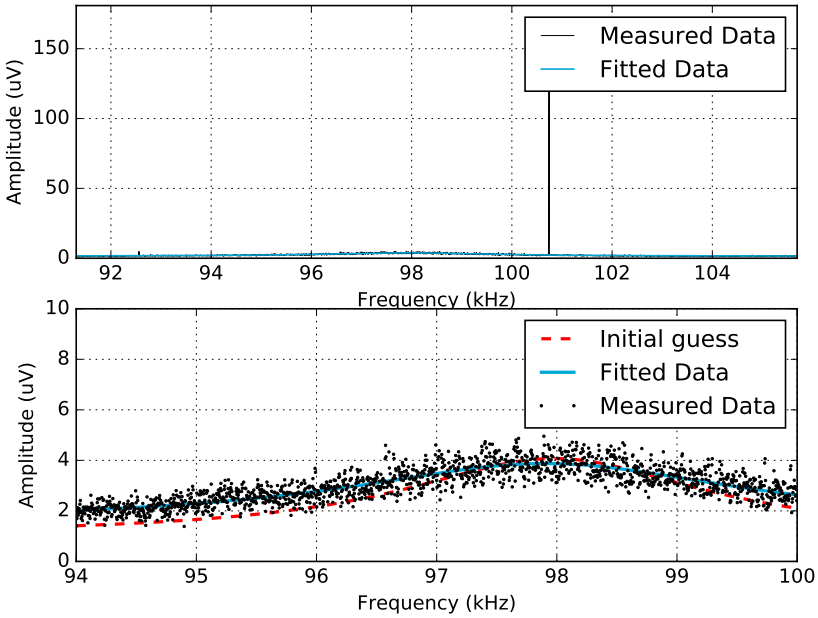

Figure E.60: Measurement in 80% CO_2, using cantilever C, near the surface.

Measurement gas - 90% - Cantilever C - 'Near surface', $Q = 21,\ f_c = 98.43\,\text{kHz}$

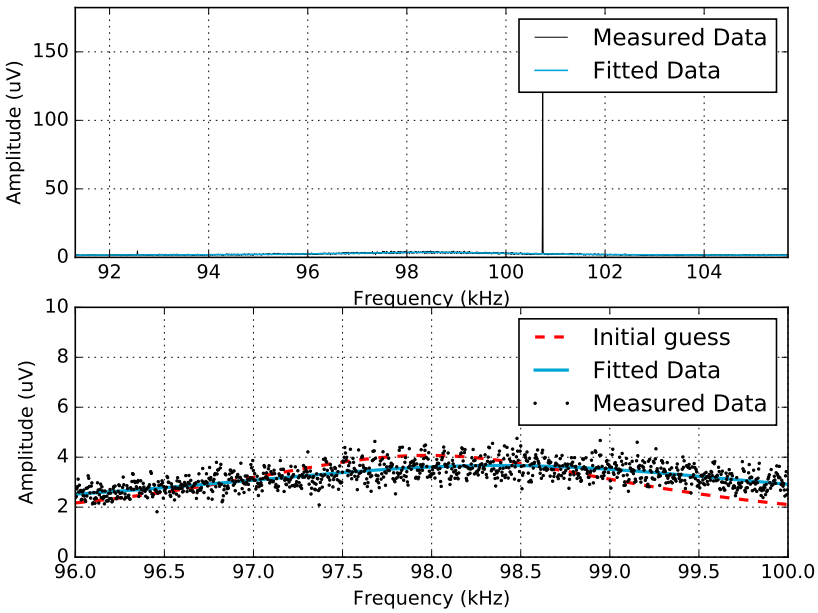

Figure E.61: Measurement in 90% CO_2, using cantilever C, near the surface.

Measurement gas - 98% - Cantilever C - 'Near surface', $Q = 22,\ f_c = 98.89\,\mathrm{kHz}$

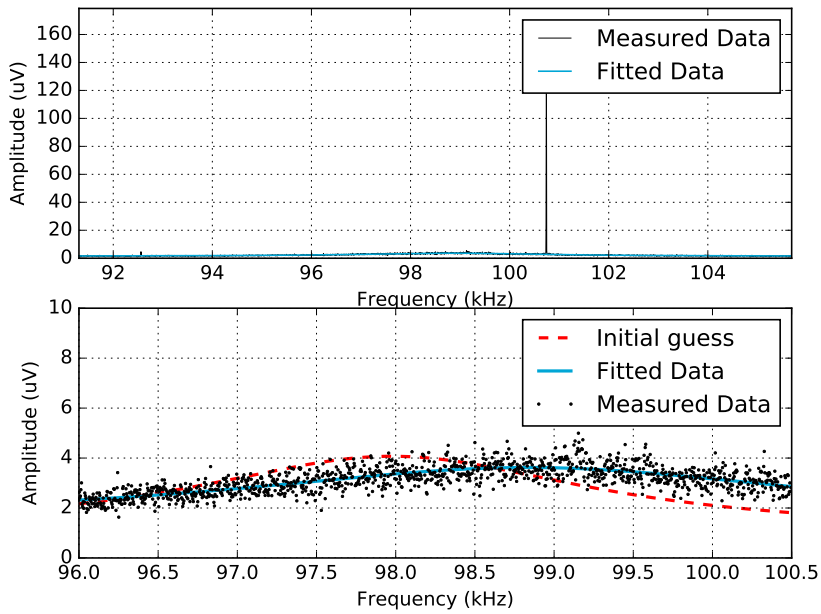

Figure E.62: Measurement in 98% CO_2, using cantilever C, near the surface.

Measurement gas - 100% - Cantilever C - 'Near surface', $Q = 25,\ f_c = 100.1\,\mathrm{kHz}$

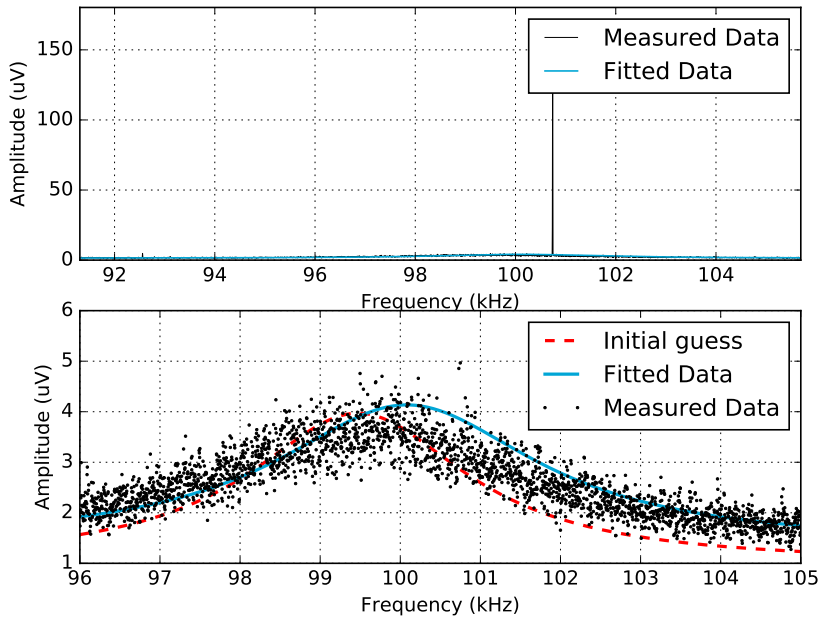

Figure E.63: Measurement in 100% CO_2, using cantilever C, near the surface.